BỘ GIÁO DỤC VÀ ĐÀO TẠO
**TRƯỜNG ĐẠI HỌC SƯ PHẠM KỸ THUẬT
THÀNH PHỐ HỒ CHÍ MINH**

ĐÀO THỊ THU THỦY

THIẾT KẾ VÀ PHÂN TÍCH CÁC GIAO THỨC NÂNG CAO HIỆU NĂNG MẠNG HỢP TÁC HAI CHIỀU

**DANH MỤC CÁC CÔNG TRÌNH ĐÃ CÔNG BỐ
NGÀNH: KỸ THUẬT ĐIỆN TỬ**

Tp. Hồ Chí Minh, tháng 07/2023

DANH MỤC CÁC CÔNG TRÌNH ĐÃ CÔNG BỐ CỦA LUẬN ÁN

[P1]. **Thu-Thuy Thi Dao**, Pham Ngoc Son, "Uplink Non-Orthogonal Multiple Access Protocol in Two-Way Relaying Networks: Realistic Operation and Performance Analysis," *2020 7th NAFOSTED Conference on Information and Computer Science (NICS)*, VNUHCM, Vietnam 11/2020 (IEEE Xplore).

[P2]. **Thu-Thuy Thi Dao**, Pham Ngoc Son, "Cancel-Decode-Encode Processing on Two-Way Cooperative NOMA Schemes in Realistic Conditions," *Wireless Communications and Mobile Computing*, vol 2021, Article ID 8828443, 15 pages, 2021 (SCIE).

[P3]. **Thu-Thuy Thi Dao**, Pham Ngoc Son, **"**Two-Way Cognitive Network supported by Reconfigurable Intelligent Surface," *2021 International Conference on Advanced Technologies for Communications (2021ATC)*, Ho Chi Minh city, Vietnam. 10/2021 (IEEE Xplore).

[P4]. **Thu-Thuy Thi Dao**, Pham Ngoc Son, "Multi-constraint two-way underlay cognitive network using, reconfigurable intelligent surface," *Wireless Networks*, 2022/04/06 2022 (SCIE).

[P5]. **Thu-Thuy Thi Dao**, Pham Ngoc Son, "Performance analysis of two-way network with nonlinear energy harvesting relay and digital network coding," *The 2nd International Conference on Advanced Technology and Sustainable Development – 2022 (ICATSD 2022)*, Ho Chi Minh city, Vietnam, 11/2022.

Uplink non-orthogonal multiple access protocol in two-way relaying networks: realistic operation and performance analysis

Thu-Thuy Thi Dao [*][†], Pham Ngoc Son [*]

[*] Ho Chi Minh City University of Technology and Education, Ho Chi Minh City, Vietnam

Email: thuydtt.ncs@hcmute.edu.vn; sonpndtvt@hcmute.edu.vn

[†] Industrial University of Ho Chi Minh City, Ho Chi Minh City, Vietnam

Abstract—In this paper, we study a two-way non-orthogonal multiple access cooperative schemes with two sources and the aid of a decode-and-forward relay under the overall effects of perfect/imperfect successive interference cancellation and perfect/imperfect channel state information. In this scheme, the digital network coding technique is used at the relay to decrypt sequentially the received data from sources, then encode these data by the XOR operation and transmit back to the sources. System performance in terms of outage probabilities and throughput is analyzed by exact and asymptotic closed-form expressions. Besides, the proposed protocol performance is compared to the performance of a conventional two-way scheme. The Monte Carlo simulation results evidence the validity of the analysis expressions.

Index Terms—Two-way cooperative scheme, perfect and imperfect SIC, perfect and imperfect CSI, digital network coding, non-orthogonal multiple access.

I. INTRODUCTION

In recent years, improving system throughput and spectrum efficiency over wireless networks has been a growing challenge because of the growing number of users and increasingly diverse Internet of Things applications. The cooperative communication has been interested in because it provides high spatial diversity gain to mitigate fading, to widen coverage, and to increase communication reliability [1]. The relaying nodes process received and transmit signals by apply methods as decode-and-forward (DF) and amplify-and-forward (AF). The AF method is simple but it amplify noises in received signals. In two-way cooperative communications, both source devices can transmit or receive from each other, so digital network coding (DNC) should be combined to improve the performance system as increasing bandwidth utilization efficiency by decreasing transmission time between devices [2]–[4].

Besides, non-orthogonal multiple access (NOMA) has considered as one of the solutions for the fifth-generation (5G) mobile communications network to meet these challenges due to its potential achievements to improve spectral efficiency, enlarge connections, reduce access latency and enhance fairness among users [5], [6]. Recently, a two-way CNOMA network has been studied to take advantage of these advantages [7]–[10]. In a power-domain NOMA scheme, transmit signals for multi-users is distributed at different power levels at the same time, frequency, and code domain using the superposition coding. And at receivers, the decoding principle is to apply the successive interference cancellation (SIC) method. In practical cases, when using SIC still happens unexpected issues caused by complexity scaling and error propagation lead to errors in decoding. And the near-user of the NOMA system will endure a residual interference signal if the fault of using SIC appears. Hence, considering the impact of imperfect SIC (ipSIC) on system performances is necessary. Moreover, in realistic applications, the system performances can be affect by hardware impairments or the collection of imperfect channel state information (CSI) [11], [12]. The imperfect CSI can occur because of the channel time-variation during the feedback delays (FDs) of the CSI and also because of the errors in the CSI estimating process [13], [14]. In [15], the authors have studied a two-way cooperative scheme in which combination of SIC and DNC confirming that performances in an asymmetric two-way cooperative scheme have better spectrum utilization efficiency the conventional two-way DF scheme with only using the DNC technique. However, the authors investigated this scheme only in condition perfect channel state information.

Motivated by previous works for the two-way network to improve spectrum utilization efficiency and system performance, we suggest a two-way cooperative scheme with a DF relay and two sources and considers the comprehensive investigation with both the perfect CSIs (pCSIs) and the imperfect CSIs (ipCSIs) in case of the perfect SICs (pSICs) and the imperfect SICs (ipSICs).

We adopt the uplink NOMA protocol to achieve high spectral efficiency, the source close to the relay is allocated a smaller transmission power than the farther source. Afterward, the relay uses the SIC technique to decrypt sequentially the received signals and uses the DNC technique to makes a new encoded signal. Finally, the encoded signal is broadcasted back to two source nodes, denoted as TTS protocol. To evaluate the system performance of the proposed TTS protocol, the exact and asymptotic closed-form expressions of the outage probabilities and the system throughput are considered. Besides, we also compare the system throughput of this proposed protocol with the system throughput of the conventional two-way DF protocol which does not use the SIC and DNC techniques, denoted as FTS protocol.

The rest of this paper is organized into sections as follows.

First time slot: $\longrightarrow$

Second time slot: $\dashrightarrow$
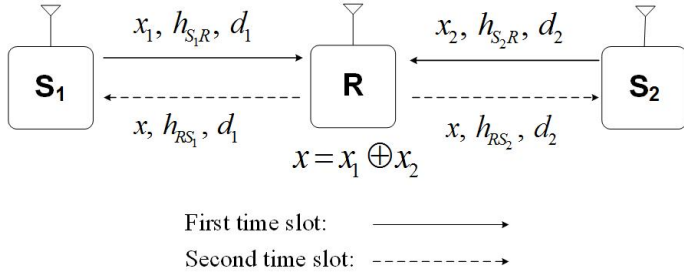
Fig. 1. Two-way cooperative model of the TTS protocol.

Section II describes a two-way cooperative model of the TTS protocol. Section III analyzes the exact and asymptotic outage probabilities and system throughput of the TTS and FTS protocols. Section IV shows simulation results to verify the theoretical analysis. Finally, the conclusions are given in Section V.

Notations: $\Pr(.)$ stands for probability operation; $f_X(.)$ and $F_X(.)$ define the probability density function (PDF) and cumulative distribution function (CDF) of a given random variable (RV) X, respectively.

II. System Model

Consider a cooperative two-way network as illustrated in figure 1, where two sources S_1 and S_2 communicate to each other with the aid of a half-duplex DF relay R. In this model, we have some assumptions as: the sources and the relay have a single antenna; the direct link between the sources S_1 and S_2 is unavailable due to severe fading and path-loss, thus communication between two sources can be established only via relay [16], [17]. We denote d_1 and d_2 as the normalized distances of link S_1 and R and S_2 and R, where $d_1 \leq d_2$. We assume that all the channels suffer from flat and block Rayleigh fading. The channel coefficients for links $S_k \rightarrow R$ and $R \rightarrow S_k$ are denoted as $h_{S_k R}$ and h_{RS_k}, respectively. In this model, the imperfect CSIs are caused by the feedback delay with a time-variant channel model and can be modeled as [12]–[14].

$$\hat{h}_f = \rho_f h_f + \sqrt{1 - \rho_f{}^2}\varepsilon_f \qquad (1)$$

where $f \in \{S_k R, RS_k\}$. Here, ε_f represents the estimation errors and $\hat{h}_f$ defines the estimated CSIs. ε_f and $\hat{h}_f$ are independent complex Gaussian RVs with zero mean and variances λ_f, $\left(\varepsilon_f, \widehat{h}_f \sim CN(0, \lambda_f)\right)$. Moreover, the correlation coefficients $0 \leq \rho_f \leq 1$ are constants (where $\rho_f = 1$ represents no delay effect and in other words, the CSI is not outdated), characterizing the average quality of channel estimations. For simplicity, we assume that $\rho_f = \rho$ for all the identical devices, $\rho = 1$ for perfect CSIs, and $\rho < 1$ for imperfect CSIs [11]–[14]. The estimated channel gains $g_{S_k R} = \left|\hat{h}_{S_k R}\right|^2$ and $g_{RS_k} = \left|\hat{h}_{RS_k}\right|^2$ are exponentially distributed RVs with PDFs $f_{g_{S_k R}}(x) = f_{g_{RS_k}}(x) = \frac{1}{\lambda_k}e^{-x/\lambda_k}$, and CDFs $F_{g_{S_k R}}(x) = F_{g_{RS_k}}(x) = 1 - e^{-x/\lambda_k}$, where

$\lambda_k = \lambda_{S_k R} = \lambda_{RS_k} = d_k^{-\beta}$ and β are a path-loss exponent [4].

The operation of the TTS protocol happens in two time slots. In the first slot, the relay receive concurrently the signals of two sources S_1 and S_2, and the relay will decode the received signals using the SIC technique. In the second slot, the relay creates an encoded signal using the DNC techniques [4], [15] and broadcasts it to two sources S_1 and S_2. In this paper, the SIC technique is considered in cases of the perfect SIC (pSIC) and imperfect SIC (ipSIC).

We denote x_1 and x_2 as the transmitted data signals by S_1 and S_2, respectively, while $x = x_1 \oplus x_2$ as the transmitted signal by the selected relay with transmit power P_R. Considering the first time slot, according to the NOMA protocol, the received signal y_R at R is a weighted sum of x_1 and x_2, and is described as an expression follows.

$$y_R = \sqrt{\alpha_1 P_S}h_{S_1 R}x_1 + \sqrt{\alpha_2 P_S}h_{S_2 R}x_2 + n_R. \qquad (2)$$

where $\alpha_1 P_S$ and $\alpha_2 P_S$ are transmit power to carry x_1 and x_2, respectively, with power allocation coefficients α_1 and α_2 to fairness between S_1 and S_2 (a higher power should be allocated to the source which is farther from relay [7], $(0 < \alpha_1, \alpha_2 < 1)$, and n_R is the AWGNs with the variance N_0 at the nodes R.

Substituting (1) into (2), we have an expression as

$$y_R = \sqrt{\alpha_1 P_S}\hat{h}_{S_1 R}x_1 - \sqrt{\alpha_1 P_S}\frac{\sqrt{1-\rho^2}}{\rho}\varepsilon_{S_1 R}x_1 \\ + \sqrt{\alpha_2 P_S}\hat{h}_{S_2 R}x_2 - \sqrt{\alpha_2 P_S}\frac{\sqrt{1-\rho^2}}{\rho}\varepsilon_{S_2 R}x_2 + n_R. \qquad (3)$$

At the first time slot, applying the SIC technique [9], [15], the relay first decode the transmitted signal x_1 by the nearby source which has better average channel quality while considering signals containing x_2 as interference. The received signal-to-interference-plus-noise ratio (SINR) for detecting x_1 can be given from (3) as

$$\gamma_{S_1 R \rightarrow x_1} = \frac{\alpha_1 \left|\hat{h}_{S_1 R}\right|^2}{\alpha_2 \left|\hat{h}_{S_2 R}\right|^2 + \underbrace{(\alpha_1 \lambda_1 + \alpha_2 \lambda_2)(1 - \rho^2) + \rho^2/\gamma}_{\phi_1}} \\ = \frac{\alpha_1 g_{S_1 R}}{\alpha_2 g_{S_2 R} + \phi_1}, \qquad (4)$$

where γ is defined as transmit SNR, $\gamma = P_S/N_0$.

After decoding x_1 successfully, the interference component $\sqrt{\alpha_1 P_S}\hat{h}_{S_1 R}$ in (3) is deleted at the relay, then the received SNR for detecting x_2 can be given as:

$$\gamma_{S_2 R \rightarrow x_2} = \frac{\alpha_2 \gamma \left|\hat{h}_{S_2 R}\right|^2}{\varepsilon\gamma|h_R|^2\rho^2 + \gamma(\alpha_1 \lambda_1 + \alpha_2 \lambda_2)(1-\rho^2) + \rho^2} \\ = \frac{\alpha_2 g_{S_2 R}}{\varepsilon\rho^2 g_R + \phi_1}. \qquad (5)$$

In the subsequent time slot, the relay R uses XOR operation to synthetic $x = x_1 \oplus x_2$ and then broadcasts x to two sources. As a result, the source S_k receives signal as following

$$y_{RS_k} = \sqrt{P_R}\hat{h}_{RS_k}x - \sqrt{P_R}\frac{\sqrt{1-\rho^2}}{\rho}\varepsilon_{RS_k}x + n_{S_k}, \qquad (6)$$

where P_R is the transmit power for the signal x at the R, and n_{S_k} is the AWGNs at the sources S_k with the variance N_0.

Then x will be detected at the source S_k with the SINR value of

$$\gamma_{RS_k \to x} = \frac{P_R \left| \hat{h}_{RS_k} \right|^2 / \rho^2}{P_R \lambda_k \left(1 - \rho^2\right) / \rho^2 + N_0} = \frac{\eta \gamma g_{RS_k}}{\eta \gamma \lambda_k \left(1 - \rho^2\right) + \rho^2}, \quad (7)$$

where $\eta = P_R / P_S$ and $\eta > 0$.

For comparison, we consider a two-way scheme using four time slots with relay in perfect and imperfect CSIs (called as the FTS protocol). The transmission process of this protocol is described as follows $S_1 \xrightarrow[\text{1st}]{x_1} R \xrightarrow[\text{2nd}]{x_1} S_2 \xrightarrow[\text{3rd}]{x_2} R \xrightarrow[\text{4th}]{x_2} S_1$.

In the first time slot, the source node S_1 transmits the data signal x_1 to the relay, the received signal and the SNR at the relay can be expressed by

$$\begin{aligned} y^C_{S_1 R} &= \sqrt{\alpha_1 P_S} h_{S_1 R} x_1 + n_R \\ &= \sqrt{\alpha_1 P_S} \, \hat{h}_{S_1 R} x_1 - \sqrt{\alpha_1 P_S} \frac{\sqrt{1-\rho^2}}{\rho} \varepsilon_{S_1 R} x_1 + n_R \end{aligned}, \quad (8)$$

$$\gamma_{S_1 R} = \frac{\alpha_1 P_S \left| \hat{h}_{S_1 R} \right|^2 / \rho^2}{\alpha_1 P_S \lambda_1 (1-\rho^2)/\rho^2 + N_0} = \frac{\alpha_1 \gamma g_{S_1 R}}{\alpha_1 \lambda_1 \gamma (1-\rho^2) + \rho^2}. \quad (9)$$

Then x_1 will be decoded and transmitted to the source S_2 in the next time slot. At the source S_2, the received signal and the SNR can be expressed by

$$y^C_{RS_2} = \sqrt{P_R} \hat{h}_{RS_2} x_1 - \sqrt{P_R} \frac{\sqrt{1-\rho^2}}{\rho} \varepsilon_{RS_2} x_1 + n_{S_2}, \quad (10)$$

$$\gamma_{RS_2} = \frac{\eta \gamma g_{RS_2}}{\eta \gamma \lambda_2 \left(1 - \rho^2\right) + \rho^2}. \quad (11)$$

Similarly, the source S_2 transmits the signal x_2 to the relay and the relay R will decode and transmit this signal to the source S_1 in the third and fourth time slots. Consequently, SINR to decode the signal x_2 at the relay R and the source S_1 can be expressed by

$$\gamma_{S_2 R} = \frac{\alpha_2 \gamma g_{S_2 R}}{\alpha_2 \lambda_2 \gamma \left(1 - \rho^2\right) + \rho^2}, \quad (12)$$

$$\gamma_{RS_1} = \frac{\eta \gamma g_{RS_1}}{\eta \gamma \lambda_1 \left(1 - \rho^2\right) + \rho^2}. \quad (13)$$

III. Performance Evaluation

In this section, we obtain expressions of the outage probability and throughput for the considered protocols. We suppose that the nodes R and S_k decrypt received signals successfully if their SINRs are larger than or equal to a target γ_t. Otherwise, these nodes will happen to the outage events.

A. Outage probability analysis

1) The proposed TTS protocol: As mentioned in section 2, to successfully transmit the signal x_1 from S_1 to S_2, first the relay R must receive and decode successfully the signal x_1 and then the node source S_2 also must detect and decode successfully with the signal x. The probability of successful decoding x_1 at S_2 will equal to $\Pr(\gamma_{S_1 R \to x_1} \geq \gamma_t, \gamma_{RS_2 \to x} \geq \gamma_t)$. Conversely, the outage probability at the source S_2 for

the $S_1 \xrightarrow{x_1} R \xrightarrow{x} S_2$ link can be described as the formula following

$$OP_{S_2} = 1 - \Pr \left[\gamma_{S_1 R \to x_1} \geq \gamma_t, \gamma_{RS_2 \to x} \geq \gamma_t\right]. \quad (14)$$

A point to remark is that $\gamma_{S_1 R \to x_1} \geq \gamma_t$ and $\gamma_{RS_2 \to x} \geq \gamma_t$ are independent events. Thus, the formula (14) can rewrite as follows

$$OP_{S_2} = 1 - \Pr \left[\gamma_{S_1 R \to x_1} \geq \gamma_t\right] \times \Pr \left[\gamma_{RS_2 \to x} \geq \gamma_t\right]. \quad (15)$$

Substituting (4) and (7) into (15), after some manipulations the outage probability at the source S_2 is obtained as in (16) at the top of next page,

For the $S_2 \xrightarrow{x_2} R \xrightarrow{x} S_1$ link. Based on the SIC operation principle, the transmission of the signal x_2 from the source node S_2 to the S_1 only successes when the relay R decodes successfully the signals (x_1, x_2) and the source S_1 also decode successfully the signal x. On the other hand, the outage probability of the S_1 occurs in three cases: the relay R decodes unsuccessfully the signal x_1; or it decodes successfully the x_1 but unsuccessfully the signal x_2; or the relay R decodes successfully both the signals x_1 and x_2 but the signal x is not decoded at the source S_1. The outage probability at the source S_1 for the S_1 for this link can be described as

$$\begin{aligned} OP_{S_1} &= 1 - \Pr \left[\gamma_{S_1 R \to x_1} > \gamma_t, \gamma_{S_2 R \to x_2} > \gamma_t, \gamma_{RS_1 \to x} > \gamma_t\right] \\ &= 1 - \Pr \left[\gamma_{S_1 R \to x_1} \geq \gamma_t, \gamma_{S_2 R \to x_2} \geq \gamma_t\right] \times \Pr \left[\gamma_{RS_1 \to x} \geq \gamma_t\right] \end{aligned}. \quad (17)$$

Substituting (4), (5) and (7) into (17), after some manipulations the outage probability at the source S_2 is obtained as in (18) at the top of next page.

Corollary 1: In the special case as $\gamma \to +\infty$, then $1/\gamma \to 0$, the asymptotic expression of OP_{S_2} and OP_{S_1} are obtained as in (19) and (20) at the top of next page, respectively.

2) The comparative protocol: The outage probability at the source S_2 for the $S_1 \xrightarrow[\text{1st}]{x_1} R \xrightarrow[\text{2nd}]{x_1} S_2$ link in the FTS protocol is described as follows

$$\begin{aligned} OP^C_{S_2} &= 1 - \Pr \left[\gamma_{S_1 R} \geq \gamma_t, \gamma_{RS_2} \geq \gamma_t\right] \\ &= 1 - \left(1 - \Pr \left[\gamma_{S_1 R} < \gamma_t\right]\right) \times \left(1 - \Pr \left[\gamma_{RS_2} < \gamma_t\right]\right) \end{aligned}. \quad (21)$$

Substituting (9) and (11) into (21), and after some manipulations we we get a final result as

$$OP^C_{S_2} = 1 - e^{-\gamma_t \left(2\left(1-\rho^2\right)+\rho^2\left(1/(\alpha_1 \lambda_1 \gamma)+1/\eta \lambda_2 \gamma\right)\right)}. \quad (22)$$

Similarly, the outage probability at the source S_1 for the $S_2 \xrightarrow[\text{3rd}]{x_2} R \xrightarrow[\text{4th}]{x_2} S_1$ link is expressed as

$$OP^C_{S_1} = 1 - e^{-\gamma_t \left(2\left(1-\rho^2\right)+\rho^2\left(1/(\alpha_2 \lambda_2 \gamma)+1/\eta \lambda_1 \gamma\right)\right)}. \quad (23)$$

Corollary 2: In the special case as $\gamma \to \infty$, asymptotic expressions of the outage probabilities at the sources S_2 and S_1 are obtained as

$$OP^C_{S_2} \bigg|_{\gamma \to +\infty} = OP^C_{S_1} \bigg|_{\gamma \to +\infty} = 1 - e^{-\gamma_t 2\left(1-\rho^2\right)}. \quad (24)$$

$$OP_{S_2} = 1 - \left(1 - \int_0^\infty f_{g_{S_2R}}(x) F_{g_{S_1R}}(\frac{\gamma_t \alpha_2}{\alpha_1} x + \frac{\gamma_t \phi_1}{\alpha_1}) dx\right) \left(1 - F_{g_{RS_2}}\left(\gamma_t \lambda_2 \left(1 - \rho^2\right) + \frac{\gamma_t \rho^2}{\eta\gamma}\right)\right)$$
$$= 1 - \frac{\alpha_1 \lambda_1 e^{-\gamma_t\left(\phi_1/\alpha_1\lambda_1 + \left(1 - \rho^2\right) + \rho^2/(\lambda_2\eta\gamma)\right)}}{\alpha_1 \lambda_1 + \gamma_t \alpha_2 \lambda_2}$$

(16)

$$OP_{S_1} = \frac{e^{-\gamma_t\left(\phi_1((1+\gamma_t)/(\alpha_1\lambda_1)+1/(\alpha_2\lambda_2))+\left(1-\rho^2\right)+\rho^2/(\lambda_1\gamma)\right)}}{\left(1 + \gamma_t \alpha_2 \lambda_2/\left(\alpha_1\lambda_1\right)\right)\left(1 + \left(1 + \gamma_t^2 \phi_1/\left(\alpha_1\lambda_1\right)\right)\gamma_t \varepsilon \rho^2 \Omega/\left(\alpha_2\lambda_2\right)\right)}.$$

(18)

$$OP_{S_2}|_{\gamma\to+\infty} = 1 - \frac{\alpha_1 \lambda_1 e^{-\gamma_t\left(1-\rho^2\right)(2+(\alpha_2\lambda_2)/(\alpha_1\lambda_1))}}{\alpha_1 \lambda_1 + \gamma_t \alpha_2 \lambda_2}.$$

(19)

$$OP_{S_1}|_{\gamma\to+\infty} = \frac{e^{-\gamma_t\left(1-\rho^2\right)((\alpha_1\lambda_1+\alpha_2\lambda_2)((1+\gamma_t)/(\alpha_1\lambda_1)+1/(\alpha_2\lambda_2))+1)}}{\left(1 + \gamma_t \alpha_2\lambda_2/\left(\alpha_1\lambda_1\right)\right)\left(1 + \gamma_t \varepsilon \rho^2 \Omega\left(1 + \gamma_t^2\left(1-\rho^2\right)\left(1 + \alpha_2\lambda_2/\left(\alpha_1\lambda_1\right)\right)\right)/\left(\alpha_2\lambda_2\right)\right)}.$$

(20)

B. Throughput analysis

Mathematically speaking, the throughput for the proposed TTS protocol and the comparative FTS protocol are obtained, respectively, as [9], [18]

$$TP_{\text{TTS}} = \frac{1}{2}\left(1 - OP_{S_1}\right) R_t + \frac{1}{2}\left(1 - OP_{S_2}\right) R_t. \quad (25)$$

$$TP_{\text{FTS}} = \frac{1}{4}\left(1 - OP_{S_1}^C\right) R_t + \frac{1}{4}\left(1 - OP_{S_2}^C\right) R_t. \quad (26)$$

where: ½ and ¼ denote that the protocols TTS and FTS operate in two time slots and four time slots, respectively; $R_t = \log_2\left(1 + \gamma_t\right)$ (bits/s/Hz).

IV. SIMULATION RESULTS

In this section, we analyze and evaluate the outage probabilities and the system throughput of two protocols (TTS and FTS). Monte Carlo simulations are used to validate the accuracy of the asymptotic and exact theory expressions (markers point to simulated results in all figures). For all our analysis and evaluations, we default set the target SINR as $\gamma_t = 1$, $\Omega = -10$(dB), the power allocation coefficients $\alpha_1 = \alpha_2 = \eta = 1$ and the path-loss exponent as $\beta = 3$. In Figure 2 and Figure 3, we choice small d_1 and infer large value of d_2 as $d_2 = 1 - d_1$. Figure 2 describes the outage probabilities of the sources S_1 and S_2 of the TTS protocol as a function of P_S/N_0(dB) in the ideal conditions (pSIC - pCSIs) and practical conditions (ipSIC- ipCSIs). From Fig. 2, we can see that the system performance of the source nodes and with the pSIC- pCSIs case outperform with the ipSIC- ipCSIs case. This result show that the significant impact of the imperfect CSIs and the imperfect SIC on the system outage probabilities at the two source nodes is clearly. Thus, we should not skip these conditions when considering a practical system. And the source S_2 have the outage probabilities smaller than the source S_1. In the pSIC - pCSIs case, the outage probability of the two sources will be equal when P_S/N_0 (dB) is enough large but

the outage probabilities of the source S_2 are always better those of the source S_1 with every P_S/N_0 (dB) in the ipSIC-ipCSIs case. We have those results because channel gain coefficients are decreased by the negative effects of imperfect CSIs as formulas (1) and the residual interference signals are added to the SNR of the signal at the relay as in formulas (5). Besides, the x_2 signal depends on interference canceling due to the SIC technique in the NOMA technology as formulas (4) and (5) lead to the SNR of the signal x_2 is effected by ipCSIs of both links $S_k \to R$. An especial notice is that there is an influence on the system outage probability for the x_2 signal transmitted from the farther source to the relay than the x_1 signal when using the SIC technique to decode the data. Based on this, we can change the transmit power coefficients accordingly so that the system outage probability can have approximately the same for both signals near and far the relay to more fairness.

Figure 3 plots system throughput for the TTS and FTS protocols as a function of P_S/N_0 (dB) with pCSIs/ipCSIs when $\varepsilon = 0$, $\rho \in \{0.92, 1\}$. We can observe that the TTS protocol is capable of achieving higher throughput compared to the FTS protocol in all P_S/N_0(dB) for both cases of pCSIs and ipCSIs since the proposed protocol uses the NOMA, SIC and DNC techniques to decrease the number of time slot for the signal transmission between nodes. Besides, the throughput of both protocols in the case of pCSIs are always better than in the case of ipCSIs because of skipping effects of the interference parts on the received SINRs. Moreover, the TTS protocol converges to the throughput ceiling in the high P_S/N_0 (dB) regions ($P_S/N_0 > 15$dB).

Figure 4 plots the system throughput for the TTS and FTS protocols as a function of d_1 with pSICs/ipCSIs $\varepsilon = 0$ and $\rho \in \{0.92, 1\}$. As saw in Fig.4, at all locations of the relay, the proposed TTS protocol always betters the FTS protocol in the pCSIs case. But in the ipCSIs case, the TTS protocol have the system throughput better than the FTS protocol only when
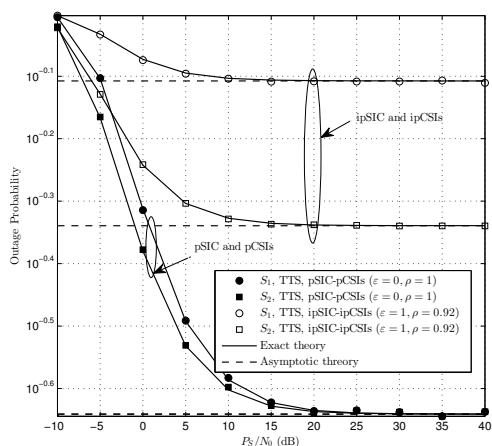
Fig. 2. Outage probabilities of the source nodes S_1 and S_2 in the proposed TTS protocol versus P_S/N_0 (dB) in the cases of pSIC- pCSIs ($\varepsilon = 0, \rho = 1$) and ipSIC- ipCSIs ($\varepsilon = 1, \rho = 0.92$)
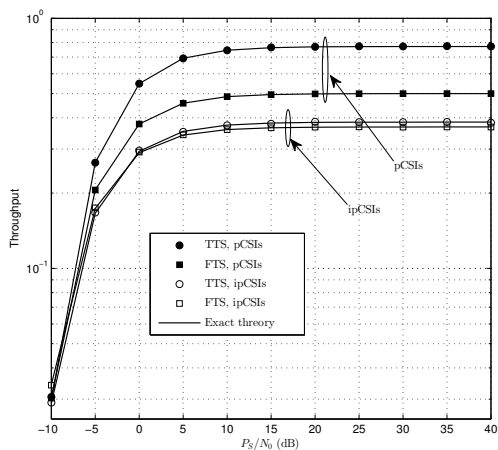
Fig. 3. Throughput of the TTS and FTS protocols versus P_S/N_0 (dB) when $\varepsilon = 0$ and $\rho \in \{0.92, 1\}$.

the distances d_1 are from 0.3 to 0.4. The throughput of the proposed TTS protocol achieves the highest value at optimal locations of the relay as $d_1 = 0.25$ (in the pCSIs case) and $d_1 = 0.37$ (in the ipCSIs case). Last but not least, the two protocols with the perfect CSI ($\rho = 1$) always exceeds with in the imperfect CSI ($\rho = 0.92$).

Finally, from Figs. 2-4, it is value noting that the asymptotic and exact theory analyses are trustful and match well the Monte Carlo simulations.

V. CONCLUSIONS

In this paper, we investigated and analyzed a practical two-way cooperative NOMA scheme under the overall effects of imperfect CSIs caused by the feedback delay and imperfect SICs caused by residual interference after the removal of interference (the TTS protocol). Outage probabilities and throughput of the system were enhanced by the combination of the techniques SIC and DNC at the relay. Our results
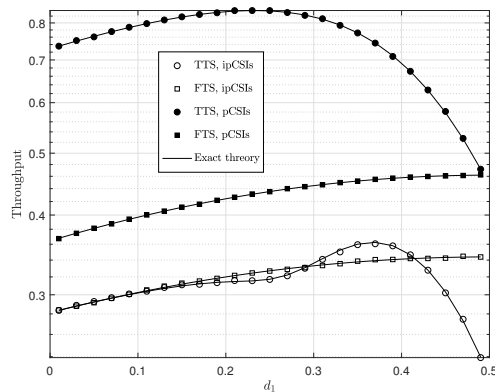
Fig. 4. Throughput of the TTS and FTS protocols versus d_1 when $P_S/N_0 = 5$(dB), $d_2 = 1 - d_1$, $\varepsilon = 0$ and $\rho \in \{0.92, 1\}$.

showed that the system performance is significantly affected by the imperfect SICs and the imperfect CSIs. Moreover, the proposed TTS protocol performs much better than the conventional two-way scheme in the pCSIs condition at all the relay location, but in the ipCSIs condition, the TTS protocol only performs better if the distances from the relay to the two sources are not too different. The significant thing was discovered as the proposed TTS protocol can achieve the best performance at optimal locations of the relay and the power appropriate coefficients of two sources.

REFERENCES

[1] P. Liu, Z. Tao, Z. Lin, E. Erkip, and S. Panwar, "Cooperative wireless communications: a cross-layer approach," *IEEE Wireless Communications*, vol. 13, pp. 84-92, 2006.
[2] T. T. Duy and H. Y. Kong, "Exact outage probability of cognitive two-way relaying scheme with opportunistic relay selection under interference constraint," *IET Communications*, vol. 6, pp. 2750-2759, 2012.
[3] E. S. Lo and K. B. Letaief, "Network coding versus superposition coding for two-way wireless communication," *IEEE Wireless Communications and Networking Conference*, pp. 1-5, 2009.
[4] P. N. Son and H. Y. Kong, "Exact outage probability of two-way decode-and-forward scheme with opportunistic relay selection under physical layer security," *Wireless Personal Communications*, vol. 77, pp. 2889-2917, 2014.
[5] Z. Ding, Y. Liu, J. Choi, Q. Sun, M. Elkashlan, I. Chih-Lin, I. Poor, H. Vincent, "Application of non-orthogonal multiple access in LTE and 5G networks," *IEEE Communications Magazine*, vol. 55, pp. 185-191, 2017.
[6] L. Dai, B. Wang, Y. Yuan, S. Han, I. Chih-Lin, and Z. Wang, "Non-orthogonal multiple access for 5G: solutions, challenges, opportunities, and future research trends," *IEEE Communications Magazine*, vol. 53, pp. 74-81, 2015.
[7] X. Wang, M. Jia, I. W.-H. Ho, Q. Guo, and F. C. Lau, "Exploiting full-duplex two-way relay cooperative non-orthogonal multiple access," *IEEE Transactions on Communications*, vol. 67, pp. 2716-2729, 2018.
[8] T.-P. Huynh, P. N. Son, and M. Vozňák, "Exact outage probability of two-way decode-and-forward NOMA scheme with opportunistic relay selection," *KSII Transactions on Internet and Information Systems*, vol.13, 2019.
[9] X. Yue, Y. Liu, S. Kang, A. Nallanathan, and Y. Chen, "Modeling and Analysis of Two-Way Relay Non-Orthogonal Multiple Access Systems," *IEEE Transactions on Communications*, vol. 66, pp. 3784-3796, 2018.

[10] H. Guo, X. Guo, C. Deng, and S. Zhao, "Performance Analysis of IQI Impaired Cooperative NOMA for 5G-Enabled Internet of Things," Wireless Communications and Mobile Computing, vol. 2020, 2020.

[11] M. J. Taghiyar, S. Muhaidat, J. Liang, and M. Dianati, "Relay selection with imperfect CSI in bidirectional cooperative networks," *IEEE Communications Letters*, vol. 16, pp. 57-59, 2011.

[12] K. Ho-Van, "Exact outage analysis of underlay cooperative cognitive networks with reactive relay selection under imperfect channel information," *Wireless Personal Communications*, vol. 84, pp. 565-585, 2015.

[13] V. Ozduran, "Leakage rate-based untrustworthy relay selection with imperfect channel state information: the outage and security trade-off analysis," *IET Communications*, vol. 13, pp. 1902-1915, 2019.

[14] V. Ozduran, B. S. B. Yarman, and J. M. Cioffi, "Opportunistic source-pair selection method with imperfect channel state information for multiuser bi-directional relaying networks," *IET Communications*, vol. 13, pp. 905-917, 2019.

[15] P. N. Son and T. T. Duy, "A new approach for two-way relaying networks: improving performance by successive interference cancellation, digital network coding and opportunistic relay selection," *Wireless Networks (2019)*, vol.26, no.2, pp.1315-1329, February 2020.

[16] Z. Cao, X. Ji, J. Wang, S. Zhang, Y. Ji, and J. Wang, "Security-Reliability Tradeoff Analysis for Underlay Cognitive Two-Way Relay Networks," *IEEE Transactions on Wireless Communications*, vol. 18, pp. 6030-6042, 2019.

[17] X. Ding, T. Song, Y. Zou, X. Chen, and L. Hanzo, "Security-Reliability Tradeoff Analysis of Artificial Noise Aided Two-Way Opportunistic Relay Selection," *IEEE Transactions on Vehicular Technology*, vol. 66, pp. 3930-3941, (2017).

[18] P. N. Son, T. T. Duy, and K. Ho-Van, "SIC-Coding Schemes for Underlay Two-Way Relaying Cognitive Networks," *Wireless Communications and Mobile Computing*, vol. 2020, Article ID 8860551, pp.1-17, Aug.2020.

WILEY | Hindawi

Research Article

Cancel-Decode-Encode Processing on Two-Way Cooperative NOMA Schemes in Realistic Conditions

Thu-Thuy Thi Dao [1,2] **and Pham Ngoc Son** [1]

[1]*Ho Chi Minh City University of Technology and Education, Ho Chi Minh City, Vietnam*
[2]*Industrial University of Ho Chi Minh City, Ho Chi Minh City, Vietnam*

Correspondence should be addressed to Thu-Thuy Thi Dao; thuydtt.ncs@hcmute.edu.vn
and Pham Ngoc Son; sonpndtvt@hcmute.edu.vn

This paper considers the effects of perfect/imperfect successive interference cancellation (SIC) and perfect/imperfect ` information (CSI) in a multiple-relay two-way cooperative network using nonorthogonal multiple access (NOMA) and digital network coding (DNC). In this model, a relay is selected by maximizing estimated channel gains to enhance the decoding capacity of the nearer source and minimize the collection time of imperfect CSI. Spectrum utilization efficiency is enhanced two times by a mixture of the SIC and DNC techniques at the selected relay (called as the SIC-2TS protocol). The system performance is considered through analysis of the exact and asymptotic expressions of the system outage probabilities and throughput. The major thing is exposed as the proposed SIC-2TS protocol can reach the best performance at optimal positions of the selected relay. Besides, the system throughput of the proposed protocol outperforms a SIC-utilized two-way relaying scheme without the DNC (called as the SIC-3TS protocol) and a conventional two-way scheme (called as the CONV-4TS protocol) for all signal-to-noise ratio regions. Lastly, the validity of the analytical expressions is verified by the Monte Carlo simulation results.

1. Introduction

Recently, wireless networks have rising challenges in enhancing system throughput and spectrum efficiency owing to the increasing user devices and increasing various Internet of Things applications. A key technology for the fifth-generation wireless network to solve these challenges is NOMA technology because of its attainments to help grow spectral efficiency, enlarge connections, decrease access latency, and increase the users' fairness [1–3]. Power domain NOMA uses the superposition coding to allocate different power levels for transmitted signals to the multiusers at the same time, frequency, and code domains. At receivers, the successive interference cancellation method is applied to decode the received signals [2, 3]. However, unexpected errors in decoding when using SIC still occur due to the complexity scale and error propagation, leading to the near user enduring a residual interference signal and the NOMA system performance impacted by this imperfect SIC (ipSIC) [3–6]. In [7],

the authors investigated the reliability and security of the ambient backscatter NOMA systems, where the source was aimed at communicating with two NOMA users in the presence of an eavesdropper. The authors in [7] considered a more practical case that nodes and backscatter devices suffer from in-phase and quadrature-phase imbalance.

Besides, cooperative communication has also been widely studied because its spatial diversity advantage helps to reduce fading, widen coverage, and increase communication preciseness [6, 8–10]. In conventional cooperative communications, relaying nodes apply the decode-and-forward (DF) method or the amplify-and-forward (AF) method to process their received and transmitted signals [6, 11]. The DF method is better because it decodes received signals at the relay, then reencodes them for forwarding to the destination so it does not amplify noises in received signals like the AF.

Cooperative models show that the selection of the best-relaying devices, including partial relay selection and opportunistic relay selection, is necessary to improve system

performance [5, 11–19]. These methods are based on the collection of channel state information to select the optimal relay to support communication. The partial relay selection does not offer the full spatial diversity, but it is not as complicated as the full relay selection, and it is useful for applications in industrial IoT and wireless sensor networks. In most practical applications, CSIs cannot be perfectly measured and there are some mismatch, known as imperfect CSIs (ipCSIs) [12, 14, 16, 19–22]. The mismatch can happen due to the feedback delays of the CSIs [12, 14, 16, 19, 22] or the faults in the CSI estimating process [20, 21]. One-way NOMA and cooperative NOMA (CNOMA) networks with the SIC have been widely discussed to increase spectral efficiency gain, improve secure performance, enlarge system energy efficiency, and enhance significantly sum throughput in several studies [1, 4, 23–25]. Besides, two-way cooperative networks have advantages in using frequency spectral efficiency over one-way networks because two sources are able to both transmit and receive signals. Moreover, network coding has the advantages of compressing data and high spectral efficiency, and it plays a crucial role in two-way relay networks [5].

In this paper, we propose a two-way cooperative network with a cluster of DF relays and two sources in which the relay will be chosen in the setup phase. The relay selection method in our work helps to enhance the decoding capacity of the nearer source and decrease the collection time of the CSIs than the opportunistic relay selection in [5]. To achieve higher spectral efficiency, we use the NOMA protocol for uplink and the DNC technique for downlink. At the selected relay, the SIC is used to decode sequentially the received signals; next, the DNC is applied to create a new encoded signal and then, this signal is transmitted back to sources, called as the SIC-2TS protocol. Moreover, this paper also investigates the effect of realistic conditions as the ipCSIs and the ipSIC on the system performance. Afterward, the system performance of the SIC-2TS protocol is evaluated based on the analysis expressions of the outage probabilities and the system throughput. Lastly, we compare the proposed protocol with the conventional two-way DF protocol, denoted as CONV-4TS protocol, and the SIC-utilized two-way relaying without the DNC, denoted as the SIC-3TS protocol.

The contributions in this paper are summarized as follows. Firstly, the exact and asymptotic expressions of the outage probabilities and throughput of two sources in the proposed scheme are analyzed and verified under the overall effects of pSIC/ipSIC and pCSIs/ipCSI conditions. Secondly, the exact and asymptotic closed-form expressions are proved valid by the simulation results. Next, the simulation results show that the ipSIC and the ipCSI conditions significantly affect the system performance. Fourthly, the performance of the SIC-2TS protocol is improved by the increased number of relays as well as the perfect operations of the SIC process and the CSI estimations. Moreover, the performance of SIC-2TS can attain the best level at optimal locations of the selected relay and the power suitable coefficients of two sources. Last but not the least, the system throughput of the proposed method outperforms the conventional CONV-

Table 1: Notation table.

Notation	Meaning
N	Number of relays
$f_X(.)$	Probability density function (PDF) of X
$F_X(.)$	Cumulative distribution function (CDF) of X
$\oplus$	XOR operation
max (.)	Find the maximum value
argmax(.)	Find an element to achieve the maximum value
α_k	Power allocation coefficient of the source S_k
Pr (.)	Probability operation
γ_t	Target signal-to-interference-plus-noise ratio (SINR)
OP_{S_k}	Outage probability at the source S_k
TP	Throughput (bits/s/Hz)

4TS and SIC-3TS protocols in both cases of pCSIs and ipCSIs for all SNR regions.

The rest of our paper is organized as follows. Section Section 2 shows some related works. Section 3 describes the system model. Section 4 analyzes the system performance of the SIC-2TS, SIC-3TS, and CONV-4TS protocols. Section 5 shows the results and respective discussions. Finally, section 6 summarizes contributions in this paper.

Notations used in this paper are listed in Table 1.

2. Related Works

In recent researches, specific two-way CNOMA (TWR CNOMA) networks have been investigated to take benefit on system performance. The performance of the NOMA-based two-way relaying network for uplink and downlink of two users or two groups in the perfect SIC (pSIC) and ipSIC conditions and Rayleigh fading was analyzed with a half-duplex DF relay in [26, 27] and a full-duplex DF relay in [28]. The works in [26–28] showed that two-way NOMA is superior to two-way orthogonal multiple access (OMA) in terms of outage probability in low signal-to-noise ratio (SNR) regimes. In [29], the joint effects of in-phase and quadrature-phase imbalance and ipSIC on the performance of TWR CNOMA networks over the Rician fading channels were studied. Besides, the realistic assumptions of the residual hardware impairments or ipCSIs of two-way or multiway CNOMA networks have also been considered in the articles [21, 22, 30].

Moreover, DNC and NOMA techniques can be combined to decreasing transmission time between devices and improve the performance system [5, 31, 32]. In [31, 32], the authors combined NOMA and DNC techniques in a two-way DF relay cooperative scheme confirming that performance in this proposed asymmetric scheme had better spectrum utilization efficiency than the traditional two-way DF OMA scheme, the two-way DF with only using the CNOMA, and the two-way relaying system with OMA in the uplink and DNC in the downlink. The authors in [31, 32] only used
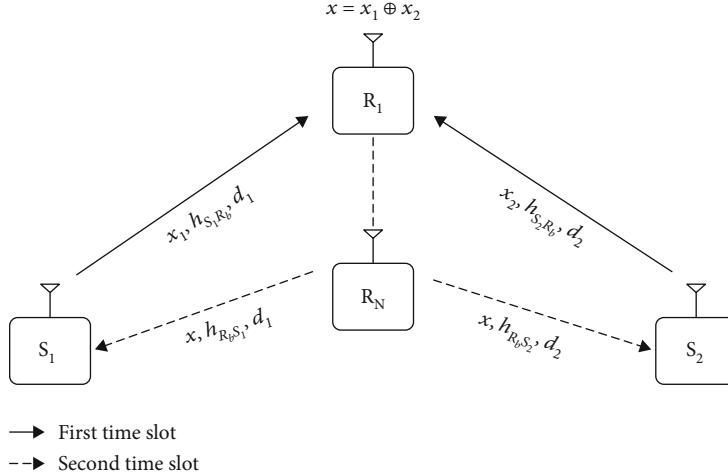
FIGURE 1: Two-way cooperative model of the SIC-2TS protocol.

a DF relay to support communication. The system performance in [31] was considered in the case of the ideal conditions. In [5], the system performance was investigated in perfect CSI (pCSI) conditions with the opportunistic relay selection.

3. System Model

A cooperative two-way network has two sources S_1 and S_2 and a closed group of N half-duplex DF relays R_i with $i \in \{1, 2, \cdots N\}$, as depicted in Figure 1. This system model can be applied for data transmission in heterogeneous cellular networks. The sources and the relays in the SIC-2TS are single antenna and HD devices. We assume that the direct link between the two sources does not exist due to severe fading and path loss, and the information exchange can be performed only via relays [32–34]; the relays are close together as a cluster [17] so the link distances between each source and the relays are identical; hence, we denote d_1 and d_2 as the normalized distances between S_1 and R_i and between S_2 and R_i, respectively. We also assume that the flat and block Rayleigh fading channels with the fading coefficients for links $S_k \longrightarrow R_i$ and $R_i \longrightarrow S_k$ are denoted as $h_{S_k R_i}$ and $h_{R_i S_k}$, respectively, where $k \in \{1, 2\}$. In addition, perfect knowledge of all links is assumed at the receivers by channel estimators that are error-free [35], and the ipCSIs are only caused by the feedback delay with a time-variant channel representation and is described by [12, 14, 16, 20, 22, 32, 35]

$$\hat{h}_\nu = \rho_\nu h_\nu + \sqrt{1 - \rho_\nu^2}\,\varepsilon_\nu, \tag{1}$$

where $\nu \in \{S_k R_i, R_i S_k\}$. Here, ε_ν stand for the estimation errors and $\hat{h}_\nu$ describes the estimated CSIs. ε_ν and $\hat{h}_\nu$ are independent complex Gaussian random variables (RVs) with zero means and variances λ_ν, $(\varepsilon_\nu, \hat{h}_\nu \sim CN(0, \lambda_\nu))$ [14, 16].

And the correlation coefficients $\rho_\nu (0 \le \rho_\nu \le 1)$ are constants (where $\rho_\nu = 1$ denotes no delay effect), characterizing the average quality of channel estimations [14, 16, 32]. For uncomplicated, we assume that $\rho_\nu = \rho$ for all the similar devices, $\rho = 1$ for perfect CSIs, and $\rho < 1$ for ipCSIs [12, 14, 16, 20, 32]. The estimated channel gains $g_{S_k R_i} = |\hat{h}_{S_k R_i}|^2$ and $g_{R_i S_k} = |\hat{h}_{R_i S_k}|^2$ are exponentially distributed RVs with PDFs $f_{g_{S_k R_i}}(x) = f_{g_{R_i S_k}}(x) = (1/\lambda_k)e^{-x/\lambda_k}$, and CDFs $F_{g_{S_k R_i}}(x) = F_{g_{R_i S_k}}(x) = 1 - e^{-x/\lambda_k}$, where $\lambda_k = \lambda_{S_k R_i} = \lambda_{R_i S_k} = d_k^{-\beta}$ and β is a path-loss exponent [15].

Prior to transmitting data, the setup phase is performed firstly by request and feedback messages through the cooperative medium access control (MAC) protocol [8]. The nearer source, denoted as S_n, $n \in \{1, 2\}$, receives all channel coefficients from it to the relays under effect of feedback delay and performs the cooperative relay selection. The SIC-2TS protocol uses two time slots for signal communication. In the first slot, two sources S_1 and S_2 send concurrently their signals x_1 and x_2, respectively, to all relays, and at the selected relay, the SIC technique is applied to decode the received signals. In the second slot, the DNC technique is used to create a new signal $x = x_1 \oplus x_2$ [5, 15, 32] and the selected relay sends it back to two sources S_1 and S_2 with transmit power P_R.

The signal which the relays receive in the first time slot is a weighted sum of x_1 and x_2 as follows:

$$y_{R_i} = \sqrt{\alpha_1 P_S}\,h_{S_1 R_i} x_1 + \sqrt{\alpha_2 P_S}\,h_{S_2 R_i} x_2 + n_{R_i}, \tag{2}$$

where $\alpha_1 P_S$ and $\alpha_2 P_S$ are transmit powers to carry x_1 and x_2, respectively; α_1 and α_2 are power allocation coefficients to fairness between two sources (a lower power should be given to the source which is nearer relays) [28], $(0 < \alpha_1, \alpha_2 < 1)$; and n_{R_i} is the AWGNs with the variance N_0 at the nodes R_i.

Substituting (1) into (2), the received signal is given by

$$y_{R_i} = \sqrt{\alpha_1 P_S} \left(\frac{\hat{h}_{S_1 R_i} - \sqrt{1-\rho^2} \varepsilon_{S_1 R_i}}{\rho} \right) x_1$$

$$+ \sqrt{\alpha_2 P_S} \left(\frac{\hat{h}_{S_2 R_i} - \sqrt{1-\rho^2} \varepsilon_{S_2 R_i}}{\rho} \right) x_2 + n_{R_i}$$

$$= \sqrt{\alpha_1 P_S} \hat{h}_{S_1 R_i} x_1 + \sqrt{\alpha_2 P_S} \hat{h}_{S_2 R_i} x_2$$

$$- \sqrt{\alpha_1 P_S} \frac{\sqrt{1-\rho^2}}{\rho} \varepsilon_{S_1 R_i} x_1$$

$$- \sqrt{\alpha_2 P_S} \frac{\sqrt{1-\rho^2}}{\rho} \varepsilon_{S_2 R_i} x_2 + n_{R_i}. \tag{3}$$

Due to the symmetry of the proposed system model in Figure 1, without loss of generality, assume that S_n and S_f are near and far sources from the relays, respectively, where $n, f \in \{1, 2\}$ and $n \neq f$. Applying the SIC technique [5, 6, 24, 27, 32], firstly, the relays decode the signal x_n of the nearby source which has better average channel quality while the signal x_f is considered as interference. The received signal-to-interference-plus-noise ratio (SINR) for detecting x_n is given by

$$\gamma_{S_n R_i \longrightarrow x_n | d_n \leq d_f} = \frac{\alpha_n P_S \left| \hat{h}_{S_n R_i} \right|^2 / \rho^2}{\alpha_f P_S \left| \hat{h}_{S_f R_i} \right|^2 / \rho^2 + \left(\alpha_n P_S \lambda_{S_n R_i} + \alpha_f P_S \lambda_{S_f R_i} \right) (1-\rho^2)/\rho^2 + N_0}$$

$$= \frac{\alpha_n \gamma \left| \hat{h}_{S_n R_i} \right|^2}{\alpha_f \gamma \left| \hat{h}_{S_f R_i} \right|^2 + \gamma(\alpha_n \lambda_n + \alpha_f \lambda_f)(1-\rho^2) + \rho^2}$$

$$= \frac{\alpha_n \left| \hat{h}_{S_n R_i} \right|^2}{\alpha_f \left| \hat{h}_{S_f R_i} \right|^2 + \underbrace{(\alpha_n \lambda_n + \alpha_f \lambda_f)(1-\rho^2) + \rho^2/\gamma}_{\phi_1}}$$

$$= \frac{\alpha_n g_{S_n R_i}}{\alpha_f g_{S_f R_i} + \phi_1}, \tag{4}$$

where γ is the transmit SNR, $\gamma = P_S/N_0$.

In this paper, the relay selection method is used by maximizing estimated channel gains to enhance the decoding capacity of the nearer source. This method has an outstanding advantage in minimizing the collection time of ipCSIs. The relay selection criterion based on the estimated channel gains has been used in [36–38] to achieve the better performance. From (4), the selected relay R_b is expressed as follows:

$$R_b = \arg \max_{i=1 \cdots N} g_{S_n R_i}. \tag{5}$$

After decoding x_n successfully, the relay R_b deletes the component containing the x_n signal in (3); then, it decodes the x_f signal and the received SINR for detecting x_f is given by

$$\gamma_{S_f R_b \longrightarrow x_f | d_n \leq d_f} = \frac{\alpha_f P_S \left| \hat{h}_{S_f R_b} \right|^2 / \rho^2}{\varepsilon P_S |h_{R_b}|^2 + (\alpha_n P_S \lambda_n + \alpha_f P_S \lambda_f)(1-\rho^2)/\rho^2 + N_0}$$

$$= \frac{\alpha_f \gamma \left| \hat{h}_{S_f R_b} \right|^2}{\varepsilon \gamma |h_{R_b}|^2 \rho^2 + \gamma(\alpha_n \lambda_n + \alpha_f \lambda_f)(1-\rho^2) + \rho^2}$$

$$= \frac{\alpha_f g_{S_f R_b}}{\varepsilon \rho^2 g_{R_b} + \phi_1}, \tag{6}$$

where h_{R_b} is a remaining interference signal with zero mean and variance Ω at the relay R_b [27], $g_{R_b} = |h_{R_b}|^2$ is exponentially distributed RVs with the PDF as $f_{g_{R_b}}(x) = (1/\Omega)e^{-x/\Omega}$, and CDF $F_{g_{R_b}}(x) = 1 - e^{-x/\Omega}$ [27, 28]. $\varepsilon = 0$ and $\varepsilon = 1$ correspond to pSIC and ipSIC at the relay R_b, respectively [5, 28].

In the second time slot, at the relay R_b, the signal $x = x_1 \oplus x_2$ is synthesized and transmitted to two sources. And the received signal at the source S_k, $k \in \{1, 2\}$, is described as follows:

$$y_{R_b S_k} = \sqrt{P_R} h_{R_b S_k} x + n_{S_k}$$

$$= \sqrt{P_R} \hat{h}_{R_b S_k} x - \sqrt{P_R} \frac{\sqrt{1-\rho^2}}{\rho} \varepsilon_{R_b S_k} x + n_{S_k}, \tag{7}$$

where n_{S_k} is the AWGNs at the sources S_k with the variance N_0.

Next, the x signal is detected at the two sources with the SINR as follows:

$$\gamma_{R_b S_k \longrightarrow x} = \frac{P_R \left| \hat{h}_{R_b S_k} \right|^2 / \rho^2}{P_R \lambda_k (1-\rho^2)/\rho^2 + N_0} = \frac{\eta \gamma g_{R_b S_k}}{\eta \gamma \lambda_k (1-\rho^2) + \rho^2}, \tag{8}$$

where $\eta = P_R/P_S$ and $\eta > 0$.

Remark 1. If the proposed SIC-2TS protocol operates without the DNC at the selected relay, the signals x_1 and x_2 are sent sequences by the R_b to the sources S_2 and S_1 in two different time slots (the second and third time slots). The received signals and the corresponding SINRs are expressed identically as formulas (7) and (8) in which the symbol x is changed to x_1 (to send S_2) and x_2 (to send S_1). We denoted the SIC-2TS protocol in this case (without the DNC) as the SIC-3TS protocol to distinguish in the rest of this paper.

We also investigate a conventional two-way CONV-4TS protocol using four time slots with relay selection. This protocol's transmission process is as follows: $S_1 \xrightarrow[\text{1st}]{x_1} R_{b_1} \xrightarrow[\text{2nd}]{x_1} S_2$ $\xrightarrow[\text{3rd}]{x_2} R_{b_2} \xrightarrow[\text{4th}]{x_2} S_1$.
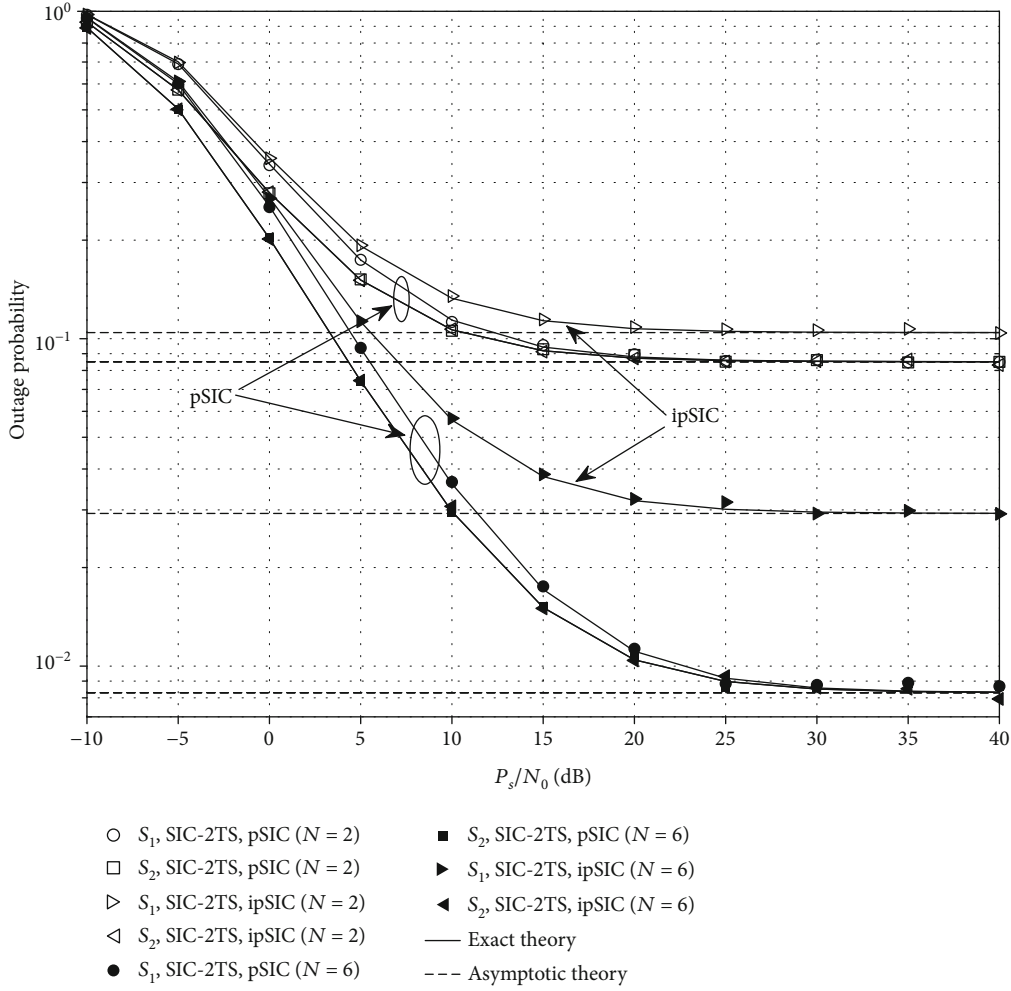
FIGURE 2: Outage probabilities of the source nodes S_1 and S_2 in the proposed SIC-2TS protocol versus P_S/N_0 (dB) when $\Omega = -10$ (dB), $d_1 = 0.4$, $d_2 = 1 - d_1$, $N \in \{2, 6\}$, $\rho \in \{0.92, 1\}$, $\varepsilon = 0$, and the power allocation coefficients $\alpha_1 = \alpha_2 = \eta = 1$.

Firstly, the data signal x_1 is transmitted from the source S_1 to all the relays; the received signal and the SINR at the relay R_i are described by

$$
\begin{aligned}
y^C_{S_1 R_i} &= \sqrt{\alpha_1 P_S} h_{S_1 R_i} x_1 + n_{R_i} \\
&= \sqrt{\alpha_1 P_S} \left(\frac{\hat{h}_{S_1 R_i} - \sqrt{1-\rho^2} \varepsilon_{S_1 R_i}}{\rho} \right) x_1 + n_{R_i} \\
&= \sqrt{\alpha_1 P_S} \hat{h}_{S_1 R_i} x_1 - \sqrt{\alpha_1 P_S} \frac{\sqrt{1-\rho^2}}{\rho} \varepsilon_{S_1 R_i} x_1 + n_{R_i},
\end{aligned}
$$

(9)

$$
\gamma_{S_1 R_i} = \frac{\alpha_1 P_S \left| \hat{h}_{S_1 R_i} \right|^2 / \rho^2}{\alpha_1 P_S \lambda_1 (1-\rho^2)/\rho^2 + N_0} = \frac{\alpha_1 \gamma g_{S_1 R_i}}{\alpha_1 \lambda_1 \gamma (1-\rho^2) + \rho^2}.
$$

(10)

Secondly, the relay R_{b_1} is selected as by formula $R_{b_1} = \arg \max_{i=1 \cdots N} g_{S_1 R_i}$ and then R_{b_1} decodes and transmits the signal

x_1 to the source S_2. The received signal and the SINR at the source S_2 are described by

$$
\begin{aligned}
y^C_{R_{b_1} S_2} &= \sqrt{P_R} h_{R_{b_1} S_2} x_1 + n_{S_2} \\
&= \sqrt{P_R} \hat{h}_{R_{b_1} S_2} x_1 - \sqrt{P_R} \frac{\sqrt{1-\rho^2}}{\rho} \varepsilon_{R_{b_1} S_2} x_1 + n_{S_2},
\end{aligned}
$$

(11)

$$
\gamma_{R_{b_1} S_2} = \frac{P_R \left| \hat{h}_{R_{b_1} S_2} \right|^2 / \rho^2}{P_R \lambda_2 (1-\rho^2)/\rho^2 + N_0} = \frac{\eta \gamma g_{R_{b_1} S_2}}{\eta \gamma \lambda_2 (1-\rho^2) + \rho^2}.
$$

(12)

In the same way, in the third and fourth time slots, the source S_2 transmits the signal x_2 to the source S_1 via the best relay R_{b_2}. We have the SINRs to decode the signal x_2 at the relay R_i and the source S_1 as follows:

$$\gamma_{S_2R_i} = \frac{\alpha_f P_S \left| \hat{h}_{S_2R_i} \right|^2 / \rho^2}{\alpha_2 P_S \lambda_2 (1 - \rho^2) / \rho^2 + N_0} = \frac{\alpha_2 \gamma g_{S_2R_i}}{\alpha_2 \lambda_2 \gamma (1 - \rho^2) + \rho^2}, \tag{13}$$

$$\gamma_{R_{b_2}S_1} = \frac{P_R \left| \hat{h}_{R_{b_2}S_1} \right|^2 / \rho^2}{P_R \lambda_1 (1 - \rho^2) / \rho^2 + N_0} = \frac{\eta \gamma g_{R_{b_2}S_1}}{\eta \gamma \lambda_1 (1 - \rho^2) + \rho^2}. \tag{14}$$

4. Performance Analysis

Section IV presents expressions of the outage probability and throughput for the protocols. We assume that the outage occurs at the nodes R_i and S_k if their SINRs are less than a predefined target γ_t. Conversely, these nodes decode signals successfully.

4.1. Outage Probability Analysis

4.1.1. The Proposed SIC-2TS Protocol

(1) The Outage Probability at the Source S_f for the $S_n \longrightarrow^{x_n} R_b \to^x S_f$ Link. The outage of the system occurs in this link when the relay R_b fails to decode the signal x_n or it decodes successfully the signal x_n but the source S_f fails to decode the signal x. Besides, the outage probability can also be calculated by the complementary event of the success transmission probability. The successful transmission is the signal x_n, and the signal x is received and decoded successfully at the R_b and the source S_f, respectively [32]. At the source S_f, the outage probability of the signal x_n can be described as

$$\begin{aligned} OP_{S_f} \Big|_{d_n \le d_f} &= \Pr \left[\gamma_{S_nR_b \longrightarrow x_n | d_n \le d_f} < \gamma_t \right] \\ &\quad + \Pr \left[\gamma_{S_nR_b \longrightarrow x_n | d_n \le d_f} \ge \gamma_t, \gamma_{R_bS_f \longrightarrow x} < \gamma_t \right] \\ &= 1 - \Pr \left[\gamma_{S_nR_b \longrightarrow x_n | d_n \le d_f} \ge \gamma_t, \gamma_{R_bS_f \longrightarrow x} \ge \gamma_t \right]. \end{aligned} \tag{15}$$

A point to remark is that $\gamma_{S_nR_b \longrightarrow x_n | d_n \le d_f} \ge \gamma_t$ and $\gamma_{R_bS_f \longrightarrow x} \ge \gamma_t$ are separate events. Thus, the $OP_{S_f} \Big|_{d_n \le d_f}$ can be given by

$$\begin{aligned} OP_{S_f} \Big|_{d_n \le d_f} &= 1 - \Pr \left[\gamma_{S_nR_b \longrightarrow x_n | d_n \le d_f} \ge \gamma_t \right] \\ &\quad \times \Pr \left[\gamma_{R_bS_f \longrightarrow x} \ge \gamma_t \right]. \end{aligned} \tag{16}$$

Lemma 2. The probability $\Pr \left[\gamma_{S_nR_b \longrightarrow x_n | d_n \le d_f} \ge \gamma_t \right]$ is calculated by

$$\Pr \left[\gamma_{S_nR_b \longrightarrow x_n | d_n \le d_f} \ge \gamma_t \right] = 1 - \lambda_n \sum_{p=0}^{N} \frac{C_N^p (-1)^p e^{-p\phi_3/\lambda_n}}{\lambda_n + p\phi_2 \lambda_f}, \tag{17}$$

where $\phi_2 = \gamma_t \alpha_f / \alpha_n$, $\phi_3 = \gamma_t \phi_1 / \alpha_n$, and $C_N^p = N! / (p! (N - p)!)$.

Proof. See the proof in "Appendix A."
The probability $\Pr \left[\gamma_{R_bS_f \longrightarrow x} \ge \gamma_t \right]$ is solved as

$$\begin{aligned} \Pr \left[\gamma_{R_bS_f \longrightarrow x} \ge \gamma_t \right] &= 1 - \Pr \left[\gamma_{R_bS_f \longrightarrow x} < \gamma_t \right] \\ &= 1 - \Pr \left[g_{R_bS_f} < \gamma_t \lambda_f (1 - \rho^2) + \frac{\gamma_t \rho^2}{\eta \gamma} \right] \\ &= 1 - F_{g_{R_bS_f}} \left(\gamma_t \lambda_f (1 - \rho^2) + \frac{\gamma_t \rho^2}{\eta \gamma} \right) \\ &= e^{-\gamma_t \left((1 - \rho^2) + (\rho^2 / (\lambda_f \eta \gamma)) \right)}. \end{aligned} \tag{18}$$

Substituting (17) and (18) into (16), the outage probability at the source S_f is obtained as

$$\begin{aligned} OP_{S_f} \Big|_{d_n \le d_f} &= 1 - \left(1 - \lambda_n \sum_{p=0}^{N} \frac{C_N^p (-1)^p e^{-p\phi_3/\lambda_n}}{\lambda_n + p\phi_2 \lambda_f} \right) \\ &\quad \cdot \left(e^{-\gamma_t \left((1 - \rho^2) + \rho^2 / (\lambda_f \eta \gamma) \right)} \right). \end{aligned} \tag{19}$$

(2) The Outage Probability at the Source S_n for the $S_f \to^{x_f} R_b \to^x S_n$ Link. The outage of the system occurs in this link when the signal x_n is not decoded successfully at relay R_b; or it is decoded successfully but the signal x_f is not decoded successfully at relay R_b; or both the signals x_n and x_f are decoded successfully at the relay R_b but the source S_n decodes unsuccessfully the signal x. Conversely, the success transmission of the signal x_f occurs when the relay R_b and the source S_n decode successfully the signals (x_n, x_f) and the signal x, respectively. At the source S_n, the outage probability of the signal x_f can be described as

$$\begin{aligned} OP_{S_n} \Big|_{d_n \le d_f} &= \Pr \left[\gamma_{S_nR_b \longrightarrow x_n | d_n \le d_f} < \gamma_t \right] \\ &\quad + \Pr \left[\gamma_{S_nR_b \longrightarrow x_n | d_n \le d_f} \ge \gamma_t, \gamma_{S_fR_b \longrightarrow x_f | d_n \le d_f} < \gamma_t \right] \\ &\quad + \Pr \left[\gamma_{S_nR_b \longrightarrow x_n | d_n \le d_f} \ge \gamma_t, \gamma_{S_fR_b \longrightarrow x_n | d_n \le d_f} \ge \gamma_t, \gamma_{R_bS_n \longrightarrow x} < \gamma_t \right] \\ &= 1 - \Pr \left[\gamma_{S_nR_b \longrightarrow x_n | d_n \le d_f} > \gamma_t, \gamma_{S_fR_b \longrightarrow x_f | d_n \le d_f} > \gamma_t, \gamma_{R_bS_n \longrightarrow x} > \gamma_t \right] \\ &= 1 - \Pr \left[\gamma_{S_nR_b \longrightarrow x_n | d_n \le d_f} \ge \gamma_t, \gamma_{S_fR_b \longrightarrow x_f | d_n \le d_f} \ge \gamma_t \right] \times \Pr \left[\gamma_{R_bS_n \longrightarrow x} \ge \gamma_t \right]. \end{aligned} \tag{20}$$
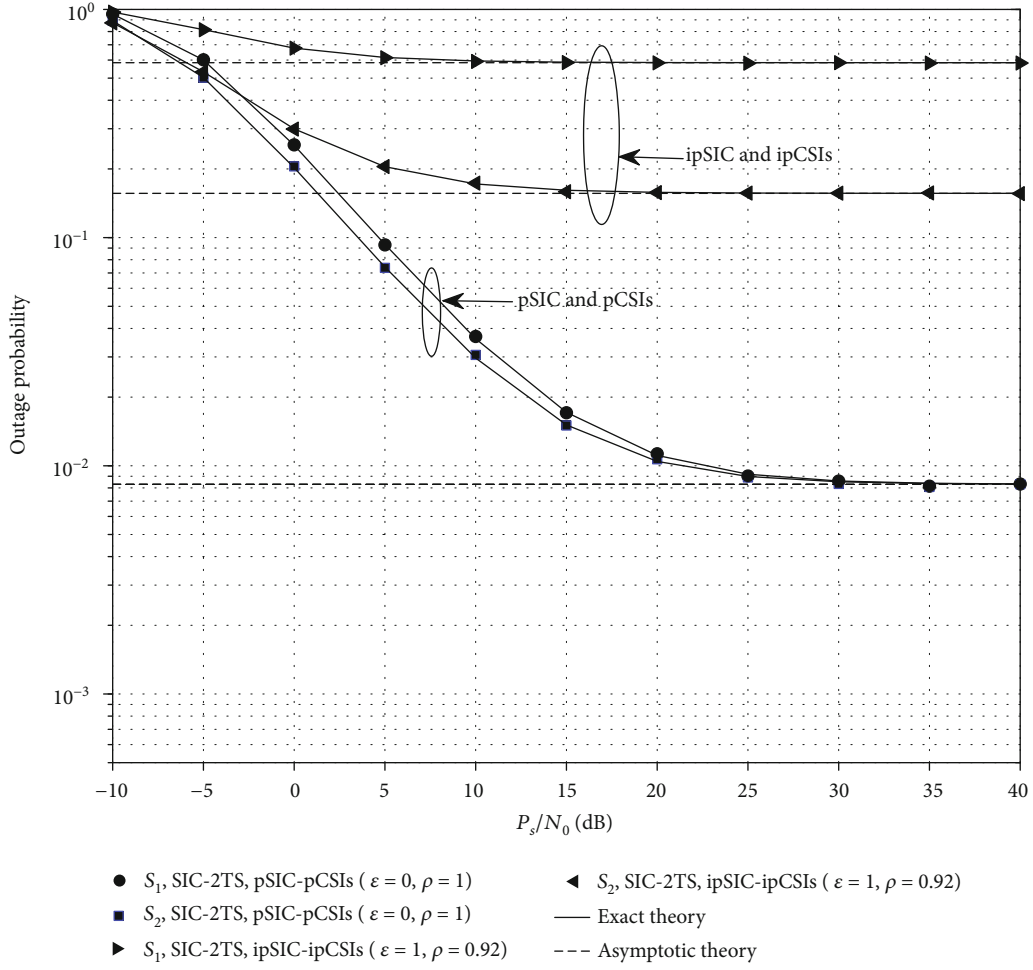
Figure 3: Outage probabilities of the source nodes S_1 and S_2 in the proposed SIC-2TS protocol versus P_S/N_0 (dB) when $\Omega = -10$ (dB), $d_1 = 0.4$, $d_2 = 1 - d_1$, $N \in \{2, 6\}$, $\rho = 1$, $\varepsilon \in \{0, 1\}$, and the power allocation coefficients $\alpha_1 = \alpha_2 = \eta = 1$.

Lemma 3. *The probability* $\Pr\left[\gamma_{S_n R_b \longrightarrow x_n | d_n \leq d_f} \geq \gamma_t, \gamma_{S_f R_b \longrightarrow x_f | d_n \leq d_f} \geq \gamma_t\right]$ *is calculated by*

$$\Pr\left(\gamma_{S_n R_b \longrightarrow x_n | d_n \leq d_f} \geq \gamma_t, \gamma_{S_f R_b \longrightarrow x_f | d_n \leq d_f} \geq \gamma_t\right)$$
$$= \frac{\lambda_f e^{-\left(\phi_5/\lambda_f\right)}}{\left(\lambda_f + \phi_4 \Omega\right)} - \sum_{p=0}^{N} \frac{\lambda_n{}^2 \lambda_f C_N^p (-1)^p e^{-\left(p(\phi_3 + \phi_5 \phi_2)/\lambda_n + \phi_5/\lambda_f\right)}}{\left(\lambda_n + p\phi_2 \lambda_f\right)\left(\lambda_n \lambda_f + \phi_4 \Omega\left(\lambda_n + p\phi_5 \phi_2 \lambda_f\right)\right)},$$

(21)

where $\phi_4 = \gamma_t \varepsilon \rho^2/\alpha_f$ and $\phi_5 = \gamma_t \phi_1/\alpha_f$.

Proof. See the proof in "Appendix B."

The final probability $\Pr\left[\gamma_{R_b S_n \longrightarrow x} \geq \gamma_t\right]$ in (20) is answered as

$$\Pr\left[\gamma_{R_b S_n \longrightarrow x} \geq \gamma_t\right] = 1 - \Pr\left[\gamma_{R_b S_n \longrightarrow x} < \gamma_t\right]$$
$$= 1 - \Pr\left[g_{R_b S_n} < \gamma_t \lambda_n\left(1 - \rho^2\right) + \frac{\gamma_t \rho^2}{\eta \gamma}\right]$$
$$= e^{-\gamma_t\left(\left(1 - \rho^2\right) + \rho^2/(\lambda_n \eta \gamma)\right)}.$$

(22)

By substituting (21) and (22) into (20), the outage probability at the source S_n is solved as

$$\left.\mathrm{OP}_{S_n}\right|_{d_n \leq d_f} = 1 - \left(\frac{\lambda_f e^{-\phi_5/\lambda_f}}{\left(\lambda_f + \phi_4 \Omega\right)} - \sum_{p=0}^{N} \frac{\lambda_n{}^2 \lambda_f C_N^p (-1)^p e^{-\left(p(\phi_3 + \phi_5 \phi_2)/\lambda_n + \phi_5/\lambda_f\right)}}{\left(\lambda_n + p\phi_2 \lambda_f\right)\left(\lambda_n \lambda_f + \phi_4 \Omega\left(\lambda_n + p\phi_5 \phi_2 \lambda_f\right)\right)}\right) \times \left(e^{-\gamma_t\left(\left(1 - \rho^2\right) + \rho^2/(\lambda_n \gamma)\right)}\right).$$

(23)
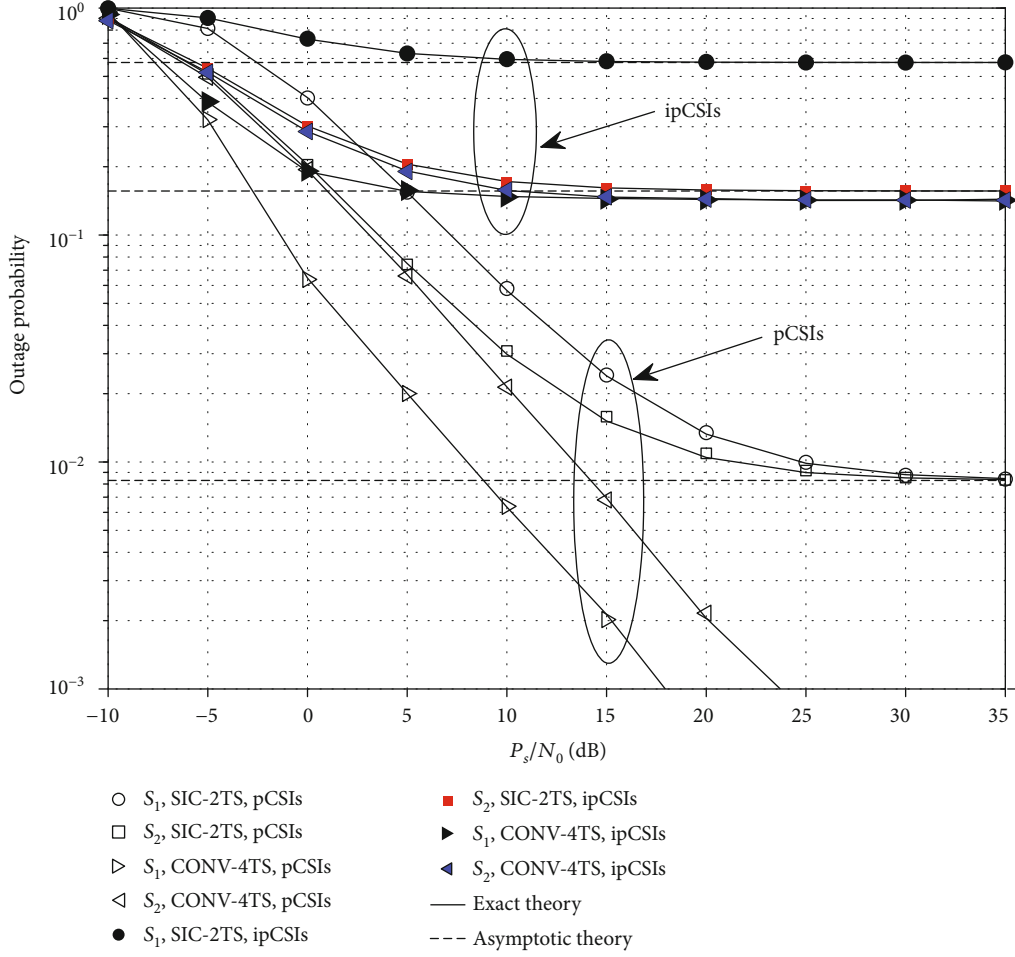
FIGURE 4: Outage probabilities of the source nodes S_1 and S_2 in the proposed SIC-2TS and CONV-4TS protocols versus P_S/N_0 (dB) when $\Omega = -10$ (dB), $d_1 = 0.4$, $d_2 = 1 - d_1$, $N = 6$, pSIC-pCSIs ($\varepsilon = 0$, $\rho = 1$), ipSIC-ipCSIs ($\varepsilon = 1$, $\rho = 0.92$), and the power allocation coefficients $\alpha_1 = \alpha_2 = \eta = 1$.

Corollary 4. *When $\gamma \longrightarrow +\infty$, we obtain asymptotic expression as*

$$\left. \mathrm{OP}_{S_f} \right|_{d_n \leq d_f}^{\gamma \longrightarrow +\infty} = 1 - \left(1 - \lambda_n \sum_{p=0}^{N} \frac{C_N^p (-1)^p e^{-p\phi_6/\lambda_n}}{\lambda_n + p\phi_2\lambda_f} \right) e^{-\gamma_t (1-\rho^2)}, \tag{24}$$

$$\left. \mathrm{OP}_{S_n} \right|_{d_n \leq d_f}^{\gamma \longrightarrow +\infty} = 1 - \left(\frac{\lambda_f e^{-\phi_7/\lambda_f}}{(\lambda_f + \phi_4\Omega)} - \sum_{p=0}^{N} \frac{\lambda_n^2 \lambda_f C_N^p (-1)^p e^{-\left(p(\phi_6 + \phi_7\phi_2)/\lambda_n + \phi_7/\lambda_f \right)}}{(\lambda_n + p\phi_2\lambda_f)(\lambda_n\lambda_f + \phi_4\Omega(\lambda_n + p\phi_7\phi_2\lambda_f))} \right) e^{-\gamma_t (1-\rho^2)}, \tag{25}$$

where $\phi_6 = (\gamma_t(\alpha_n\lambda_n + \alpha_f\lambda_f)(1 - \rho^2))/\alpha_n$ and $\phi_7 = (\gamma_t(\alpha_n\lambda_n + \alpha_f\lambda_f)(1 - \rho^2))/\alpha_f$.

Remark 5. In the SIC-3TS protocol, the outage probabilities and the asymptotic expressions of the sources S_f and S_n are

also identified as closed-form formulas (19), (23), (24), and (25), respectively.

4.1.2. The CONV-4TS Protocol. The outage probability at the source S_2 for the $S_1 \xrightarrow[\text{1st}]{x_1} R_{b_1} \xrightarrow[\text{2nd}]{x_1} S_2$ link in the

CONV-4TS protocol is described as follows:

$$
\begin{aligned}
OP_{S_2}^C &= 1 - \Pr\left[\gamma_{s_1 R_{b1}} \geq \gamma_t, \gamma_{R_{b1} S_2} \geq \gamma_t\right] \\
&= 1 - \Pr\left[\gamma_{s_1 R_{b1}} \geq \gamma_t\right] \times \Pr\left[\gamma_{R_{b1} S_2} \geq \gamma_t\right] \\
&= 1 - \left(1 - \Pr\left[\gamma_{s_1 R_{b1}} < \gamma_t\right]\right) \times \left(1 - \Pr\left[\gamma_{R_{b1} S_2} < \gamma_t\right]\right).
\end{aligned}
\tag{26}
$$

Substituting $\gamma_{S_1 R_{b1}}$ and $\gamma_{R_{b1} S_2}$ in (10) and (12) into ((26), we obtain

$$
\begin{aligned}
OP_{S_2}^C &= 1 - \left(1 - \Pr\left[\frac{\alpha_1 \gamma g_{S_1 R_{b1}}}{\alpha_1 \lambda_1 \gamma (1-\rho^2) + \rho^2} < \gamma_t\right]\right) \\
&\quad \cdot \left(1 - \Pr\left[\frac{\gamma g_{R_{b1} S_2}}{\gamma \lambda_2 (1-\rho^2) + \rho^2} < \gamma_t\right]\right) \\
&= 1 - \left(1 - \Pr\left[g_{S_1 R_{b1}} < \underbrace{\gamma_t \lambda_1 (1-\rho^2) + \gamma_t \rho^2/(\alpha_1 \gamma)}_{\phi_8}\right]\right) \\
&\quad \times \left(1 - \Pr\left[g_{R_{b1} S_2} < \underbrace{\gamma_t \lambda_2 (1-\rho^2) + \gamma_t \rho^2/\gamma}_{\phi_9}\right]\right) \\
&= 1 - \left(1 - F_{g_{S_1 R_{b1}}}(\phi_8)\right)\left(1 - F_{g_{R_{b1} S_2}}(\phi_9)\right) \\
&= 1 - \left(1 - \left(1 - e^{-\phi_8/\lambda_1}\right)^N\right) e^{-\phi_9/\lambda_2} \\
&= 1 - \left(1 - \sum_{p=0}^{N} C_N^p (-1)^p e^{-p\phi_8/\lambda_1}\right) e^{-\phi_9/\lambda_2}.
\end{aligned}
\tag{27}
$$

Similarly, the outage probability at the source S_1 for the $S_2 \xrightarrow{x_2} R_{b_2} \xrightarrow{x_2} S_1$ link is expressed as

$$
\begin{aligned}
OP_{S_1}^C &= 1 - \Pr\left(\gamma_{S_2 R_{b2}} \geq \gamma_t, \gamma_{R_{b2} S_1} \geq \gamma_t\right) \\
&= 1 - \Pr\left(\gamma_{S_2 R_{b2}} \geq \gamma_t\right) \times \Pr\left(\gamma_{R_{b2} S_1} \geq \gamma_t\right).
\end{aligned}
\tag{28}
$$

By substituting $\gamma_{S_2 R_{b2}}$ and $\gamma_{R_{b2} S_1}$ in (13) and (14), respectively, into (28) and after some manipulations as finding the outage probability $OP_{S_2}^C$, we get a final result as

$$
OP_{S_1}^C = 1 - \left(1 - \sum_{p=0}^{N} C_N^p (-1)^p e^{-p\phi_{10}/\lambda_2}\right) e^{-\phi_{11}/\lambda_1},
\tag{29}
$$

$\rho^2) + \gamma_t \rho^2/\gamma$.

Corollary 6. *When $\gamma \longrightarrow \infty$, asymptotic expressions of the outage probabilities at the sources S_2 and S_1 are obtained as*

$$
\begin{aligned}
OP_{S_2}^C\Big|_{\gamma \longrightarrow +\infty} &= 1 - \left(1 - \sum_{p=0}^{N} C_N^p (-1)^p e^{-p\gamma_t(1-\rho^2)}\right) e^{-\gamma_t(1-\rho^2)}, \\
OP_{S_1}^C\Big|_{\gamma \longrightarrow +\infty} &= 1 - \left(1 - \sum_{p=0}^{N} C_N^p (-1)^p e^{-p\gamma_t(1-\rho^2)}\right) e^{-\gamma_t(1-\rho^2)}.
\end{aligned}
\tag{30}
$$

4.2. Throughput Analysis. The system throughput of the SIC-2TS, SIC-3TS, and the CONV-4TS protocols is obtained in the following, respectively [39]:

$$
TP_{SIC-2TS}\Big|_{d_n \leq d_f} = \frac{1}{2}\left(1 - OP_{S_n}\Big|_{d_n \leq d_f}\right)R_t + \frac{1}{2}\left(1 - OP_{S_f}\Big|_{d_n \leq d_f}\right)R_t,
\tag{31}
$$

$$
TP_{SIC-3TS}\Big|_{d_n \leq d_f} = \frac{1}{3}\left(1 - OP_{S_n}\Big|_{d_n \leq d_f}\right)R_t + \frac{1}{3}\left(1 - OP_{S_f}\Big|_{d_n \leq d_f}\right)R_t,
\tag{32}
$$

$$
TP_{CONV-4TS} = \frac{1}{4}\left(1 - OP_{S_1}^C\right)R_t + \frac{1}{4}\left(1 - OP_{S_2}^C\right)R_t,
\tag{33}
$$

where 1/2, 1/3, and 1/4 denote that the protocols SIC-2TS, SIC-3TS, and CONV-4TS work in two, three, and four time slots, respectively; $R_t = \log_2(1 + \gamma_t)$ (bits/s/Hz) [40].

Remark 7. The SIC-3TS protocol without the DNC operates in three time slots to send two data; thus, the throughput is obtained by the formula (32) where the outage probabilities $OP_{S_n}\big|_{d_n \leq d_f}$ and $OP_{S_f}\big|_{d_n \leq d_f}$ are taken from the proposed SIC-2TS protocol.

5. Numerical Results and Discussion

In this section, the outage probabilities and system throughput of three protocols SIC-2TS, SIC-3TS, and CONV-4TS are analyzed and evaluated. The exactness of the asymptotic and exact theory extractions is validated by Monte Carlo simulations (simulated results are shown by the marker point in all figures). We default the threshold SINR as $\gamma_t = 1$ and the path-loss exponent as $\beta = 3$ in all the analyses and evaluations. From Figures 2–5, the distance d_1 has smaller value and $d_2 = 1 - d_1$.

In Figure 2, we examine the outage probabilities of the two sources S_1 and S_2 in the proposed SIC-2TS protocol as a function of the P_S/N_0 (dB) with assuming perfect CSIs ($\rho = 1$) when $\Omega = -10$ (dB), $d_1 = 0.4$, $d_2 = 1 - d_1$, $N \in \{2, 6\}$, and $\alpha_1 = \alpha_2 = \eta = 1$ in both pSIC case ($\varepsilon = 0$) and ipSIC case ($\varepsilon = 1$). Figure 2 shows that the outage probabilities of the source S_2 are equal in the pSIC case and the ipSIC case as formula (19). The outage probabilities of the source S_1 in the pSIC case are higher than those of the source S_2 at the low P_S/N_0 (dB) regions, and they move to the same saturation values at the high P_S/N_0 (dB) regions. The outage
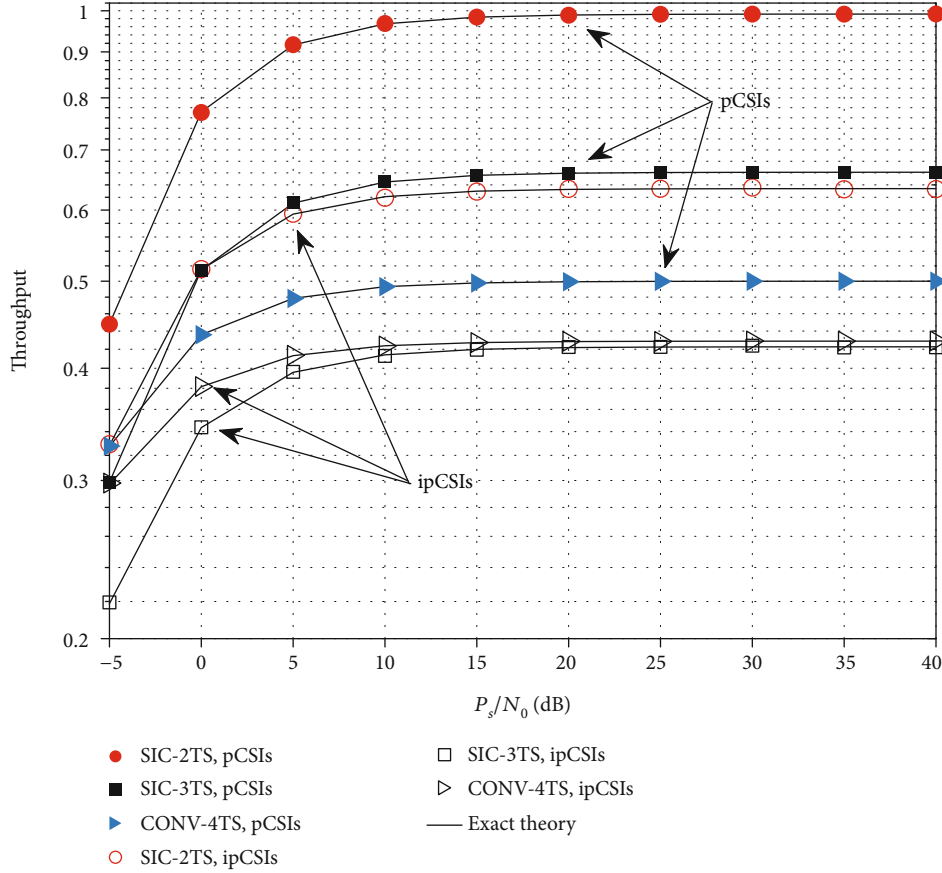
FIGURE 5: Throughput of the SIC-2TS, SIC-3TS, and CONV-4TS protocols versus P_S/N_0 (dB) when $\Omega = -10$ (dB), $d_1 = 0.4$, $d_2 = 1 - d_1$, $N = 6$, $\varepsilon = 0$, $\rho \in \{0.92, 1\}$, and the power allocation coefficients $\alpha_1 = \alpha_2 = \eta = 1$.

probabilities of the source S_1 in the ipSIC case are higher than those in the pSIC case with every P_S/N_0 (dB) due to adding the residual interference signals to the SINR of the signal x_2 at the relay as in formulas (6). Furthermore, the system diversity capacity increases because of using the relay selection methods as in (5) and (17) so the system performance of the proposed SIC-2TS protocol is better when the number of relays increases. Finally, the asymptotic and exact theory analysis lines of the outage probabilities also coincide well with their Monte Carlo simulation lines.

Figure 3 illustrates the outage probabilities of the sources S_1 and S_2 in the proposed SIC-2TS protocol as a function of P_S/N_0 (dB) in both ideal (pSIC-pCSIs) and practical (ipSIC-ipCSIs) conditions when $\Omega = -10$ (dB), $d_1 = 0.4$, $d_2 = 1 - d_1$, $N = 6$, and the power allocation coefficients $\alpha_1 = \alpha_2 = \eta = 1$. Figure 3 shows that the outage probabilities of the two sources with the pSIC- pCSI condition are better than with the ipSIC-ipCSI condition. In the pSIC-pCSI condition, the outage probabilities of the two source nodes have a small difference. But in the ipSIC-ipCSI case, the system outage probability for the source nodes S_1 is a lot higher. These results happen because the SIC technique is used to decode the signal at the relay to make the signal of the farther source more influenced in imperfect cases. In order to have fairness, meaning the two sources can have the nearly same system

outage probability in the ipSIC-ipCSI condition, we can provide the higher transmit power for the farther source by changing the transmit power coefficients (α_1, α_2) in formula (2). Finally, the asymptotic and exact theory analysis lines of the outage probabilities also coincide well with their Monte Carlo simulation lines.

In Figure 4, we consider the outage probabilities of the two sources S_1 and S_2 in the proposed SIC-2TS and CONV-4TS protocols as a function of P_S/N_0 (dB) with assuming perfect SIC ($\varepsilon = 0$) when $\Omega = -10$ (dB), $d_1 = 0.4$, $d_2 = 1 - d_1$, $N = 6$, and $\alpha_1 = \alpha_2 = \eta = 1$ [5, 13] in both pCSI case ($\rho = 1$) and ipCSI case ($\rho = 0.92$). Considering the SIC-2TS protocol in Figure 4, firstly, the outage probabilities of two sources in the pCSI case are smaller than those in the ipCSI case and all of them have the floor values when P_S/N_0 (dB) is large. Secondarily, the outage probabilities of the source S_1 has higher than the source S_2. Thirdly, if the P_S/N_0 (dB) has enough large value the outage probability of the two sources will be equal in the pCSI condition, but the source S_1 outage probabilities are always bigger than the outage probabilities of the source S_2 at all P_S/N_0 (dB) values in the ipCSI condition. Those SIC-2TS protocol results occur because the negative effects of imperfect CSIs lead to channel gain coefficients decrease as formula (1); and in case of $d_1 \leq d_2$, decoding the signal x_2 is decided by the SIC technique
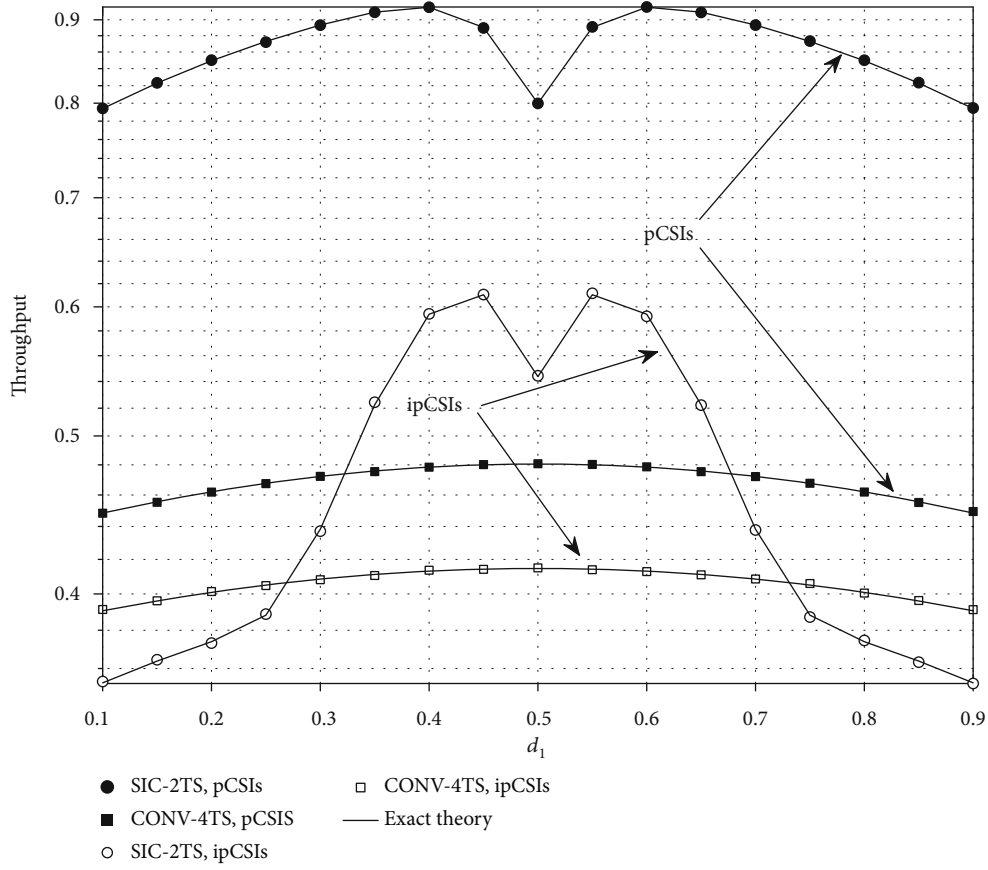
FIGURE 6: Throughput of the SIC-2TS and CONV-4TS protocols versus d_1 when $P_S/N_0 = 5$ (dB), $\Omega = -10$ (dB), $d_2 = 1 - d_1$, $N = 6$, $\varepsilon = 0$, $\rho \in \{0.92, 1\}$, and the power allocation coefficients $\alpha_1 = \alpha_2 = \eta = 1$.
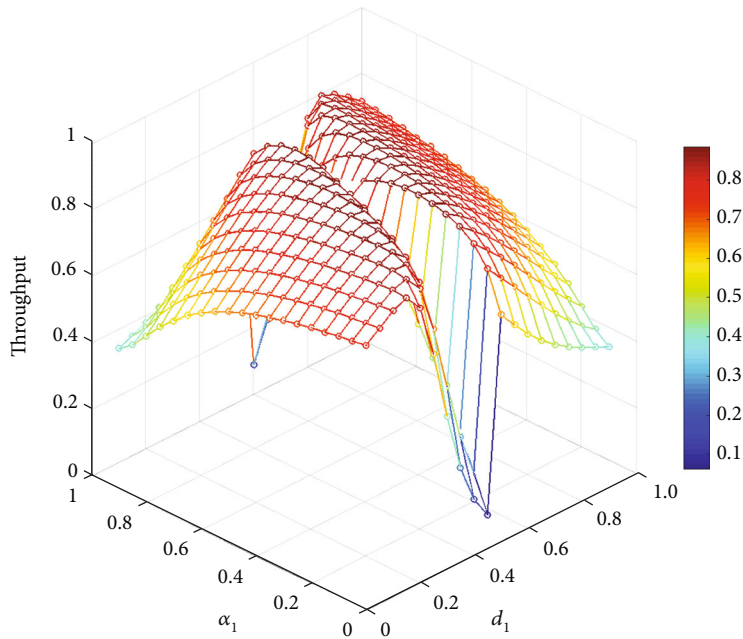
FIGURE 7: Throughput of the SIC-2TS protocol as a function of α_1 and d_1 when $P_S/N_0 = 5$ (dB), $\Omega = -10$ (dB), $d_2 = 1 - d_1$, $N = 6$, $\varepsilon = 0$, $\rho = 1$, and the power allocation coefficients $\alpha_2 = 1 - \alpha_1$ and $\eta = 1$.

TABLE 2: The maximum throughput values corresponding to the distances d_1 and the power allocation coefficient α_1.

d_1	0.1	0.2	0.3	0.4	0.5	0.6	0.7	0.8	0.9
α_1	0.1	0.1	0.3	0.5	0.3	0.5	0.7	0.9	0.9
Maximum throughput	0.7839	0.8413	0.8715	0.8853	0.8754	0.8853	0.8715	0.8413	0.7839

SIC-2TS, pSIC, $N = 1$
SIC-2TS, pSIC, $N = 6$
Exact theory
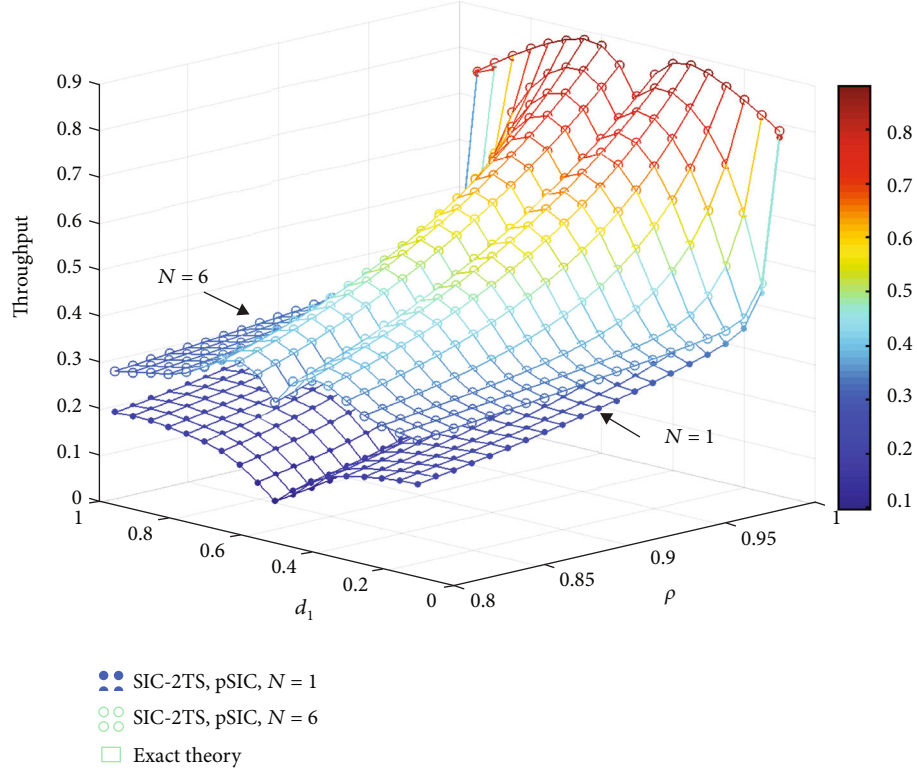
FIGURE 8: Throughput of the SIC-2TS protocol as a function of d_1 and ρ when $P_S/N_0 = 5(dB)$, $\Omega = -10(dB)$, $d_2 = 1 - d_1$, $N = \{1, 6\}$, $\varepsilon = 0$, $\rho = 0$, $\alpha_1 = d_1$, $\alpha_2 = 1 - \alpha_1$, and $\eta = 1$.

as (4) and (6) so the SINR of the x_2 is affected by the ipCSIs of both links $S_1 \longrightarrow R_i$ and $S_2 \longrightarrow R_i$. Moreover, we also see that the CONV-4TS protocol has a smaller outage probabilities than the SIC-2TS protocol in both the pCSI and the ipCSI conditions, but this conventional protocol will take a lot of time and energy to transmit the signals. Lastly, the asymptotic and exact theory analysis lines of the outage probabilities coincide well with their Monte Carlo simulation lines.

Figure 5 plots the system throughput for the SIC-2TS, SIC-3TS, and CONV-4TS protocols as a function of P_S/N_0 (dB) with pCSIs/ipCSIs $\rho \in \{0.92, 1\}$ when $\Omega = -10$ (dB), $d_1 = 0.4$, $d_2 = 1 - d_1$, $N = 6$, and the power allocation coefficients $\alpha_1 = \alpha_2 = \eta = 1$ for case $d_1 \leq d_2$ in formulas (31), (32), and (33), respectively. We can see that the proposed SIC-2TS protocol has the ability to achieve higher throughput than the CONV-4TS and SIC-3TS protocols in all P_S/N_0(dB) for both pCSI and ipCSI cases because it combines the NOMA, SIC, and DNC techniques to help degrade the number of the time slot of the transmission between two sources. In addition, the interference parts on the received SINRs are skipped in the case of pCSIs so the throughput of protocols in this condition is always better than that in the ipCSI condition. Furthermore,

the SIC-2TS protocol throughput converges at the same value in the high P_S/N_0 (dB) regions ($P_S/N_0 > 15$ dB). Finally, the exact theory values of the system throughput of three protocols fix well the Monte Carlo simulations.

Figure 6 demonstrates the system throughput of the SIC-2TS and CONV-4TS protocols versus d_1 in cases of pCSIs/ipCSIs $\rho \in \{0.92, 1\}$ when $P_S/N_0 = 5$(dB), $\Omega = -10$ (dB), $N = 6$, and the power allocation coefficients $\alpha_1 = \alpha_2 = \eta = 1$. Figure 6 shows that the SIC-2TS protocol has the system throughput higher than the CONV-4TS protocol in the pCSI case. But in the ipCSI case, its throughput is only better when the distances d_1 are about from 0.3 to 0.7. Moreover, the throughput of the SIC-2TS protocol reaches the highest values at optimal locations of the selected relay as $d_1 = 0.4$ (in the pCSIs) and $d_1 = 0.45$ (in the ipCSIs). Besides, the CONV-4TS protocol has the highest system throughput when the relay is at an equidistant point of the two sources ($d_1 = 0.5$). Lastly, in the perfect CSI ($\rho = 1$), the throughput of the two protocols is always better than in the imperfect CSI ($\rho = 0.92$) case.

Figure 7 observes the throughput of the proposed SIC-2TS protocol versus α_1 and d_1. The scopes of α_1 and d_1 are from 0.05 to 0.95. The throughput of the proposed SIC-2TS protocol

is the highest at about 0.8853 when joint pairs $\{\alpha_1, d_1\} = \{0.4, 0.5\}$ and $\{\alpha_1, d_1\} = \{0.6, 0.5\}$. Table 2 shows the detail of the maximum throughput value corresponding to the distance d_1 and the power coefficient α_1 of the S_1. The coefficients α_1 and α_2 help to adjust the transmit powers of the source nodes; a smaller power is set to the source node nearer to the relay cluster and higher power for the farther source node. The transmit power allocation can achieve the best throughput performance for the proposed SIC-2TS protocol.

Figure 8 presents the throughput of the proposed SIC-2TS protocol as functions of ρ and d_1. The range of ρ is from 0.8 to 1, and the range of d_1 is set from 0.05 to 0.95. The power coefficients α_1 and α_2 also vary according to distance d_1 and d_2, respectively, to achieve the best throughput performance as mentioned in Figure 7. It is seen that a small range decrease in ρ will result in a large range reduction in throughput so obviously, it is necessary to consider the effect of feedback delay when examining a real system. In other words, channel error estimation in cooperation networks becomes principally important and any ineffective estimation can have detrimental consequences for system performance and it should be not omitted when surveying a cooperation network model. Furthermore, the relative distance between the two sources and the relay cluster also affects different throughput decreases as ρ decreases. When the distance d_1 is in the range $[0.3 : 0.4]$ and $[0.6 : 0.7]$, the throughput performance of the system is affected by reduction less than the rest. At last, the larger the number of the relay is, the larger the throughput; therefore, this shows the advantage of using multiple relays.

6. Conclusion

In this article, a two-way cooperative NOMA model with two sources and multiple relaying nodes under the reality conditions as the ip/pCSIs and the ip/pSIC is studied. In the proposed protocol, a relay was selected in the setup phase by the MAC layer protocol to enhance the decoding capacity of the nearer source and minimize the collection time of imperfect CSIs. Spectrum utilization efficiency was improved by using the SIC and DNC techniques at the selected relay. In order to analyze and evaluate the system performance, exact and asymptotic closed-form outage probabilities and throughput expressions were considered and demonstrated by the Monte Carlo simulations. Our results showed that the performance of the proposed SIC-2TS protocol is significantly improved by the increased number of relays as well as the perfect operations of the SIC process and the CSI estimations. Besides, the system performance is decreased in the ipSIC and the ipCSI conditions. The noteworthy thing is found as the proposed SIC-2TS protocol can reach the best performance at optimal locations of the relay cluster and suitable values of power coefficients. In the pCSI condition, the proposed SIC-2TS protocol always has the system performance much better than the CONV-4TS and SIC-3TS protocols. However, in the ipCSI condition, the SIC-2TS protocol only performs better if the distances from two sources to the relay cluster are not very different. Finally, the analysis expressions of the outage probabilities and system throughput are validated by the Monte Carlo simulations.

Appendix

A. Proof of Lemma 2

We have an equivalent expression of $\Pr\left(\gamma_{S_n R_b \longrightarrow x_n | d_n \leq d_f} \geq \gamma_t\right)$ as

$$\Pr\left(\gamma_{S_n R_b \longrightarrow x_n | d_n \leq d_f} \geq \gamma_t\right) = 1 - \Pr\left(\gamma_{S_n R_b \longrightarrow x_n | d_n \leq d_f} < \gamma_t\right). \tag{A.1}$$

Substituting in (4) into (A.1), we have

$$\begin{aligned}
&\Pr\left(\gamma_{S_n R_b \longrightarrow x_n | d_n \leq d_f} \geq \gamma_t\right) \\
&= 1 - \Pr\left(\frac{\alpha_n g_{S_n R_b}}{\alpha_f g_{S_f R_b} + \phi_1} < \gamma_t\right) \\
&= 1 - \Pr\left(g_{S_n R_b} < \underbrace{\frac{\gamma_t \alpha_f}{\alpha_n} g_{S_f R_b}}_{\phi_2} + \underbrace{\frac{\gamma_t \phi_1}{\alpha_n}}_{\phi_3}\right) \\
&= 1 - \Pr\left(g_{S_n R_b} < \phi_2 g_{S_f R_b} + \phi_3\right) \\
&= 1 - \int_0^\infty f_{g_{S_f R_b}}(x) F_{g_{S_n R_b}}(\phi_2 x + \phi_3) dx.
\end{aligned} \tag{A.2}$$

In (A.2), $F_{g_{S_n R_b}}(x)$ is the CDF of $g_{S_n R_b}$ and can find the following:

$$\begin{aligned}
F_{g_{S_n R_b}}(x) &= \Pr\left[g_{S_n R_b} < x\right] = \Pr\left[\max_{i=1,2,\cdots,N} g_{S_n R_i} < x\right] \\
&= \prod_{i=1}^N \Pr\left[g_{S_n R_i} < x\right] \\
&= \prod_{i=1}^N F_{g_{S_n R_i}}(x) = \left(1 - e^{-x/\lambda_n}\right)^N.
\end{aligned} \tag{A.3}$$

Substituting the PDF of $g_{S_f R_b}$ as $f_{g_{S_f R_b}}(x) = (1/\lambda_f) e^{-x/\lambda_f}$ and (A.3) into (A.2), we obtain a result as

$$\begin{aligned}
&\Pr\left(\gamma_{S_n R_b \longrightarrow x_n | d_n \leq d_f} \geq \gamma_t\right) \\
&= 1 - \int_0^\infty \frac{1}{\lambda_f} e^{-x/\lambda_f} \left(1 - e^{-(\phi_2 x + \phi_3)/\lambda_n}\right)^N dx \\
&= 1 - \int_0^\infty \frac{1}{\lambda_f} e^{-x/\lambda_f} \sum_{p=0}^N C_N^p (-1)^p e^{-(p(\phi_2 x + \phi_3)/\lambda_n)} dx \\
&= 1 - \frac{1}{\lambda_f} \sum_{p=0}^N C_N^p (-1)^p e^{-p\phi_3/\lambda_n} \int_0^\infty e^{-x\left((1/\lambda_f) + (p\phi_2/\lambda_n)\right)} dx \\
&= 1 - \lambda_n \sum_{p=0}^N \frac{C_N^p (-1)^p e^{-p\phi_3/\lambda_n}}{\lambda_n + p\phi_2 \lambda_f}.
\end{aligned}$$

Hence, Lemma 2 is proven completely.

B. Proof of Lemma 3

Substituting (4) and (6) into the probability $\Pr\left(\gamma_{S_nR_b\longrightarrow x_n|d_n\leq d_f}\geq\gamma_t, \gamma_{S_fR_b\longrightarrow x_f|d_n\leq d_f}\geq\gamma_t\right)$, we have

$$
\begin{aligned}
&\Pr\left(\gamma_{S_nR_b\longrightarrow x_n|d_n\leq d_f}\geq\gamma_t, \gamma_{S_fR_b\longrightarrow x_f|d_n\leq d_f}\geq\gamma_t\right)\\
&=\Pr\left[\frac{\alpha_n g_{S_nR_b}}{\alpha_f g_{S_fR_b}+\phi_1}\geq\gamma_t, \frac{\alpha_f g_{S_fR_b}}{\varepsilon\rho^2 g_{R_b}+\phi_1}\geq\gamma_t\right]\\
&=\Pr\left[g_{S_nR_b}\geq\underbrace{\frac{\gamma_t\alpha_f}{\alpha_n}}_{\phi_2}g_{S_fR_b}+\underbrace{\frac{\gamma_t\phi_1}{\alpha_n}}_{\phi_3}, g_{S_fR_b}\geq\underbrace{\frac{\gamma_t\varepsilon\rho^2}{\alpha_f}}_{\phi_4}g_{R_b}+\underbrace{\frac{\gamma_t\phi_1}{\alpha_f}}_{\phi_5}\right]\\
&=\int_0^\infty f_{g_b}(z)\left(\int_{\phi_4z+\phi_5}^\infty f_{g_{S_fR_b}}(x)\left(\int_{\phi_2x+\phi_3}^\infty f_{g_{S_nR_b}}(y)dy\right)dx\right)dz\\
&=\int_0^\infty f_{g_b}(z)\left(\int_{\phi_4z+\phi_5}^\infty f_{g_{S_fR_b}}(x)\left(1-F_{g_{S_nR_b}}(\phi_2x+\phi_3)\right)dx\right)dz.
\end{aligned}
\tag{B.1}
$$

Substituting PDF of g_{R_b}, $g_{S_fR_b}$, and CDF of $g_{S_nR_b}$ into (B.1), we obtain

$$
\begin{aligned}
&\Pr\left(\gamma_{S_nR_b\longrightarrow x_n|d_n\leq d_f}\geq\gamma_t, \gamma_{S_fR_b\longrightarrow x_f|d_n\leq d_f}\geq\gamma_t\right)\\
&=\int_0^\infty\frac{1}{\Omega}e^{-z/\Omega}\times\left(\int_{\phi_4z+\phi_5}^\infty\frac{1}{\lambda_f}e^{-x/\lambda_f}\left(1-\sum_{p=0}^N C_N^p(-1)^p e^{-p(\phi_2x+\phi_3)/\lambda_n}\right)dx\right)dz\\
&=\frac{\lambda_f e^{-\phi_5/\lambda_f}}{(\lambda_f+\phi_4\Omega)}-\sum_{p=0}^N\frac{\lambda_n^2\lambda_f C_N^p(-1)^p e^{-\left(p(\phi_3+\phi_5\phi_2)/\lambda_n+\phi_5/\lambda_f\right)}}{(\lambda_n+p\phi_2\lambda_f)\left(\lambda_n\lambda_f+\phi_4\Omega(\lambda_n+p\phi_5\phi_2\lambda_f)\right)}.
\end{aligned}
\tag{B.2}
$$

Therefore, Lemma 3 is proven completely.

Data Availability

The data used to support the findings of this study are included in the article.

Conflicts of Interest

The authors declare that they have no conflicts of interest.

References

[1] Z. Ding, Y. Liu, J. Choi et al., "Application of non-orthogonal multiple access in LTE and 5G networks," *IEEE Communications Magazine*, vol. 55, no. 2, pp. 185–191, 2017.

[2] L. Dai, B. Wang, Y. Yuan, S. Han, I. Chih-Lin, and Z. Wang, "Non-orthogonal multiple access for 5G: solutions, challenges, opportunities, and future research trends," *IEEE Communications Magazine*, vol. 53, no. 9, pp. 74–81, 2015.

[3] H. Guo, X. Guo, C. Deng, and S. Zhao, "Performance analysis of IQI impaired cooperative NOMA for 5G-enabled Internet of Things," *Wireless Communications and Mobile Computing*, vol. 2020, Article ID 3812826, 12 pages, 2020.

[4] Z. Yang, Z. Ding, P. Fan, and N. Al-Dhahir, "The impact of power allocation on cooperative non-orthogonal multiple access networks with SWIPT," *IEEE Transactions on Wireless Communications*, vol. 16, pp. 4332–4343, 2017.

[5] P. N. Son and T. T. Duy, "A new approach for two-way relaying networks: improving performance by successive interference cancellation, digital network coding and opportunistic relay selection," *Wireless Networks*, vol. 26, no. 2, pp. 1315–1329, 2020.

[6] X. Yue, Y. Liu, S. Kang, A. Nallanathan, and Z. Ding, "Exploiting full/half-duplex user relaying in NOMA systems," *IEEE Transactions on Communications*, vol. 66, pp. 560–575, 2018.

[7] X. Li, M. Zhao, Y. Liu, L. Li, Z. Ding, and A. Nallanathan, "Secrecy analysis of ambient backscatter NOMA systems under I/Q imbalance," *IEEE Transactions on Vehicular Technology*, vol. 69, pp. 12286–12290, 2020.

[8] P. Liu, Z. Tao, Z. Lin, E. Erkip, and S. Panwar, "Advances in smart antennas - cooperative wireless communications: a cross-layer approach," *IEEE Wireless Communications*, vol. 13, pp. 84–92, 2006.

[9] A. Nosratinia, T. E. Hunter, and A. Hedayat, "Cooperative communication in wireless networks," *IEEE Communications Magazine*, vol. 42, pp. 74–80, 2004.

[10] F. Xing, H. Yin, X. Ji, and V. C. Leung, "Joint relay selection and power allocation for underwater cooperative optical wireless networks," *IEEE Transactions on Wireless Communications*, vol. 19, pp. 251–264, 2019.

[11] L. Pan, Z. Li, Z. Wang, and F. Zhang, "Joint relay selection and power allocation for the physical layer security of two-way cooperative relaying networks," *Wireless Communications and Mobile Computing*, vol. 2019, Article ID 1839256, 7 pages, 2019.

[12] V. Ozduran, "Leakage rate-based untrustworthy relay selection with imperfect channel state information: the outage and security trade-off analysis," *IET Communications*, vol. 13, pp. 1902–1915, 2019.

[13] T. T. Duy and H. Y. Kong, "Exact outage probability of cognitive two-way relaying scheme with opportunistic relay selection under interference constraint," *IET Communications*, vol. 6, pp. 2750–2759, 2012.

[14] M. J. Taghiyar, S. Muhaidat, J. Liang, and M. Dianati, "Relay selection with imperfect CSI in bidirectional cooperative networks," *IEEE Communications Letters*, vol. 16, pp. 57–59, 2012.

[15] P. N. Son and H. Y. Kong, "Exact outage probability of two-way decode-and-forward scheme with opportunistic relay selection under physical layer security," *Wireless Personal Communications*, vol. 77, pp. 2889–2917, 2014.

[16] K. Ho-Van, "Exact outage analysis of underlay cooperative cognitive networks with reactive relay selection under imperfect channel information," *Wireless Personal Communications*, vol. 84, pp. 565–585, 2015.

[17] P. N. Son and H. Y. Kong, "Exact outage analysis of energy harvesting underlay cooperative cognitive networks," *IEICE Transactions on Communications*, vol. 98, pp. 661–672, 2015.

[18] T.-P. Huynh, P. N. Son, and M. Voznak, "Exact outage probability of two-way decode-and-forward NOMA scheme with opportunistic relay selection," *KSII Transactions on Internet and Information Systems*, vol. 13, 2019.

[19] P. N. Son, "Joint impacts of hardware impairments, imperfect CSIs, and interference constraints on underlay cooperative

cognitive networks with reactive relay selection," *Telecommunication Systems*, vol. 71, pp. 65–76, 2019.

[20] V. Ozduran, B. S. B. Yarman, and J. M. Cioffi, "Opportunistic source-pair selection method with imperfect channel state information for multiuser bi-directional relaying networks," *IET Communications*, vol. 13, pp. 905–917, 2019.

[21] X. Li, J. Li, Y. Liu, Z. Ding, and A. Nallanathan, "Residual transceiver hardware impairments on cooperative NOMA networks," *IEEE Transactions on Wireless Communications*, vol. 19, pp. 680–695, 2019.

[22] Y. Chen, T. Zhang, Y. Liu, and X. Qiao, "Physical layer security in NOMA-enabled cognitive radio networks with outdated channel state information," *IEEE Access*, vol. 8, pp. 159480–159492, 2020.

[23] Z. Ding, M. Peng, and H. V. Poor, "Cooperative non-orthogonal multiple access in 5G systems," *IEEE Communications Letters*, vol. 19, pp. 1462–1465, 2015.

[24] T.-T. T. Dao, N.-L. Nguyen, H.-N. Nguyen et al., "Exploiting secure performance of full-duplex decode and forward in optimal relay selection networks," *Elektronika ir Elektrotechnika*, vol. 24, no. 4, 2018.

[25] M. Zhang, J. Zheng, and Y. He, "Secure transmission scheme for SWIPT-powered full-duplex relay system with multi-antenna based on energy cooperation and cooperative jamming," *Telecommunication Systems*, vol. 74, pp. 55–66, 2020.

[26] A. Agarwal and A. K. Jagannatham, "Performance analysis for non-orthogonal multiple access (NOMA)-based two-way relay communication," *IET Communications*, vol. 13, pp. 363–370, 2018.

[27] X. Yue, Y. Liu, S. Kang, A. Nallanathan, and Y. Chen, "Modeling and analysis of two-way relay non-orthogonal multiple access systems," *IEEE Transactions on Communications*, vol. 66, pp. 3784–3796, 2018.

[28] X. Wang, M. Jia, I. W.-H. Ho, Q. Guo, and F. C. Lau, "Exploiting full-duplex two-way relay cooperative non-orthogonal multiple access," *IEEE Transactions on Communications*, vol. 67, pp. 2716–2729, 2018.

[29] X. Tian, Q. Li, X. Li et al., "I/Q imbalance and imperfect SIC on two-way relay NOMA systems," *Electronics*, vol. 9, pp. 1–16, 2020.

[30] X. Li, Q. Wang, Y. Liu, T. A. Tsiftsis, Z. Ding, and A. Nallanathan, "UAV-aided multi-way NOMA networks with residual hardware impairments," *IEEE Wireless Communications Letters*, vol. 9, no. 9, pp. 1538–1542, 2020.

[31] F. Wei, T. Zhou, T. Xu, and H. Hu, "Modeling and analysis of two-way relay networks: a joint mechanism using NOMA and network coding," *IEEE Access*, vol. 7, pp. 152679–152689, 2019.

[32] T.-T. T. Dao and P. N. Son, "Uplink non-orthogonal multiple access protocol in two-way relaying networks: realistic operation and performance analysis," in *2020 7th NAFOSTED Conference on Information and Computer Science (NICS)*, pp. 399–404, Ho Chi Minh City, Vietnam, 2020.

[33] Z. Cao, X. Ji, J. Wang, S. Zhang, Y. Ji, and J. Wang, "Security-reliability tradeoff analysis for underlay cognitive two-way relay networks," *IEEE Transactions on Wireless Communications*, vol. 18, pp. 6030–6042, 2019.

[34] X. Ding, T. Song, Y. Zou, X. Chen, and L. Hanzo, "Security-reliability tradeoff analysis of artificial noise aided two-way opportunistic relay selection," *IEEE Transactions on Vehicular Technology*, vol. 66, pp. 3930–3941, 2017.

[35] H. A. Suraweera, P. J. Smith, and M. Shafi, "Capacity limits and performance analysis of cognitive radio with imperfect channel knowledge," *IEEE Transactions on Vehicular Technology*, vol. 59, pp. 1811–1822, 2010.

[36] H. Huang, Z. Li, J. Si, and L. Guan, "Underlay cognitive relay networks with imperfect channel state information and multiple primary receivers," *IET Communications*, vol. 9, pp. 460–467, 2014.

[37] H. Cui, R. Zhang, L. Song, and B. Jiao, "Capacity analysis of bidirectional AF relay selection with imperfect channel state information," *IEEE Wireless Communications Letters*, vol. 2, pp. 255–258, 2013.

[38] R. Jiang, K. Xiong, P. Fan, L. Zhou, and Z. Zhong, "Outage probability and throughput of multirelay SWIPT-WPCN networks with nonlinear EH model and imperfect CSI," *IEEE Systems Journal*, vol. 14, pp. 1206–1217, 2020.

[39] P. N. Son and T. T. Duy, "Performance analysis of underlay cooperative cognitive full-duplex networks with energy-harvesting relay," *Computer Communications*, vol. 122, pp. 9–19, 2018.

[40] A. A. Nasir, X. Zhou, S. Durrani, and R. A. Kennedy, "Relaying protocols for wireless energy harvesting and information processing," *IEEE Transactions on Wireless Communications*, vol. 12, no. 7, pp. 3622–3636, 2013.

Two-Way Cognitive Network supported by Reconfigurable Intelligent Surface

1st Thu-Thuy Thi Dao
Faculty of Electrical and Electronics Engineering
Ho Chi Minh City University of Technology and Education
Ho Chi Minh City, Vietnam
thuydtt.ncs@hcmute.edu.vn
Faculty of Electronics Technology
Industrial University of Ho Chi Minh City
Ho Chi Minh City, Vietnam
daothithuthuy@iuh.edu.vn

2nd Pham Ngoc Son
Faculty of Electrical and Electronics Engineering
Ho Chi Minh City University of Technology and Education
Ho Chi Minh City, Vietnam
sonpndtvt@hcmute.edu.vn

Abstract—In this paper, we propose an underlay two-way (UTW) scheme in which two secondary sources transmit simultaneously their data to each other through the Reconfigurable Intelligent Surface (RIS). The proposed scheme is designed to operate in the full-duplex mode under an interference constraint of a primary receiver (PR). The exact closed-form expressions of outage probabilities are considered to evaluate the system performance. The results show that the secondary system performance increases as the number of reflected elements, the distances between PR and secondary sources, the maximum interference power-noise ratio at primary receivers (Q dB), and the maximum signal-noise ratio at the secondary sources (γ_0 dB) increase. Moreover, if the value of the Q or the γ_0 is large enough, the outage probabilities of the secondary network will fall into a saturation state. Finally, the Monte Carlo simulation results are collected to evidence the validity of the analytical expressions of the outage probabilities.

Index Terms—Underlay two-way scheme, reconfigurable intelligent surface, full-duplex.

I. INTRODUCTION

Nowadays, the growing number of users and increasingly diverse mobile multimedia applications lead to a rising challenge about using spectral efficiency (SE), energy efficiency (EE), and cost-efficiency in the deployment and operation of wireless networks. Recently, Reconfigurable Intelligent Surface has been considered as an emerging cost-saving technology for future wireless communication systems. These artificial surfaces include reconfigurable electromagnetic materials that can be controlled and programmed using integrated electronics and integrated into the existing infrastructure [1]. In particular, RIS is able to change the signal transmission direction with low-cost passive devices. In this way, RIS is able to create favorable wireless propagation environments without consuming power. Furthermore, RIS can be readily coated on the facades of buildings, which reduces implementation cost and complexity. In addition, RIS passively reflects the signal without processing while a relay actively processes the received signal before re-transmitting. Lead to the RIS-supported communication betters the relay-supported one about the spectrum efficiency and the energy efficiency [2].

Besides, two-way relay cooperation networks are also one of the solutions to enhance the system performance and SE because of their ability to exchange signals of two device users over the same shared channel, especially in full-duplex communication [3].

In addition, the authors in [4] shows that the usage of the registered frequency spectrum against time and space is not high. Thus the cognitive radio (CR) network was proposed to allow the primary network to share its frequency band with the secondary network to improve SE. In CR networks, there are three protocols (underlay, overlay, and interweave) were proposed so the secondary users can operate flexibly and smartly to access the licensed frequency spectra of the primary users as long as the primary network still maintains the quality of services [5]–[7]. In the underlay CR protocol, the secondary and primary networks operate on the same frequency band, but the secondary sources must adjust the transmit power so as not to affect the operation of the primary receivers [5]. The cognitive two-way relay networks combined with other techniques are considered and valuated under an interference constraint of a primary receiver [8], [9].

A. Related work and motivation

In [2], the authors analyzed and compared the performance of two wireless systems with aid of RIS and amplify-and-forward (AF) relaying. The results showed that RIS-assisted wireless systems outperform the corresponding AF-relaying ones. To take advantage of both SE and EE, the one-way cognitive network had multiple primary receivers (PR) and a single secondary receiver (SR) combined with a RIS half-duplex [10] and full-duplex [11].

Recently, the two–way network in which two users communicate via a common RIS were investigated [12], [13]. In [12], outage probability and average throughput were derived with assuming that uplink and downlink communication channels between two users and the RIS can be reciprocal. In [13], the channels between the two users and RIS can either be reciprocal or non-reciprocal, and the authors proposed the

optimal phases and approximation methods for each case to
derive the outage probability and the SE of the system.

Motivated by previous works for a two-way network to
improve SE and EE, we suggest a RIS-supported underlay
two-way scheme, called as RIS-UTW, in which two secondary
sources operate in the full-duplex mode with aid of a RIS
under the limit condition of a primary receiver.

To consider and evaluate the system performance, the outage
probability of the system is investigated according to parame-
ters such as the maximum interference power-noise ratio that
the PR can decode information in the primary network (Q);
the maximum signal-noise ratio that the secondary network
hardware can satisfy (γ_0); the relative position of the RIS and
the PR; the change in the number of reflected elements of
the RIS; and the loop interference suppression ability of the
full-duplex transmission.

B. Contributions

The contributions in this paper are summarized as follows.
First, the exact and asymptotic expressions of the outage prob-
abilities of two secondary users in the RIS-UTW scheme are
analyzed and then proved validity by the simulation. Next the
parameters affecting the outage probabilities of the secondary
system are examined.The simulation and analysis results show
that the number of reflected elements or the distance between
PR and secondary sources increase, the outage probabilities
of the two secondary sources decrease. Addition on, with any
number of reflected elements, the outage probabilities of both
sources decrease quickly when Q increases in a small value
region, and attains a saturation value in the greater Q region.
Finally, the lines OP of the sources versus γ_0 also decreases
when γ_0 is less than about -10 dB, then the OP stays at the
same value even though γ_0 still increases.

C. Paper organization and notations

The rest of the paper is organized into sections as follows.
Section 2 presents the proposed system model. Section 3
analyzes outage probabilities. Results and discussions are
shown in section 4. Lastly, section 5 is the conclusion.

The notations: $f_\Lambda(\cdot)$ and $F_\Lambda(\cdot)$ present respectively the
probability density function (PDF) and the cumulative distri-
bution function (CDF) of a random variable (RV) Λ; $\Pr[\Xi]$
presents the probability operation of an event Ξ; $\Gamma[.]$ is the
Gamma function [14] (eq.8.310); $\gamma[.,.]$ is the lower incom-
plete Gamma function [14] (eq.8.350.1); $\Gamma[.,.]$ is the upper
incomplete Gamma function [14] (eq.8.350.2); $W,()$ is the
Whittaker function [14] (eq.9.222); $CN()$ denotes the complex
normal distribution.

II. SYSTEM MODEL

A system model of RIS-supported underlay two-way net-
work is shown in Figure 1 in which two-antenna secondary
sources S_1 and S_2 send simultaneously their data x_1 and x_2
($x_1 \in S_1$ and $x_2 \in S_2$) to each other through an RIS with T
metasurfaces MS_t , $t = \{1, 2, ..., T\}$. The S_1 and S_2 tolerate
interference constraint of the primary receiver, denoted as I.
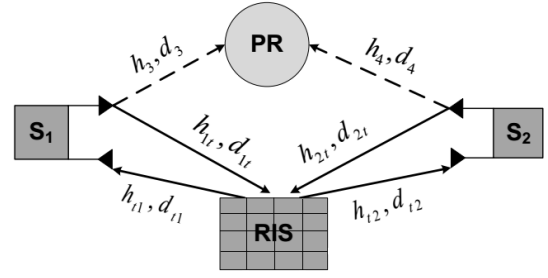
Fig. 1. System model of an RIS-supported underlay two-way network

In Figure 1,(h_{1t}, d_{1t}), (h_{t1}, d_{t1}), (h_{2t}, d_{2t}), (h_{t2}, d_{t2}), (h_3, d_3)
and (h_4, d_4) denote the fading channel coefficients and the
normalized distances of links $S_1 - MS_t, MS_t - S_1, S_2 -
MS_t, MS_t - S_2, S_1 - PR$ and $S_2 - PR$, respectively. We
have some assumptions as: 1) direct links between node pairs
(S_1, S_2) and (MS_t, PR) does not exist due to the far distance,
deep shadow fading or beamforming of the RIS; 2) additive
noises at the S_1 and S_2 are $CN(0, N_0)$ with zero-mean and
identical variance N_o; 3) each MS_t is close to others, and
thus the normalized distances can be set as $d_{1t} = d_{t1} = d_1$,
$d_{2t} = d_{t2} = d_2$; 4) wireless channels between node pairs
(S_1, MS_t) and (S_2, MS_t) are reciprocal, i.e $h_{t1} = h_{1t}$ and
$h_{t1} = h_{1t}$ [6], [13]; all fading channel coefficients are complex
normal RVs, i.e. $h_{t1} = h_{1t} = |h_{1t}| e^{\varphi_{1t}} \in CN(0, 1/\lambda_1)$,
$h_{t2} = h_{2t} = |h_{2t}| e^{\varphi_{2t}} \in CN(0, 1/\lambda_2)$, $h_3 \in CN(0, 1/\lambda_3)$
and $h_4 \in CN(0, 1/\lambda_4)$, where φ_{1t} and φ_{2t} are phase values
of reciprocal channels h_{1t} and h_{2t}, $\lambda_u = d_u^\beta$, β is a path-loss
exponent, and $u \in \{1, 2, 3, 4\}$; 5) loop-back signals from the
transmit antenna to the receive antenna are filtered to cancel
completely.

Under operation conditions of the underlay cognitive radio
network, the transmit power of the secondary sources S_q
(denoted by P_q, $q \in \{1, 2\}$) must be below a maximum power
(denoted by $P_{q,max}$) and satisfies the interference constraint of
the primary network. Therefore, P_q is set maximally as [7]

$$P_q = \min\left(P_{q,max}, I/g_{(q+2)}\right) \qquad (1)$$

where $g_{(q+2)} = |h_{(q+2)}|^2$ with $h_{(q+2)} \in \{h_3, h_4\}$.

At the same time, the secondary sources S_1 and S_2 send
simultaneously the data x_1 and x_2 respectively to each other
through the RIS with the same frequency. More specifically,
the S_1 will receive the signal including the desired data x_2,
and is affected by self-interference signal including the own
data x_1 from the reverse reflection of the RIS, and by internal
additive noise. The received signal at the S_1 is presented as
[12], [13].

$$y_1 = \underbrace{\sqrt{P_2}x_2\left(\sum_{t=1}^{T} h_{2t}r_t h_{t1}\right)}_{Desired\ signal} + \underbrace{\sqrt{P_1}x_1\left(\sum_{t=1}^{T} h_{1t}r_t h_{t1}\right)}_{Self-inteference\ signal} + n_1$$

$$(2)$$

where r_t is the unit-adjusted response of the MS_t and can be
expressed as $r_t = e^{j\phi_t}$, ϕ_t is the adjustable phase induced by

the MS_t; the additive Gaussian noise n_1 is $CN(0, N_0)$ and $E\{|x_1|^2\} = E\{|x_2|^2\} = 1$.

In (2), the S_1 can cancel perfectly the self-inference signal $\sqrt{P_1} x_1 \left(\sum_{t=1}^{T} h_{1t} r_t h_{t1} \right)$ because of holding the parameters h_{1t}, h_{t1} and r_t in the setup phase and combining with own parameters P_1 and x_1. In addition, the phase ϕ_t of the MS_t is selected optimally as $\phi_t = -(\varphi_{1t} + \varphi_{2t})$ [2], [12], [13]. The formula (2) is rewritten as

$$y_1 = \sqrt{P_2} x_2 \left(\sum_{t=1}^{T} |h_{t1}| \times |h_{2t}| \right) + n_1 \qquad (3)$$

Hence, the received signal-noise ratio (SNR) at the S_1 to decode x_2 is obtained from (3) as

$$\gamma_1 = \frac{\left| \sqrt{P_2} x_2 \left(\sum_{t=1}^{T} |h_{t1}| \times |h_{2t}| \right) \right|^2}{|n_1|^2} = \frac{P_2 \left(\sum_{t=1}^{T} |h_{t1}| \times |h_{2t}| \right)^2}{N_0}, \qquad (4)$$

For simplicity in analyses, we set as $P_{1,\max} = P_{2,\max} = P_{\max}$. In addition, we also defined as

$$\gamma_0 = P_{\max}/N_0, Q = I/N_0, \Psi = \sum_{t=1}^{T} |h_{t1}| \times |h_{2t}|. \quad (5)$$

Substituting in (1) and (5) into (4), we have:

$$\gamma_1 = \min(\gamma_0, \frac{Q}{g_4})\Psi^2, \qquad (6)$$

Similarly, the received signal and the SNR at the S_2 to decode x_1 are inferred respectively as

$$y_2 = \underbrace{\sqrt{P_1} x_1 \left(\sum_{t=1}^{T} h_{1t} r_t h_{t2} \right)}_{\text{Desired signal}} + \underbrace{\sqrt{P_2} x_2 \left(\sum_{t=1}^{T} h_{2t} r_t h_{t2} \right)}_{\text{Self-inteference signal}} + n_2, \qquad (7)$$

$$\gamma_2 = \frac{P_1 \left(\sum_{t=1}^{T} |h_{1t}| \times |h_{t2}| \right)^2}{N_0} = \min(\gamma_0, \frac{Q}{g_3})\Psi^2, \quad (8)$$

where the additive Gaussian noise n_2 is $CN(0, N_0)$.

III. OUTAGE PROBABILITY ANALYSIS

The outage probability (OP) of the secondary source S_p occurs when the S_p cannot successfully decode the desired data x_w of the opposite secondary source S_w in one transmission phase, $(p, w = \{1, 2\})$ and $p \neq w$. The outage probability of S_p is defined as $OP_{S_p} = \Pr[R_{S_p} < R_{th}]$, where R_{S_p} is the achievable data rate at the S_p and is expressed as $R_{S_p} = \log_2(1 + \gamma_p)$, and R_{th} is the threshold data rate

(bits/s/Hz). The outage probability of the S_p in RIS-UTW scheme is presented as

$$OP_{S_p} = \Pr\left[\gamma_p < 2^{R_{th}} - 1 \right]$$

$$= \Pr\left[\min(\gamma_0, \frac{Q}{g_{(w+2)}})\Psi^2 < \underbrace{(2^{R_{th}} - 1)}_{\alpha_1} \right]$$

$$= \underbrace{\Pr\left[\gamma_0 \Psi^2 < \alpha_1, \gamma_0 < \frac{Q}{g_{(w+2)}} \right]}_{\Upsilon_1} + \qquad (9)$$

$$+ \underbrace{\Pr\left[\frac{Q}{g_{(w+2)}}\Psi^2 < \alpha_1, \gamma_0 \geq \frac{Q}{g_{(w+2)}} \right]}_{\Upsilon_2}$$

To analyze the probability OP_{S_p} in (9), the CDF and PDF of the RV Ψ are presented by Lemma 1.

Lemma 1: In formula (5), Ψ is the sum of T independent and identical double Rayleigh RVs, the PDF of the Ψ can be closely approximated as the first term of a Laguerre series expansion [15] (eq.2.76). The PDF and CDF of the RV Ψ is obtained respectively as [2]

$$f_\Psi(x) \simeq \frac{x^a}{b^{a+1}\Gamma(a+1)} \exp\left(-\frac{x}{b}\right) \qquad (10)$$

$$F_\Psi(x) \simeq \frac{\gamma\left(a+1, \frac{x}{b}\right)}{\Gamma(a+1)} \qquad (11)$$

where $a = \frac{k_1^2}{k_2} - 1$, $b = \frac{k_2}{k_1}$, $k_1 = \frac{T\pi}{4\sqrt{\lambda_1 \lambda_2}}$, and $k_2 = \frac{T}{\lambda_1 \lambda_2}\left(1 - \frac{\pi^2}{16}\right)$.

The Υ_1 in the (9) is determined as followed

$$\Upsilon_1 = \Pr\left[\Psi < \sqrt{\frac{\alpha_1}{\gamma_0}}, g_{(w+2)} < \frac{Q}{\gamma_0} \right]$$

$$= F_\Psi\left(\sqrt{\frac{\alpha_1}{\gamma_0}}\right) \times F_{g_{(w+2)}}\left(\frac{Q}{\gamma_0}\right) \qquad (12)$$

where the estimated channel gain $g_{(w+2)} = |h_{(w+2)}|^2$ is exponentially distributed RVs with CDF $F_{g_{(w+2)}}(x) = 1 - e^{-\lambda_{(w+2)}x}$ and PDF $f_{g_{(w+2)}}(x) = \lambda_{(w+2)} e^{-\lambda_{(w+2)}x}$ [6].

And substituting (11) into (12), we obtain

$$\Upsilon_1 = \frac{\gamma\left(a+1, \frac{1}{b}\sqrt{\frac{\alpha_1}{\gamma_0}}\right)}{\Gamma(a+1)} \times \left(1 - e^{-\lambda_{(w+2)}Q/\gamma_0}\right) \qquad (13)$$

Next, the Υ_2 in the (9) is determined as followed

$$\Upsilon_2 = \Pr\left[\Psi < \underbrace{\sqrt{\alpha_1/Q}}_{\alpha_2} \sqrt{g_{(w+2)}}, g_{(w+2)} \geq \underbrace{Q/\gamma_0}_{\alpha_3} \right]$$

$$= \int_{\alpha_3}^{\infty} f_{g_{(w+2)}}(x) \times F_\Psi(\alpha_2 \sqrt{x}) dx \qquad (14)$$

Substituting (11) into (14), we obtain

$$\Upsilon_2 = \int_{\alpha_3}^{\infty} \frac{\lambda_{(w+2)}}{\Gamma(a+1)} e^{-\lambda_{(w+2)}x} \gamma\left(a+1, \frac{\alpha_2}{b}\sqrt{x}\right) dx \qquad (15)$$

After some analysis we have the following result of the Υ_2 in two forms: the integral expression and the infinite sum expression with the formulas (16) and (17), respectively.

$$\Upsilon_2 = 2^{-\left(a+\frac{1}{2}\right)}\left(\frac{\alpha_2}{b}\right)^{\left(a+\frac{1}{2}\right)}\lambda_{(w+2)}{}^{-\frac{1}{2}(a+1/2)} \times$$
$$\times W_{-\frac{1}{2}(a+1/2),-\frac{1}{4},\left(\frac{\alpha_2{}^2}{4b^2\lambda_{(w+2)}}\right)}{}^{+}$$
$$+ \int_0^{\alpha_3} \frac{\lambda_{(w+2)}}{\Gamma(a+1)} e^{-\lambda_{(w+2)}x} \gamma\left(a+1, \frac{\alpha_2}{b}\sqrt{x}\right) dx \tag{16}$$

$$\Upsilon_2 = 2^{-\left(a+\frac{1}{2}\right)}\left(\frac{\alpha_2}{b}\right)^{\left(a+\frac{1}{2}\right)}\lambda_{(w+2)}{}^{-\frac{1}{2}(a+1/2)} \times$$
$$\times W_{-\frac{1}{2}(a+1/2),-\frac{1}{4},\left(\frac{\alpha_2{}^2}{4b^2\lambda_{(w+2)}}\right)}{}^{+}$$
$$+ \frac{\lambda_{(w+2)}}{\Gamma(a+1)} \sum_{n=0}^{\infty} \frac{(-1)^n}{n!(a+1+n)} \left(\lambda_{(w+2)}\right)^{-\left(\frac{1}{2}(a+1+n)+1\right)} \times$$
$$\times \gamma\left(\frac{1}{2}(a+1+n)+1, \lambda_{(w+2)}\alpha_3\right) \tag{17}$$

Substituting (13) and (16) or (17) into (9), we obtain OP_{S_p} in (18) or (19) at the top of next page.

Corollary 1: In special case as $\gamma_0 \to +\infty$ then $e^{-\lambda_{(w+2)}Q/\gamma_0} \to 1 \Rightarrow$ in formula (13) $\Upsilon_1 \to 0$ and in formula (15) $\alpha_3 = Q/\gamma_0 \to 0$, so we obtain asymptotic expression of the OP of the S_p in formula (19) when $\gamma_0 \to +\infty$ as

$$OP_{S_p}^{\gamma_0 \to \infty} = 2^{-\left(a+\frac{1}{2}\right)}\left(\frac{\alpha_2}{b}\right)^{\left(a+\frac{1}{2}\right)}\lambda_{(w+2)}{}^{-\frac{1}{2}(a+1/2)} \times$$
$$\times W_{-\frac{1}{2}(a+1/2),-\frac{1}{4},\left(\frac{\alpha_2{}^2}{4b^2\lambda_{(w+2)}}\right)} \tag{20}$$

Corollary 2: In special case as $Q \to +\infty$ then $e^{-\lambda_{(w+2)}Q/\gamma_0} \to 0$, $\alpha_2 \to 0$ and $\alpha_3 \to +\infty$ we obtain asymptotic expression of the OP in formula (19) when $Q \to +\infty$ as

$$OP_{S_p}^{Q \to \infty} = \frac{\gamma\left(a+1, \frac{1}{b}\sqrt{\frac{\alpha_1}{\gamma_0}}\right)}{\Gamma(a+1)} \tag{21}$$

IV. RESULTS AND DISCUSSIONS

This section presents analysis and simulation results in terms of outage probabilities of the proposed RIS-UTW scheme. The simulation results are executed by the Monte Carlo method to prove the analyzed expressions. Coordinates of the nodes S_1, S_2, the PR and the RIS are set as $S_1(0,0)$, $S_2(1,0)$, $PR(x_{PR}, y_{PR})$, $RIS(x_R, y_R)$, where $0 < x_R < 1$. The normalized distances are calculated from the coordinates as $d_1 = \sqrt{x_R^2 + y_R^2}$, $d_2 = \sqrt{(1-x_R)^2 + y_R^2}$, $d_3 = \sqrt{(x_{PR})^2 + (y_{PR})^2}$, and $d_4 = \sqrt{(1-x_{PR})^2 + y_{PR}^2}$. It is assumed that the threshold data rate and the path-loss exponent are fixed by $R_{th} = 1(bits/s/Hz)$ and $\beta = 3$, and Q (dB) on the x-axis is defined as $Q = 10 \times \log_{10}(I/N_o)$ (dB). Markers denote simulated results.

Figure 2 shows the exact and asymptotic outage probabilities of the secondary sources S_1 and S_2 versus Q (dB) as formula (18) and (19) when $\gamma_0 = -15(dB)$, $T \in \{2, 5, 8\}$, $x_R = 0.5$, $y_R = -0.5$, $x_{PR} = 0.5$, $y_{PR} = 1$. Firstly, as selecting the above parameters, we have a symmetrical model

with normalized distances $d_1 = d_2$, and $d_3 = d_4$, so the lines drawing the two sources outage probabilities nearly overlap. Secondly, the outage probabilities of both sources decrease as the interference constraint parameters Q (dB) increases in the region Q (dB) value is small and attains a saturation (floor) value in the high Q (dB) ones. Due to large values of Q (dB), the transmit powers of the nodes S_1, S_2 increase as in (1) which correspond to large SNRs to decode the data x_1, x_2 in (4) and (8). And the transmit powers in (1) also have a limit by the maximum power of each source so the transmit powers will attain a saturation when Q achieves a high threshold value. Moreover, when the number of metasurfaces increases, the system outage probability decreases, or in other words, the system performance increases proportionally with the number of metasurfaces. Besides, in Fig 2, the outage probabilities of the secondary sources are plotted according to two analytical formulas in the infinite sum form (18) and the integral form (19). The results show that the curves represented by the integral formula coincides with the Monte Carlo simulation lines, while the curves represented by the infinite sum (with the first 25 terms selected) is closer to the simulation curves in case of the number of the RIS reflective cell increased.

Figure 3 considers the outage probabilities of the secondary sources S_1 and S_2 versus $\gamma_0 = Pmax/N_0$ (dB) when $Q = -10$ (dB), $T \in \{2, 5, 8\}$, $x_R = 0.5$, $y_R = -0.5$, $x_{PR} = 0.5$, $y_{PR} = 1$. Firstly, similar to Fig. 2 with these selected parameters, Fig. 3 also has the outage probabilities of the two sources overlap. Next, the outage probabilities of the sources quickly decrease as γ_0 (dB) increases to about -10 dB, then they remain constant even though γ_0 (dB) still increases. It shows that the higher the maximum capacity the hardware is able to handle, the better the system performance is, however it has a saturation value because the transmit power depends on two parameters like formula (1). Furthermore, the system performance increases proportionally with the number of metasurfaces as Fig. 2.

Fig. 4 examines the effect of the distances between PR and secondary sources on the outage probability of the secondary system versus Q (dB). When this distances increase leading to the outage probabilities of the system decrease. We have the result because in (4) and (8) the SNRs decrease when the transmit power of the secondary sources increases. And the transmit power of the secondary sources increases when the distances between PR and secondary increase due to the interference effect of the secondary network to PR decreases as in formula (1). Last but not least, the asymptotic and exact theory analysis curves of all figures always match well with their Monte Carlo simulation ones.

V. CONCLUSIONS

In this paper, we proposed and analyzed the underlay two-way RIS scheme with two secondary sources and a primary receiver, known as the UTW-RIS. To evaluate the system performance, the paper investigated the outage probability via parameters such as Q (dB), γ_0 (dB), number of reflected elements of RIS. The notable results are that the system outage

$$OP_{S_p} = \frac{\gamma\left(a+1,\frac{1}{b}\sqrt{\frac{\alpha_1}{\gamma_0}}\right)}{\Gamma(a+1)} \times \left(1 - e^{-\lambda_{(w+2)}Q/\gamma_0}\right) + 2^{-\left(a+\frac{1}{2}\right)}\left(\frac{\alpha_2}{b}\right)^{\left(a+\frac{1}{2}\right)}\lambda_{(w+2)}^{-\frac{1}{2}(a+1/2)} \times$$
$$\times W_{-\frac{1}{2}(a+1/2),-\frac{1}{4}}\left(\frac{\alpha_2^2}{4b^2\lambda_{(w+2)}}\right) + \int\limits_0^{\alpha_3}\frac{\lambda_{(w+2)}}{\Gamma(a+1)}e^{-\lambda_{(w+2)}x}\gamma\left(a+1,\frac{\alpha_2}{b}\sqrt{x}\right)dx \quad (18)$$

$$OP_{S_p} = \frac{\gamma\left(a+1,\frac{1}{b}\sqrt{\frac{\alpha_1}{\gamma_0}}\right)}{\Gamma(a+1)} \times \left(1 - e^{-\lambda_{(w+2)}Q/\gamma_0}\right) + 2^{-\left(a+\frac{1}{2}\right)}\left(\frac{\alpha_2}{b}\right)^{\left(a+\frac{1}{2}\right)}\lambda_{(w+2)}^{-\frac{1}{2}(a+1/2)} \times W_{-\frac{1}{2}(a+1/2),-\frac{1}{4}}\left(\frac{\alpha_2^2}{4b^2\lambda_{(w+2)}}\right) +$$
$$+ \frac{\lambda_{(w+2)}}{\Gamma(a+1)}\sum_{n=0}^{\infty}\frac{(-1)^n}{n!(a+1+n)}\left(\lambda_{(w+2)}\right)^{-\left(\frac{1}{2}(a+1+n)+1\right)}\times\gamma\left(\frac{1}{2}(a+1+n)+1,\lambda_{(w+2)}\alpha_3\right) \quad (19)$$

Fig. 2. The outage probabilities of the secondary sources S_1 and S_2 versus Q (dB) when $\gamma_0(dB) = -15(dB)$, $T \in \{2,5,8\}$, $x_R = 0.5$, $y_R = -0.5$, $x_{PR} = 0.5$, $y_{PR} = 1$.
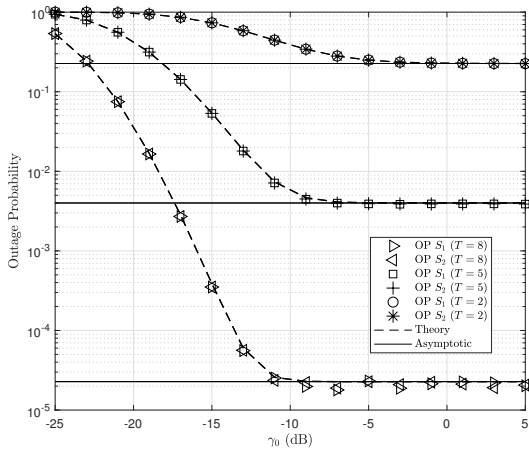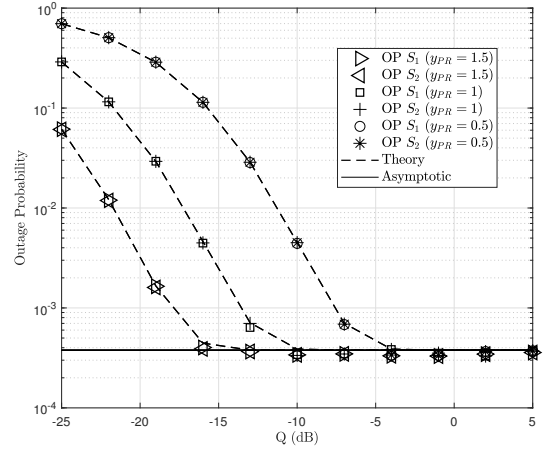
Fig. 4. The outage probabilities of the secondary sources S_1 and S_2 versus Q (dB) when $\gamma_0(dB) = -15(dB)$, $T = 8$, $x_R = 0.5$, $y_R = -0.5$, $x_{PR} = 0.5$, $y_{PR} \in \{0.5,1,1.5\}$.

Fig. 3. The outage probabilities of the secondary sources S_1 and S_2 versus $\gamma_0 = Pmax/N_0$(dB) when $Q = -10$ (dB), $T \in \{2,5,8\}$, $x_R = 0.5$, $y_R = -0.5$, $x_{PR} = 0.5$, $y_{PR} = 1$.

probabilities decrease a lot when the number of reflected elements increase. Besides, the system outage probabilities decrease fastly when Q (dB) or γ_0 (dB) increase at their small value region, and reach the saturation value at their high value region. Finally, the analysis results of the outage probabilities were validated by the Monte Carlo simulations.

REFERENCES

[1] E. Basar, M. Di Renzo, J. De Rosny, M. Debbah, M.-S. Alouini, and R. Zhang, "Wireless communications through reconfigurable intelligent surfaces," IEEE Access, vol. 7, pp. 116753-116773, 2019.

[2] A.-A. A. Boulogeorgos and A. Alexiou, "Performance Analysis of Reconfigurable Intelligent Surface-Assisted Wireless Systems and Comparison With Relaying," IEEE Access, vol. 8, pp. 94463-94483, 2020.

[3] H. Cui, M. Ma, L. Song, and B. Jiao, "Relay selection for two-way full duplex relay networks with amplify-and-forward protocol," IEEE Transactions on Wireless Communications, vol. 13, pp. 3768-3777, 2014.

[4] I. F. Akyildiz, W.-Y. Lee, M. C. Vuran, and S. Mohanty, "NeXt generation/dynamic spectrum access/cognitive radio wireless networks: A survey," Computer networks, vol. 50, pp. 2127-2159, 2006.

[5] A. Goldsmith, S. A. Jafar, I. Maric, and S. Srinivasa, "Breaking spectrum gridlock with cognitive radios: An information theoretic perspective," Proceedings of the IEEE, vol. 97, pp. 894-914, 2009.

[6] Pham Ngoc Son, D. Har and H. Y. Kong, "Smart Power Allocation for Secrecy Transmission in Reciprocally Cooperative Spectrum Sharing," IEEE Transactions on Vehicular Technology, vol. 64, no. 11, pp. 5395-5400, Nov. 2015.

[7] H. Van Toan, V.-N. Q. Bao, and H. Nguyen-Le, "Cognitive two-way relay systems with multiple primary receivers: exact and asymptotic outage formulation," IET Communications, vol. 11, pp. 2490-2497, 2017.

[8] R. T. Al-Zubi, M. T. Abu Issa, O. Jebreil, K. A. Darabkh, and Y. Khattabi, "Outage performance of cognitive two-way amplify-and-forward relay network under different transmission schemes," Transactions on Emerging Telecommunications Technologies, p. e4004, 2020.

[9] P. N. Son, T. T. Duy, and K. Ho-Van, "SIC-Coding Schemes for Underlay Two-Way Relaying Cognitive Networks," Wireless Communications and Mobile Computing, vol. 2020, 2020.

[10] J. Yuan, Y.-C. Liang, J. Joung, G. Feng, and E. G. Larsson, "Intelligent reflecting surface (IRS)-enhanced cognitive radio system," in ICC 2020-2020 IEEE International Conference on Communications (ICC), 2020, pp. 1-6.

[11] D. Xu, X. Yu, Y. Sun, D. W. K. Ng, and R. Schober, "Resource allocation for IRS-assisted full-duplex cognitive radio systems," IEEE Transactions on Communications, vol. 68, pp. 7376-7394, 2020.

[12] S. Atapattu, R. Fan, P. Dharmawansa, G. Wang, and J. Evans, "Two–way communications via reconfigurable intelligent surface," in 2020 IEEE Wireless Communications and Networking Conference (WCNC), 2020, pp. 1-6.

[13] S. Atapattu, R. Fan, P. Dharmawansa, G. Wang, J. Evans, and T. A. Tsiftsis, "Reconfigurable intelligent surface assisted two–way communications: Performance analysis and optimization," IEEE Transactions on Communications, vol. 68, pp. 6552-6567, 2020.

[14] I. S. G. a. I. M. Ryzhik, Table of integrals, series, and products, Seventh ed.: Elsevier, 2007.

[15] S. Primak, V. Kontorovich, and V. Lyandres, "Stochastic methods and their applications to communications," Stochastic Differential Equations Approach. John Wiley and Sons, 2004.

ORIGINAL PAPER

Multi-constraint two-way underlay cognitive network using reconfigurable intelligent surface

Thu-Thuy Thi Dao[1] · Pham Ngoc Son[1]

Abstract

This article proposes an underlay two-way (UTW) scheme in which the Reconfigurable Intelligent Surface (RIS) is used to support two secondary sources that transmit their data to each other in full-duplex mode. This scheme is operated under interference constraints of multiple primary receivers (MPR), called the MPR-UTW-RIS scheme. To evaluate the secondary system performance, exact and asymptotic closed-form expressions for outage probabilities of two sources are considered. We also investigate the effect of parameters on the outage probabilities of the secondary system included the number of metasurfaces, the loop interference suppression ability of full-duplex transmission, the distances between primary receivers and secondary sources, the maximum interference power-to-noise ratio at primary receivers (Q), the maximum signal-to-noise ratio at the secondary sources ($Pmax/N_0$), and the number of primary receivers. The results reveal that the outage probabilities of the two sources will fall into a saturation state if the value of Q or $Pmax/N_0$ is large enough. In addition, when Q reaches a sufficiently large value, the number of primary receivers no longer affects the system performance. Furthermore, the RIS position equidistant from the two secondary sources gives the best outage probability for two sources. Finally, the Monte Carlo simulation results validate the analytical expressions of the outage probabilities.

1 Introduction

In recent decades, wireless networks in general and mobile networks in particular have experienced particularly rapid and revolutionary development. The number of users and intelligent multimedia applications is increasing rapidly, along with the volume of data communication on wireless networks also increasing at a sudden rate, leads to great challenges in using the frequency spectral-efficiency (SE), the energy-efficiency (EE), and the cost-efficiency (CE) in the deployment and operation of the future 6th generation (6G) and beyond wireless communication systems. In recent times, an emerging cost-saving technology of great

interest to researchers is RIS. The RIS is created by reconfigurable electromagnetic materials that can be controlled and programmed by low-cost passive electronic circuits and have wireless communication capabilities [1]. In [1], the authors showed a worth thing that the RIS can effectively control the properties of the received signals, including the phase, amplitude, frequency, and polarization, without the requirement of complex decoding, encoding, and signal processing operations as the relay. Besides, the RIS has the distinguishable features that are nearly passive and ideally; not affected by receiver noise; not amplify nor create noise when reflecting the signals and always provide a full-duplex (FD) mode; have full-band response; can work at all signal frequencies. Moreover, the RIS can be effortlessly coated on the ceilings, walls, furniture, clothes, any objects in the indoor and outdoor environments at a low cost [2]. With the above characteristics, the RIS can create a favorable wireless transmission environment with high received signal quality, saving-costs deployment, not consuming power nor time processing the

✉ Pham Ngoc Son
  sonpndtvt@hcmute.edu.vn

  Thu-Thuy Thi Dao
  thuydtt.ncs@hcmute.edu.vn

1 Ho Chi Minh City University of Technology and Education, Ho Chi Minh City, Vietnam

received signal like relay devices, and a specially worth point is that RIS technology is a promising to enhance the EE of wireless systems. RIS networks are typically classified into two categories anomalous reflectors or diffuse scatters for mmWave and sub-6GHz networks, respectively [3]. RISs may be modeled as diffusers, when the size of them is comparable to the wavelength for the sub-6GHz networks. In [4], the authors gave two types to the channel state information (CSI) acquisition between the RIS and users. When each of RIS elements can be equipped with a low-power receive radio frequency (RF) chain to enable the sensing capability for channel estimation, the channels from the users to the RIS can be estimated at the RIS based on their training signals. In contrast, the RIS cannot estimate the channels with users directly if its elements are not equipped receive RF chains. Instead of estimating the user channels separately, the authors estimate their concatenated channel with some known RIS reflection patterns. This means that the RIS beamforming coefficients for a new user are obtained by interpolating those at its nearby locations obtained in the past.

In [5], the authors considered and compared the performance of RIS and amplify-and-forward (AF) relaying wireless systems through the ergodic capacity (EC) as well as the outage probability (OP) and symbol error rate (SER). The results showed that the wireless system with RIS supports better than conventional AF relay systems in terms of average signal-to-noise ratio (SNR), OP, SER and EC. In [6], a multi-user communications system aided by a RIS and a unmanned aerial vehicle is studied to suppose the provisioning of modern services within a smart city. The authors showed that the RIS technology allows for the significant power savings and the creation of a more controllable smart wireless communications environment. The advantages of RIS in multi-input multi-output (MIMO) communications were studied in articles [7, 8]. In [7], through the outage performance analysis of RIS-aided MIMO systems over cascaded Rayleigh fading channels, the authors exposed that the increase of the number of metasurfaces is advantageous for the improvement of the diversity gain of MIMO systems and the number of metasurfaces at the RIS should be bigger than the total number of transmit and receive antennas to avoid the degradation of the MIMO diversity order. In [8], the authors studied the achievable rate optimization for multistream MIMO systems with RIS- aided, and formulated a joint optimization problem of the covariance matrix of the transmitted signal and the RIS elements based on the projected gradient method. The results demonstrated that the RIS application is particularly suitable to increase the achievable rate in indoor environments, as even a small number of RIS elements can provide a substantial achievable rate gain. The authors in [9, 10] showed that the RIS can appreciably improve the performance of TeraHertz wireless transmissions in the fluctuating two-ray fading model under misalignment and hardware impairments [9] and in $\alpha - \mu$ fading model with pointing errors [10]. The physical layer security of the downlink RIS-aided transmission for randomly located users in the presence of a multi-antenna eavesdropper was studied in [11]. The authors indicated that the security performance is improved significantly by increasing the number of reflecting elements of a RIS and the RIS-aided system offers better security performance to compare with traditional MIMO systems.

A. Related works and motivations

Besides, two-way networks and two-way cooperation networks are also one of the solutions to enhance spectral efficiency when compared to one-way networks because of their ability to simultaneously exchange signals of two device users. There are many studies to improve the performance of two-way relay network by combining with different signal processing techniques such as the method of using digital network coding (DNC) technique at relay [12]; using a relay cluster in combination with different relay selection methods [13]; using non-orthogonal multiple access technique [14, 15]. Recently, in order to combine the strengths of RIS and two-way communication, two-way networks with the help of RIS for information transmission have also begun to receive the research attention [16–18]. In [16], considering a two-way network with two users in case of reciprocal channels, the authors showed that OP and the average throughput of scheme are better if number of metasurfaces (MS) of the RIS rises. In [17], the authors investigated closed-form expressions for the OP and SE of the two-way communication between two users assisted by a RIS over Rayleigh fading channel in both cases of reciprocal and non-reciprocal channels. And the results showed that the rate of spectral efficiency increment or transmit power saving reduces when number of metasurfaces increases. The system performance in case of reciprocal channels outperforms in nonreciprocal channels. In [18], the authors proposed a multi-user RIS-aided full duplex two-way communication network and optimized the precoding matrix of the base station and the reflection coefficients of the RIS to maximize the weighted minimum rate of all users, subject to maximum transmit power to enhance user fairness.

In fact, the frequency range of radio waves is considered a finite resource and must be licensed to use it. Meanwhile, the efficiency of using licensed spectrum resources is still low [19]. In order to improve using the SE, cognitive radio technology has been born and has always been of interest to research, especially in the context of the explosion of mobile devices and applications today. This technology has three protocols (underlay, overlay, and interweave) to

allow the secondary network to dynamically access or share the licensed frequency range of the primary network in condition that the primary network still maintains its quality of services [20].

The underlay cognitive two-way relay networks are considered and valuated with an interference constraint of the primary receiver [21–24]. The authors in [21] considered the outage performance of a half-duplex (HD) AF relay model consisted of two primary users and two secondary users (SUs), in which the channel model between the SUs were Nakagami fading, under three transmission schemes with two, three and four time slots. The results showed that the transmit power by the primary transmitter and the positions of primary transmitter and receiver as well as the relay node, have significant effect on the OP of the secondary network. A HD decode-and-forward (DF) relay cluster with opportunistic relay selection method and DNC technique were used in order to achieve a better outage performance in [22] with three-time-slot scheme. And in [23], the author combined the superposition coding to reduce into two time slots to enhance the system throughput. The OP and the symbol error probability of SUs in underlay cognitive FD AF relaying networks were analyzed in [24]. Using FD relay mode helps to reduce the total transceiver time of the signal since the nodes can transmit and receive the signal at the same time, but also increases the complexity of signal processing techniques than the HD relay mode [25, 26].

Besides, to take advantage of both SE and EE, the one-way cognitive network combined with the RIS was studied and published in [27–29]. In [27], a single SU coexists with multiple PRs, the authors maximized the achievable rate of SU by optimizing the beamforming vector at SU and the phase shifts at the RIS. In [28], the authors investigated a secondary network employs an full-duplex base station for serving multiple users concurrently with aid of a RIS, in which the total sum rate of the secondary system is maximized by optimizing the transmit and receive beamforming vectors at the FD base station, the transmit power of the uplink users, and the phase shift matrix at the RIS. In [29], the authors investigated the diversity order of OP and the EE of the RIS-assisted device-to-device communication system under Nakagami-m fading in both overlay and underlay modes. In [30], a simple underlay two-way scheme was considered in which two secondary sources transmit their data through the RIS under an interference constraint of only one PR and in ideally condition of FD mode, the loop-back signals from the transmit antenna to the receive antenna are filtered to cancel completely.

Motivated by prior works for a two-way network to enhance the SE, EE and CE, we propose a RIS-supported underlay two-way scheme operating in sub-6GHz bands, called as MPR-UTW-RIS, in which two secondary sources

work in the FD mode with support of a RIS under the limit conditions of multiple PRs.

B. Contributions

The main contributions of this article are summarized as follows.

- Our two-way system model with the RIS-aided FD mode in which the two secondary sources transmit and receive signals at the same time brings the advantages reducing the transmission time slot as well as the cost of signal processing leading to increase system throughput and improve system performance compared to conventional two -way system models using AF relays.

- We evaluate the system performance based on the OPs of the two secondary sources in conditions that have the residual loop-back interference after cancelling at the receive antenna. To get an overview of the influence of factors on the system performance, we consider the OP change according to the following parameters: the maximum interference power to plus noise ratio that PUs can decode information in the primary network (Q); the maximum signal-to-plus-noise ratio that SU hardware can satisfy (SNR); the relative position of the RIS and the PU cluster; the change in the number of reflected elements of the RIS; and the loop interference suppression ability of FD transmission.

- The exact and asymptotic expressions of the OP of two sources in the proposed scheme are derived. And the analysis results about the effect of parameters on the OPs of the secondary system are proved validly by the simulation results.

- The simulation and analysis results show that the number of reflected elements increases, the OPs of the two secondary sources decrease.

- Next the OPs of both sources decrease quickly when Q (dB) or $Pmax/N_0$ (dB) increases in a small value region ($Q < -10$dB or $Pmax/N_0 < -15$dB), and attains a saturation value in their high value region.

- Besides, the OP of the SUs decreases as the number of PRs (K) increases but will fall into the saturation value when Q is larger than a threshold value. A noted thing is that this saturation value is the same with all different K values (meaning there exists a threshold value which Q is greater than it, the number of K no longer affects the performance of the secondary network).

- Moreover, the RIS position equidistant from the two sources gives the best system performance for the secondary network.

- Additionally, the position of the PRs cluster is farther from the secondary sources, the OPs of these sources are smaller and vice versa.

- Finally, the system performance of the two-way network with the RIS-aided is better than the similar network with the AF relay-aided.

C. Paper organization and notations

The article is arranged as follows. The system model of an underlay two-way RIS scheme with multiple primary receivers is described in Sect. 2. Outage probabilities of two secondary sources are analyzed in Sect. 3. Simulation results and discussions are presented in Sect. 4. Finally, Sect. 5 summarizes contributions of this article.

Notations used in this article are listed in Table 1.

2 System model

Figure 1 shows the system model of the MPR-UTW-RIS scheme, which has two secondary sources S_q, $q \in \{1, 2\}$, a RIS with T MS_t, $t = \{1, 2, ..., T\}$ and K primary receivers PR_i, $i = \{1, 2, ..., K\}$. To the channel estimation, RIS is equipped a controller to achieve CSI acquisition and information transmission [4]. The CSI of two secondary sources and PRs can be obtained by applying the conventional channel estimation. The S_q tolerate interference constraints of primary receivers, denoted as I_i. In addition, each source has a two-antenna and works in full-duplex mode. In Fig. 1, (h_{qt}, d_{qt}), (h_{tq}, d_{tq}), and $(h_{(q+2)i}, d_{(q+2)i})$ denote the fading channel coefficients and the normalized distances of links $S_q - MS_t$, $MS_t - S_q$, and $S_q - PR_i$, respectively. In this paper, there are some assumptions as: 1) direct links between node pairs (S_1, S_2) and (MS_t, PR_i) does not exist due to the far distance, deep

shadow fading or low reflecting power of the RIS [32]; 2) additive noises at the S_q are $CN(0, N_0)$ with zero-mean and identical variance N_0; 3) all primary receivers PR_i are distributed in the cluster and each MS_t is close to others, and thus the normalized distances can be set as $d_{qt} = d_{tq} = d_q$ and $d_{(q+2)i} = d_{q+2}$; 4) wireless channels between node pairs (S_q, MS_t) are reciprocal, i.e $h_{qt} = h_{tq}$ [16, 17, 33]; 5) all channel coefficients are independent and identically distributed (i.i.d.) complex Gaussian fading, i.e. $h_{tq} = h_{qt} = |h_{qt}| e^{\varphi_{qt}} \in CN(0, 1/\lambda_q)$ and $h_{(q+2)i} \in CN(0, 1/\lambda_{(q+2)})$, where φ_{qt} are phase values of reciprocal channels h_{qt}, $\lambda_u = d_u^\beta$, β is a path-loss exponent, and $u \in \{q, q+2\}$. So channel magnitudes $|h_{qt}|$ and $|h_{(q+2)i}|$ are random variables (RVs) with the Rayleigh distribution [31].

In line with the underlay cognitive radio network conditions, the secondary network can operates parallel with the primary network but the transmit power of the secondary sources S_q(symbolized by P_q) need be lower a maximum power (symbolized by $P_{q,max}$) and gratifies all interference constraints of the primary network. Thus, P_q is expressed as followed [34]

$$P_q = \min\left(P_{q,max}, I_1/g_{(q+2)1}, I_2/g_{(q+2)2}, ..., I_K/g_{(q+2)K}\right),$$

$$(1)$$

where $g_{(q+2)i} = |h_{(q+2)i}|^2$, $i = \{1, 2, ..., K\}$.

According to the full-duplex transmit protocol, the secondary sources S_q send simultaneously the data x_q to each other via the RIS at the same time. And each source will receive the signal including the desired data and undesired data by the reverse reflection of its own signal from the RIS, by residual loop-back interference from

Table 1 Notation table

Notation	Meaning
$f_X(.)$	Probability Density Function (PDF) of X
$F_X(.)$	Cumulative Distribution Function (CDF) of X
$\Pr[\Xi]$	Probability operation of an event Ξ
$E[.]$	Expectation operator
$V[.]$	Variance operator
$\binom{p}{M}$	Binomial coefficient $\left(\binom{p}{M} = \frac{M!}{p!(M-p)!}\right)$
$\Gamma[.]$	Gamma function; [27](eq.8.310)
$\gamma[.,.]$	Lower incomplete Gamma function; [27] (eq.8.350.1)
$\Gamma[.,.]$	Upper incomplete Gamma function; [27] (eq.8.350.2)
$W, ()$	Whittaker function; [27] (eq.9.222)
$X \sim CN(0, \sigma^2)$	Complex Gaussian random variable (RV)X with zero mean and variance σ^2
$| \, |$	Magnitude
$|\,|^2$	Gain

Fig. 1 System model of the MPR-UTW-RIS scheme
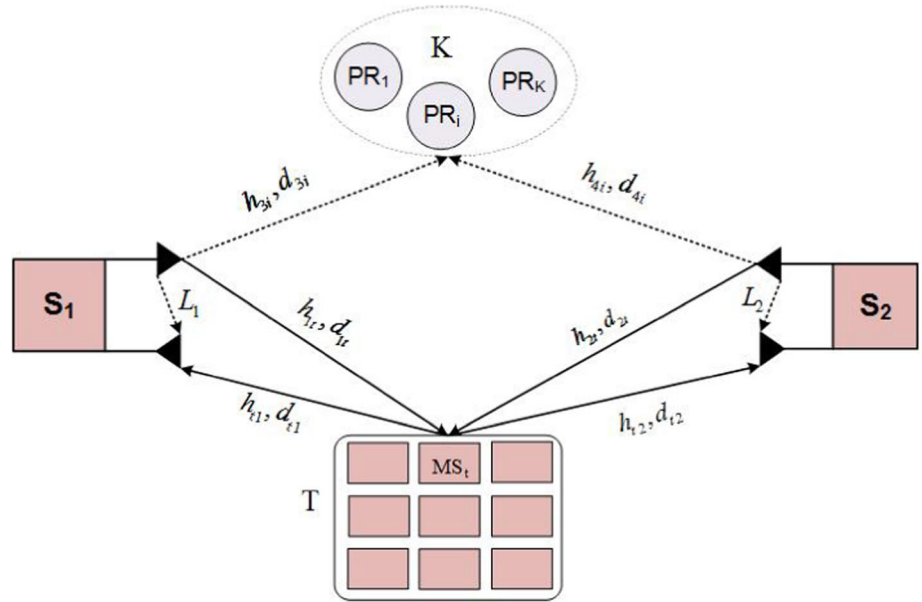
transmit antenna to receive antenna, and by internal additive noise. Specifically, the received signal at the S_1 is expressed as follow [16, 17]

$$y_1 = \sqrt{P_2}x_2 \left(\sum_{t=1}^{T} h_{2t}r_t h_{t1} \right) + \underbrace{\sqrt{P_1}x_1 \left(\sum_{t=1}^{T} h_{1t}r_t h_{t1} \right)}_{\text{Self-inteference signal}} +$$
$$+ \underbrace{L_1}_{\text{residual loop-back inteference signal}} + \underbrace{n_1}_{\text{additive noise}},$$

(2)

where $r_t = |r_t|e^{j\phi_t}$ [3, 31], in which $|r_t| \in [0,1]$ and $\phi_t \in [0, 2\pi)$ denote the reflection amplitude and phase shift of the MS_t on the RIS, respectively, without loss of generality, the reflection amplitude is fixed with a constant value, equal 1 [5, 17, 36, 37]; L_1 is the residual loop-back interference after cancelling at the receive antenna and can be modelled as $CN(0, \mu_1 N_0)$, $\mu_1 \geq 0$ [17, 25]; n_1 is the additive Gaussian noise $CN(0, N_0)$ and $E\{|x_1|^2\} = E\{|x_2|^2\} = 1$. Besides, the source S_1 holds the parameters h_{1t}, h_{t1}, r_t in the setup phase and its values P_1, x_1, so it can cancel perfectly the self-inference signal $\sqrt{P_1}x_1 \left(\sum_{t=1}^{T} h_{1t}r_t h_{t1} \right)$ in (2). In addition, to maximize the instantaneous received signal-to-interference-plus-noise ratio (SINR) of each user, the phase ϕ_t of the MS_t is configured as $\phi_t = -(\varphi_{1t} + \varphi_{2t})$ [5, 16, 17]. The formula (2) is rephrased as

$$y_1 = \sqrt{P_2}x_2 \left(\sum_{t=1}^{T} |h_{2t}| \times |h_{t1}| \right) + L_1 + n_1.$$

(3)

So the SINR at S_1 can be written as

$$\gamma_1 = \frac{\left| \sqrt{P_2}x_2 \left(\sum_{t=1}^{T} |h_{2t}| \times |h_{t1}| \right) \right|^2}{|L_1|^2 + |n_1|^2} = \frac{P_2 \left(\sum_{t=1}^{T} |h_{1t}| \times |h_{2t}| \right)^2}{(1 + \mu_1)N_o}.$$

(4)

For easiness in analyses, we assume as $I_1 = I_2 = ... = I_K = I$, and $P_{1,\max} = P_{2,\max} = P_{\max}$. The the formula (4) can be rewritten as

$$\gamma_1 = \min(\gamma_0, \frac{Q}{\underbrace{\max_{i=1...K} g_{4i}}_{g_{4k}}}) \frac{\Psi^2}{(1 + \mu_1)},$$

(5)

where

$$\gamma_0 = P_{\max}/N_o, Q = I/N_o, \Psi = \sum_{t=1}^{T} |h_{1t}| \times |h_{2t}|.$$

(6)

In the same way, the received signal and the SINR at S_2 can be written as, respectively

$$y_2 = \underbrace{\sqrt{P_1}x_1 \left(\sum_{t=1}^{T} h_{1t}r_t h_{t2} \right)}_{\text{Desired signal}} + \underbrace{\sqrt{P_2}x_2 \left(\sum_{t=1}^{T} h_{2t}r_t h_{t2} \right)}_{\text{Self-inteference signal}} + L_2 + n_2,$$

(7)

$$\gamma_2 = \frac{\left|\sqrt{P_1}\left(\sum_{t=1}^{T}|h_{1t}| \times |h_{t2}|\right)\right|^2}{|L_2|^2 + |n_2|^2} = \frac{P_1\left(\sum_{t=1}^{T}|h_{1t}| \times |h_{t2}|\right)^2}{(1+\mu_2)N_o}$$

$$= \min\left(\gamma_0, \underbrace{\frac{Q}{\max_{i=1...K} g_{3i}}}_{g_{3k}}\right)\frac{\Psi^2}{(1+\mu_2)},$$

(8)

where $L_2 \in CN(0, \mu_2 N_0)$, $\mu_2 \geq 0$, μ_2 is a ratio coefficient to the noise power N_0 of the residual loop-back interference at S_2, and assumed $\mu_2 = \mu_1 = \mu$; n_2 is the additive Gaussian noise $CN(0, N_0)$.

3 Outage probability analysis

In this section, we investigate the OPs of the two sources of the secondary network, denoted S_p and S_w, $(p, w = \{1, 2\})$ and $p \neq w$. The outage event of S_p happens when the S_p cannot successfully decrypt the data x_w of the S_w in one transmission phase. The OP at S_p is described as $OP_{S_p}^{out} = \Pr[R_{S_p} < R_{th}]$, where R_{S_p} is the achievable data rate at the S_p and is expressed as $R_{S_p} = \log_2(1 + \gamma_p)$, and R_{th} is the threshold data rate (*bits/s/Hz*) . The OP of the S_p in MPR-UTW-RIS model is presented as

$$OP_{S_p}^{out} = \Pr[\gamma_p < 2^{R_{th}} - 1]$$

$$= \Pr\left[\min\left(\gamma_0, \frac{Q}{g_{(w+2)k}}\right)\Psi^2 < \underbrace{(2^{R_{th}} - 1)(1 + \mu_p)}_{\alpha_1}\right]$$

$$= \underbrace{\Pr\left[\gamma_0\Psi^2 < \alpha_1, \gamma_0 < \frac{Q}{g_{(w+2)k}}\right]}_{\Upsilon_1}$$

(9)

$$+ \underbrace{\Pr\left[\frac{Q}{g_{(w+2)k}}\Psi^2 < \alpha_1, \gamma_0 \geq \frac{Q}{g_{(w+2)k}}\right]}_{\Upsilon_2}.$$

To analyze the probability $OP_{S_p}^{out}$ in (9), the CDFs and PDFs of the RV Ψ and $g_{(w+2)k}$ are presented by Lemma 1 and Lemma 2, respectively.

Lemma 1 *From* (6), Ψ *is the sum of T independent and identical double Rayleigh RVs, the PDF of the Ψ can be tightly approximated as the first term of a Laguerre series expansion* [38](*eq.2.76*) *and is given as follows* [5]

$$f_\Psi(x) \simeq \frac{x^a}{b^{a+1}\Gamma(a+1)}\exp\left(-\frac{x}{b}\right),$$

(10)

and CDF is obtained in (11)

$$F_\Psi(x) \simeq \frac{\gamma\left(a+1, \frac{x}{b}\right)}{\Gamma(a+1)} = 1 - \frac{\Gamma\left(a+1, \frac{x}{b}\right)}{\Gamma(a+1)},$$

(11)

where $a = \frac{k_1^2}{k_2} - 1$; $b = \frac{k_2}{k_1}$; $k_1 = \frac{T\pi}{4\sqrt{\lambda_1\lambda_2}}$ and $k_2 = \frac{T}{\lambda_1\lambda_2}\left(1 - \frac{\pi^2}{16}\right)$.

Proof See the proof of Lemma 1 in Appendix A.

Lemma 2 *We have* $g_{(w+2)k} = \max_{i=1...K} g_{(w+2)i}$, *so the CDF of the RV* $g_{(w+2)k}$ *is found as* [14, 34]

$$F_{g_{(w+2)k}}(x) = \Pr\left[\max_{i=1...K} g_{(w+2)i} < x\right]$$

$$= \prod_{i=1}^{K}\Pr[g_{(w+2)i} < x] = \prod_{i=1}^{K}F_{g_{(w+2)i}}(x).$$

(12)

The estimated channel gains $g_{(w+2)i} = |h_{(w+2)i}|^2$ are exponentially distributed RVs with CDF $F_{g_{(w+2)i}}(x) = 1 - e^{-\lambda_{(w+2)}x}$ [39], so we have

$$F_{g_{(w+2)k}}(x) = \left(1 - e^{-\lambda_{(w+2)}x}\right)^K = \sum_{m=0}^{K}(-1)^m\binom{m}{K}e^{-(w+2)mx}.$$

(13)

And the PDF of the RV $g_{(w+2)k}$ is expressed as follows

$$f_{g_{(w+2)k}}(x) = K\lambda_{(w+2)}\left(1 - e^{-\lambda_{(w+2)}x}\right)^{K-1}e^{-\lambda_{(w+2)}x}$$

$$= K\lambda_{(w+2)}\sum_{m=0}^{K-1}(-1)^m\binom{m}{K-1}e^{-\lambda_{(w+2)}mx}.$$

(14)

Then we find the expression Υ_1 of the formula (9). The Υ_1 can rewrite as follows

$$\Upsilon_1 = \Pr\left[\Psi < \sqrt{\frac{\alpha_1}{\gamma_0}}, g_{(w+2)k} < \frac{Q}{\gamma_0}\right] = F_\Psi\left(\sqrt{\frac{\alpha_1}{\gamma_0}}\right)$$

$$\times F_{g_{(w+2)k}}\left(\frac{Q}{\gamma_0}\right).$$

(15)

Substituting (11) and (13) into (15), we have

$$\Upsilon_1 = \frac{\gamma\left(a+1, \frac{1}{b}\sqrt{\frac{\alpha_1}{\gamma_0}}\right)}{\Gamma(a+1)} \times \left(1 - e^{-\lambda_{(w+2)}Q/\gamma_0}\right)^K.$$

(16)

Next the Υ_2 expression in the formula (9) can be rewritten and calculated as follows

$$\Upsilon_2 = \Pr\left[\Psi < \underbrace{\sqrt{\alpha_1/Q}}_{\alpha_2}\sqrt{g_{(w+2)k}}, g_{(w+2)k} \ge \underbrace{Q/\gamma_0}_{\alpha_3}\right] \quad (17)$$
$$= \int_{\alpha_3}^{\infty} f_{g_{(w+2)k}}(x) \times F_{\Psi}(\alpha_2\sqrt{x})dx.$$

For easy calculation, we dispense the formula (17) into two integrations as follows

$$\Upsilon_2 = \underbrace{\int_0^{\infty} f_{g_{(w+2)k}}(x) \times F_{\Psi}(\alpha_2\sqrt{x})dx}_{\zeta_1} - \underbrace{\int_0^{\alpha_3} f_{g_{(w+2)k}}(x) \times F_{\Psi}(\alpha_2\sqrt{x})dx}_{\zeta_2}. \quad (18)$$

Substituting (11) and (14) into the expression ζ_1 of (18), we have

$$\zeta_1 = \int_0^{\infty} K\lambda_{(w+2)}\left(1 - e^{-\lambda_{(w+2)}x}\right)^{K-1}e^{-\lambda_{(w+2)}x}\frac{\gamma(a+1,\frac{\alpha_2}{b}\sqrt{x})}{\Gamma(a+1)}dx$$
$$= K\left(\frac{\alpha_2}{2b\sqrt{\lambda_{(w+2)}}}\right)^{(a+\frac{1}{2})}\sum_{m=0}^{K-1}\binom{m}{K-1}(-1)^m(m+1)^{-\frac{1}{2}(a+\frac{5}{2})}$$
$$\times e^{\left(\frac{\alpha_2^2}{8b^2\lambda_{(w+2)}(m+1)}\right)}W_{-\frac{1}{2}(a+1/2),-\frac{1}{4}}\left(\frac{\alpha_2^2}{4b^2\lambda_{(w+2)}(m+1)}\right). \quad (19)$$

The expression ζ_2 in the formula (18) is shown in two forms: the integral expression and the infinite sum expression. In the first form, we substitute (11) and (14) into the expression ζ_2, so the integral expression form is obtained below:

$$\zeta_2 = \int_0^{\alpha_3} K\lambda_{(w+2)}\left(1 - e^{-\lambda_{(w+2)}x}\right)^{K-1}e^{-\lambda_{(w+2)}x} \times \left(1 - \frac{\Gamma(a+1,\frac{x}{b})}{\Gamma(a+1)}\right)dx$$
$$= (1 - e^{-\lambda_{(w+2)}\alpha_3})^K - \int_0^{\alpha_3} K\lambda_{(w+2)}\left(1 - e^{-\lambda_{(w+2)}x}\right)^{K-1}e^{-\lambda_{(w+2)}x}$$
$$\times \frac{\Gamma(a+1,\frac{\alpha_2}{b}\sqrt{x})}{\Gamma(a+1)}dx. \quad (20)$$

In the remaining form , solving the integral problem, we get the result in the infinite sum expression as the formula (21)

$$\zeta_2 = \int_0^{\alpha_3} K\lambda_{(w+2)}\left(1 - e^{-\lambda_{(w+2)}x}\right)^{K-1}e^{-\lambda_{(w+2)}x}\frac{\gamma(a+1,\frac{\alpha_2}{b}\sqrt{x})}{\Gamma(a+1)}dx$$
$$= \frac{K\lambda_{(w+2)}}{\Gamma(a+1)}\sum_{n=0}^{\infty}\frac{(-1)^n}{n!(a+1+n)}\sum_{m=0}^{K-1}\binom{m}{K-1}(-1)^m\left(\lambda_{(w+2)}(m+1)\right)^{-\left(\frac{1}{2}(a+1+n)+1\right)}$$
$$\times \gamma\left(\frac{1}{2}(a+1+n)+1, \lambda_{(w+2)}(m+1)\alpha_3\right). \quad (21)$$

Substituting (16) and (18) into (9), and then using (20) and (21), we obtain $OP_{S_p}^{out}$ in two forms as (22) and (23), respectively:

$$OP_{S_p}^{out} = \frac{\gamma\left(a+1,\frac{1}{b}\sqrt{\frac{\alpha_1}{\gamma_0}}\right)}{\Gamma(a+1)} \times \left(1 - e^{-\lambda_{(w+2)}Q/\gamma_0}\right)^K +$$
$$+ K\left(\frac{\alpha_2}{2b\sqrt{\lambda_{(w+2)}}}\right)^{(a+\frac{1}{2})}\sum_{m=0}^{K-1}\binom{m}{K-1}(-1)^m(m+1)^{-\frac{1}{2}(a+\frac{5}{2})}e^{\left(\frac{\alpha_2^2}{8b^2\lambda_{(w+2)}(m+1)}\right)} \times$$
$$\times W_{-\frac{1}{2}(a+1/2),-\frac{1}{4}}\left(\frac{\alpha_2^2}{4b^2\lambda_{(w+2)}(m+1)}\right) - (1 - e^{-\lambda_{(w+2)}\alpha_3})^K +$$
$$+ \int_0^{\alpha_3} K\lambda_{(w+2)}\left(1 - e^{-\lambda_{(w+2)}x}\right)^{K-1}e^{-\lambda_{(w+2)}x}\frac{\Gamma(a+1,\frac{\alpha_2}{b}\sqrt{x})}{\Gamma(a+1)}dx, \quad (22)$$

$$OP_{S_p}^{out} = \frac{\gamma\left(a+1,\frac{1}{b}\sqrt{\frac{\alpha_1}{\gamma_0}}\right)}{\Gamma(a+1)} \times \left(1 - e^{-\lambda_{(w+2)}Q/\gamma_0}\right)^K +$$
$$K\left(\frac{\alpha_2}{2b\sqrt{\lambda_{(w+2)}}}\right)^{(a+\frac{1}{2})}\sum_{m=0}^{K-1}\binom{m}{K-1}(-1)^m(m+1)^{-\frac{1}{2}(a+\frac{5}{2})} \times$$
$$e^{\left(\frac{\alpha_2^2}{8b^2\lambda_{(w+2)}(m+1)}\right)} \times W_{-\frac{1}{2}(a+1/2),-\frac{1}{4}}\left(\frac{\alpha_2^2}{4b^2\lambda_{(w+2)}(m+1)}\right) - \frac{K\lambda_{(w+2)}}{\Gamma(a+1)} \times$$
$$\sum_{n=0}^{\infty}\frac{(-1)^n}{n!(a+1+n)}\sum_{m=0}^{K-1}\binom{m}{K-1}(-1)^m\left(\lambda_{(w+2)}(m+1)\right)^{-\left(\frac{1}{2}(a+1+n)+1\right)} \times$$
$$\gamma\left(\frac{1}{2}(a+1+n)+1, \lambda_{(w+2)}(m+1)\alpha_3\right). \quad (23)$$

Remark 1 The infinite sum form in (23) can be evaluated for accuracy by the error metric [40] as

$$\xi_p = \frac{\left|OP_{S_p}^{out}(22) - OP_{S_p}^{out}(23)\right|}{OP_{S_p}^{out}(22)}, \quad (24)$$

where $OP_{S_p}^{out}(22)$ and $OP_{S_p}^{out}(23)$ are the exact OP form obtained by (22) and the approximated OP form taken by (23) of the S_p, respectively.

Remark 2 In special case as $\gamma_0 \to +\infty$ then $e^{-\lambda_{(w+2)}Q/\gamma_0} \to 1 \Rightarrow \Upsilon_1 \to 0$ and $\alpha_3 \to 0 \Rightarrow \Upsilon_2 \to \zeta_1$ we obtain asymptotic expression as

$$OP_{S_p}^{out,\gamma_0\to\infty} = \zeta_1 = K\left(\frac{\alpha_2}{2b\sqrt{\lambda_{(w+2)}}}\right)^{\left(a+\frac{1}{2}\right)} \times \sum_{m=0}^{K-1}\binom{m}{K-1}(-1)^m\times$$

$$\times(m+1)^{-\frac{1}{2}\left(a+\frac{5}{2}\right)}e^{\left(\frac{\alpha_2^2}{8b^2\lambda_{(w+2)}(m+1)}\right)}W_{-\frac{1}{2}(a+1/2),-\frac{1}{4}}\left(\frac{\alpha_2^2}{4b^2\lambda_{(w+2)}(m+1)}\right).$$

$$(25)$$

Remark 3 In special case as $Q \to +\infty$ then $e^{-\lambda_{(w+2)}Q/\gamma_0} \to 0$, $\alpha_2 \to 0$ and $\alpha_3 \to +\infty$ we obtain asymptotic expression as

$$OP_{S_p}^{out,Q\to\infty} = \frac{\gamma\left(a+1,\frac{1}{b}\sqrt{\frac{\alpha_1}{\gamma_0}}\right)}{\Gamma(a+1)}. \qquad (26)$$

4 Results and discussions

In this section, we compare the theoretical and simulation results for OPs of the two secondary sources of the proposed MPR-UTW-RIS system with different system parameters. The Monte-Carlo method is used all through computer simulations to validate the analyzed expressions. We set coordinates of the nodes S_1, S_2, the PR and the RIS as $S_1(0,0)$, $S_2(1,0)$, $PR(x_{PR}, y_{PR})$, $RIS(x_R, y_R)$, where $0 < x_R < 1$. So we have the normalized distances $d_1 = \sqrt{x_R^2 + y_R^2}$, $d_2 = \sqrt{(1-x_R)^2 + y_R^2}$, $d_3 = \sqrt{(x_{PR})^2 + (y_{PR})^2}$, and $d_4 = \sqrt{(1-x_{PR})^2 + y_{PR}^2}$. The threshold data rate fixed as $R_{th} = 1(bits/s/Hz)$, the path-loss exponent is $\beta = 3$, and Q (dB) on the x-axis is defined as $Q = 10 \times \log_{10}(I/N_o)$ (dB). Additionally, we compare our proposed model with the AF relay-supported underlay two-way model [24, 33]. All the figures, solid lines denote analyzed results and markers indicate simulated ones.

Figure 2 evaluates the error metric ξ_p (%) in (24) versus term number of infinity sum (denoted I_n) when $Q = -5$ (dB), $\gamma_0 = -15$ (dB), $\mu = 0.5$, $K = 15$, $x_R = 0.5$, $y_R = -0.5$, $x_{PR} = 0.5$, $y_{PR} = 1$, $p \in \{1, 2\}$, and $T \in \{7, 10, 15\}$. From Fig. 2, when the number of reconfigurable reflectors T increases, we need the smaller term number of infinity sum (I_n) in (23) to achieve a better approximation, e.g. $\xi_p < 0.02\%$ at $I_n \geq 1$ with $T = 15$. Therefore, the infinity-sum formed OP of the S_p as in (23) can be meet to the exact form as in (22) at the larger number of reconfigurable reflectors with the limited number of the sum. Table 2 shows the detail of the error value
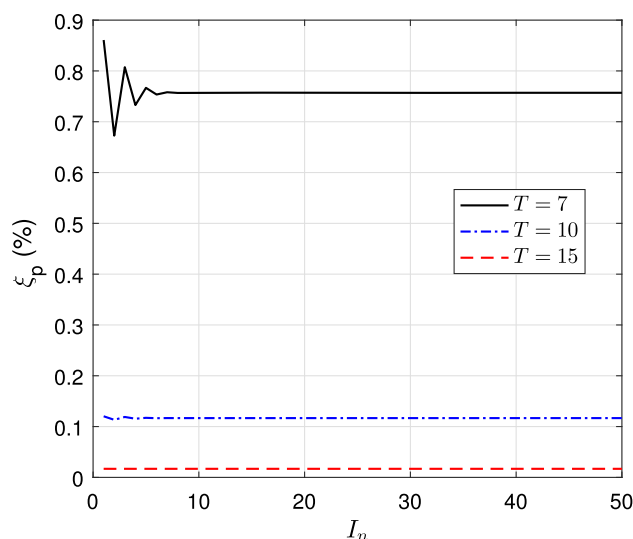
Fig. 2 The error metric ξ_p (%) versus I_n when $Q = -5$ (dB), $\gamma_0 = -15$ (dB), $\mu = 0.5$, $K = 15$, $x_R = 0.5$, $y_R = -0.5$, $x_{PR} = 0.5$, $y_{PR} = 1$, and $T \in \{7, 10, 15\}$

Table 2 Minimum the error value corresponding to the number of reconfigurable reflectors and the term number of infinity sum for parameters $Q = -5$ (dB), $\gamma_0 = -15$ (dB), $\mu = 0.5$, $K = 15$, $x_R = 0.5$, $y_R = -0.5$, $x_{PR} = 0.5$, $y_{PR} = 1$

T	I_n	$\xi_p(\%)$
7	$I_n > 10$	0.757%
10	$I_n > 5$	0.117%
15	$I_n > 1$	0.017%

[41] corresponding to the number of reconfigurable reflectors and the term number of infinity sum.

Figure 3 illustrates the exact and asymptotic OPs of the two secondary sources S_1 and S_2 versus Q (dB) when $\gamma_0 = -15$ (dB), $T \in \{4, 7, 10\}$, $K = 15$, $x_R = 0.5$, $y_R = -0.5$, $x_{PR} = 0.5$, $y_{PR} = 1$ as formulas (22), (23) and (26). We observe from Fig. 3 that the OPs of two secondary sources are roughly the same because our choice of the coordinate parameters of the nodes leads to the normalized distances $d_1 = d_2$ and $d_3 = d_4$. Fig. 3 exposes that in the small interference constraint parameter value region (between -25dB and -10dB), the OPs of both sources decrease when Q increases, and in the high Q value region (over -10dB), the OPs reach a saturation value. We have those results because when Q increases, the transmit powers of the S_1 and S_2 increase as in the formula (1) and lead to the SINRs are also better as in formulas (4) and (8). However, the formula (1) also shows that the transmit powers have a limit by the maximum power of each source, so when Q increases to a high threshold value, the transmit powers
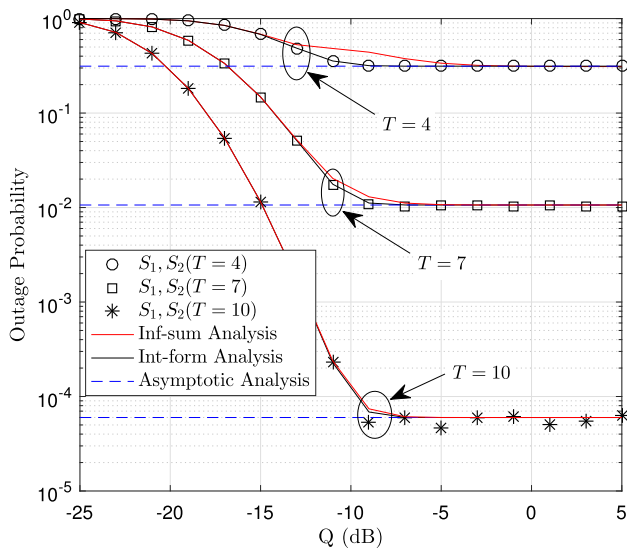
Fig. 3 The outage probabilities of the secondary sources S_1 and S_2 versus Q (dB) when $\gamma_0 = -15$ (dB), $\mu = 0.5$, $T \in \{4, 7, 10\}$, $K = 15$, $x_R = 0.5$, $y_R = -0.5$, $x_{PR} = 0.5$, $y_{PR} = 1$

cannot increase more, and the system performance attains the saturation state. Moreover, riser number of metasurfaces are, better the system performance is. Please note that the theoretical expressions of the OPs are plotted in the infinite sum and the integral forms as the formulas (22) and (23), respectively. It is observed that the lines (black solid) of the integral formula coincides perfectly with the simulation lines, while the lines (red solid) of the infinite sum formula (using the first 25 terms) are closer to the simulations when the number of metasurfaces increases.
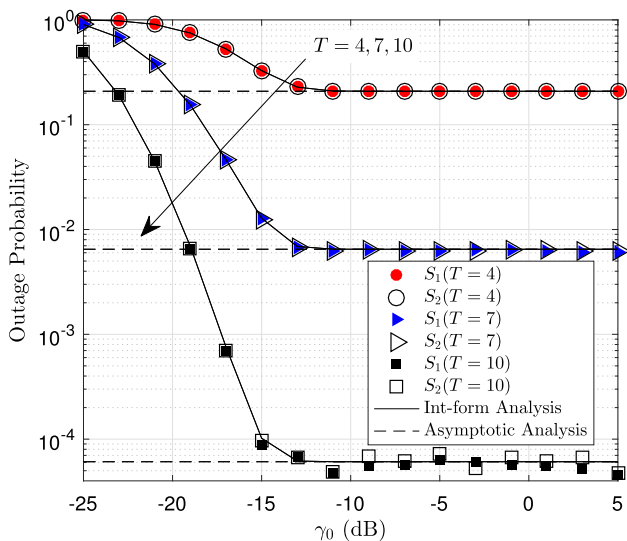
Finally, the asymptotic theory analyzes are reasonable when Q achieves to infinity values.

Figure 4 illustrates the exact and asymptotic outage probabilities of the secondary sources S_1 and S_2 versus γ_0 (dB) as formulas (22) and (25), respectively, when $Q = -10$ (dB), $T \in \{4, 7, 10\}$, $K = 15$, $x_R = 0.5$, $y_R = -0.5$, $x_{PR} = 0.5$, $y_{PR} = 1$. First observing (Fig. 4), we see that the OPs of the two sources are almost the same because we choose the coordinates of the RIS and PRs where are equidistant from the two sources. The second worth noting is that the OPs of the sources decrease rapidly when γ_0 (dB) increases between -25dB and -15dB , then stays the same value even though γ_0 (dB) still increases. This means that the maximum capacity the hardware is able to handle higher, the system performance is better, but it has a saturation value caused by the transmit powers depend on two-parameter sets as formula (1). In addition, the values of the OPs of the two sources are inverse with the number of metasurfaces similar as Fig. 3.

Figure 5 illustrates the effect of the number of primary receivers on the OPs of the secondary sources. As can be observed, when the Q value is less than -10dB, increasing the number of PRs causes an increase in OPs of the secondary sources (this means that the system performance of the secondary network will degrade when the number of PRs increases). Actually, it is clear that adding the number of PRs increases the possibility of a large channel gain between the secondary source and the PR. And this leads to a decrease in transmit power and the SINR of the secondary sources as shown in formulas (5) and (8). Though, when Q is greater than a certain value (-10dB), the number of primary receivers no longer affects the

Fig. 4 Outage probabilities of the source nodes S_1 and S_2 versus γ_0 (dB) when $Q = -10$ (dB), $\mu = 0.5$, $T \in \{4, 7, 10\}$, $K = 15$, $x_R = 0.5$, $y_R = -0.5$, $x_{PR} = 0.5$, $y_{PR} = 1$
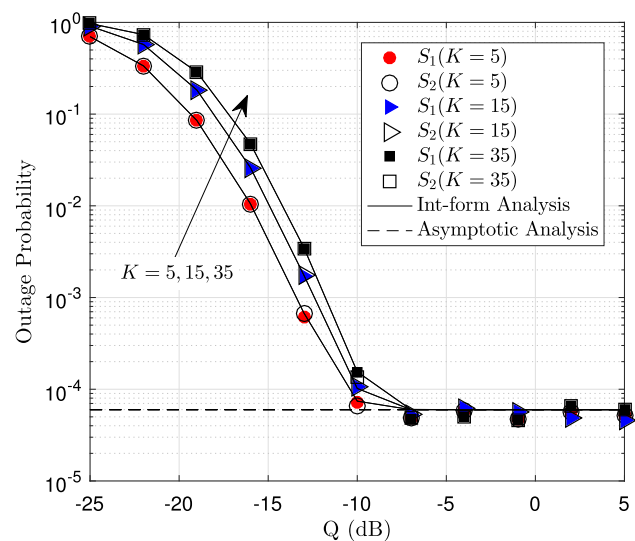
Fig. 5 The outage probabilities of the secondary sources S_1 and S_2 versus Q (dB) when $\gamma_0 = -15$ (dB), $\mu = 0.5$, $T = 10$, $K \in \{5, 15, 35\}$, $x_R = 0.5$, $y_R = -0.5$, $x_{PR} = 0.5$, $y_{PR} = 1$

performance of the secondary network. This happens because when Q is large enough the SINR will depend mainly on the limited transmission power of the secondary sources as seen in formulas (5) and (8). Finally, the OPs of the two sources are almost overlap caused of choosing the nodes coordinates the same as previous figures.

The effect of the residual loop-back interference by full-duplex mode on the OPs of the secondary sources versus Q is examined in Fig. 6. This figure shows that increasing the residual loop-back interference will degrade the performance of secondary network. And the OPs of the two secondary sources are best when $\mu = 0$, which corresponds to the perfect loop-back interference cancellation case. This result occurs because an increase in leads to a decrease in the transmit power and SINR of the sources as formulas (4) and (8). Finally, the OPs also decrease as Q increases and reach a saturation value when Q is large enough.

Figure 7 investigates the effect of the relative position of the RIS with two secondary sources on the OPs of the secondary system in case that the primary receivers are equidistant from two sources. Firstly, Fig. 7 shows that the OP curves of two sources nearly overlap. Secondly, with the same y_R values, the RIS position equidistant from two sources gives the best OP and the OPs of the sources are equal when the RIS is at positions with equal total distances from the RIS to the two sources. Finally, with the same x_R value, the OPs will decrease when the y_R changes from -0.7 to -0.4. We have those results because phase values of channel coefficients depend on the normalized distances between the sources and RIS.
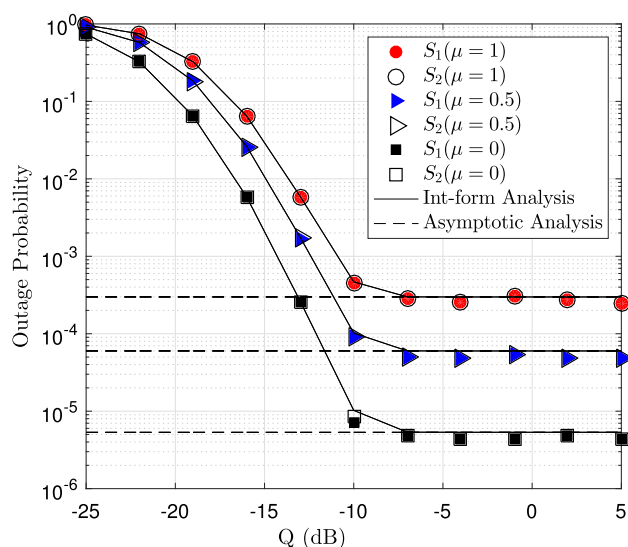
Figure 8 illustrates the influence of the relative position of the primary receivers and two sources on the OP of the secondary system. Figure 8 shows that when RIS is equidistant from sources, the farther the position of the cluster of primary receivers is, the smaller the outage probability of that source is and vice versa. Additionally, when the PRs are equidistant from the two sources, the outage probabilities of two sources are identical. In the rest cases, the source closer to PRs has a smaller outage probability and reverse. These results are obtained because when the distance between each secondary source and the PRs decreases, lead to the increase of the channel gains between these nodes and the transmit power of secondary sources will decrease as formula (1).

Figure 9 compares the outage probabilities of two secondary sources of the proposed MPR-UTW-RIS model with a two-way cooperative cognitive network model in duplex mode using AF relay similar to in paper [24], but there are some changes that use only one AF relay and equip multiple primary receivers. Besides, in order to increase the fairness in the comparison between RIS and relay, assume that the relay cancels perfectly the loop-back interference caused by the full-duplex mode. The transmit power of relay is chosen to be equal to the maximum transmit power of the two secondary sources. The results show that the system with RIS supporting communication has much better performance than the system using AF relay even in the case of only one metasurface.

5 Conclusions

In this article, we proposed and investigated the underlay two-way RIS scheme with two secondary sources and multiple primary receivers, known as the MPR-UTW-RIS scheme. To evaluate the system performance, the paper investigated the outage probability via parameters such as Q (dB), $Pmax/N_0$(dB), number of reflected elements of RIS, number of primary receivers, the residual loop-back interference due to duplex transmission, the distances between RIS and two sources, and the distances between primary receivers and two sources. The notable results are that the system performance increases by increasing of the number of reflected elements, Q, $Pmax/N_0$, the distance between the primary receivers cluster and two secondary sources, and by decreasing of the residual loop-back interference due to duplex transmission. Moreover, the parameters Q and $Pmax/N_0$(dB) have a threshold value in that the outage probabilities will fall into a saturation state, meaning the outage probabilities do not decrease even though these parameters still increase. Besides, when the number of primary receivers increases, the outage probabilities increase if the Q values are in the smaller region,

Fig. 6 The outage probabilities of the secondary sources S_1 and S_2 versus Q (dB) when $\gamma_0 = -15$ (dB), $\mu \in \{0, 0.5, 1\}$, $T = 10$, $K = 15$, $x_R = 0.5$, $y_R = -0.5$, $x_{PR} = 0.5$, $y_{PR} = 1$

Fig. 7 The outage probabilities of the secondary sources S_1 and S_2 versus x_R and y_R when $\gamma_0 = -15$ (dB), $Q \in \{-10, -15\}$ (dB), $\mu = 0.5$, $T = 10$, $K = 15$, $x_{PR} = 0.5$, $y_{PR} = 1$
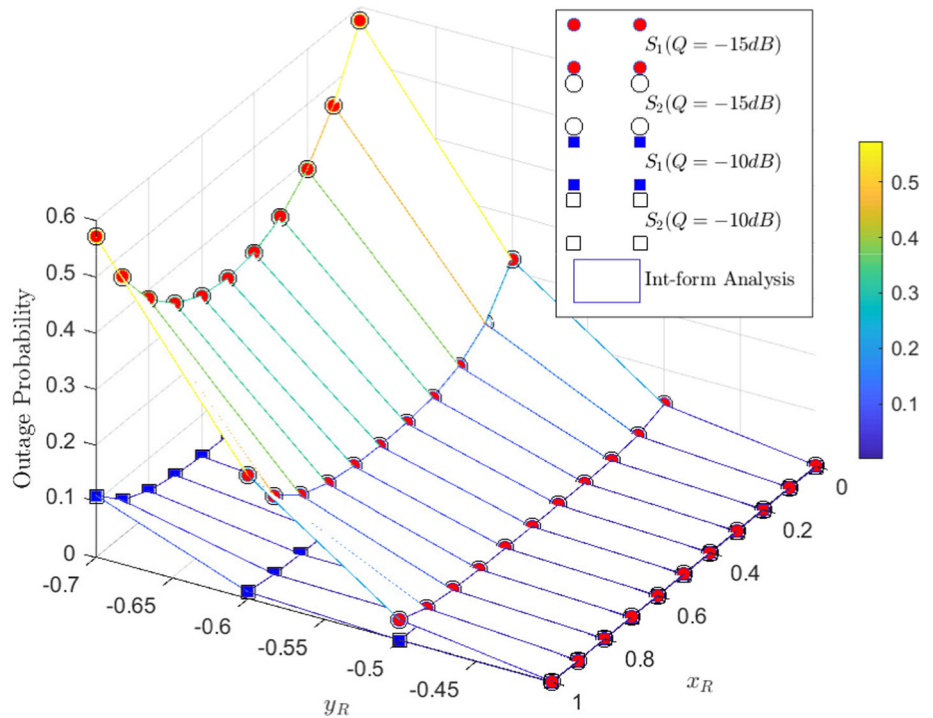
Fig. 8 The outage probabilities of the secondary sources S_1 and S_2 versus x_{PR} and y_{PR} when $\gamma_0 = -15$ (dB), $Q = -15$ (dB), $\mu = 0.5$, $T = 10$, $K = 15$, $x_R = 0.5$, $y_R = 0.5$
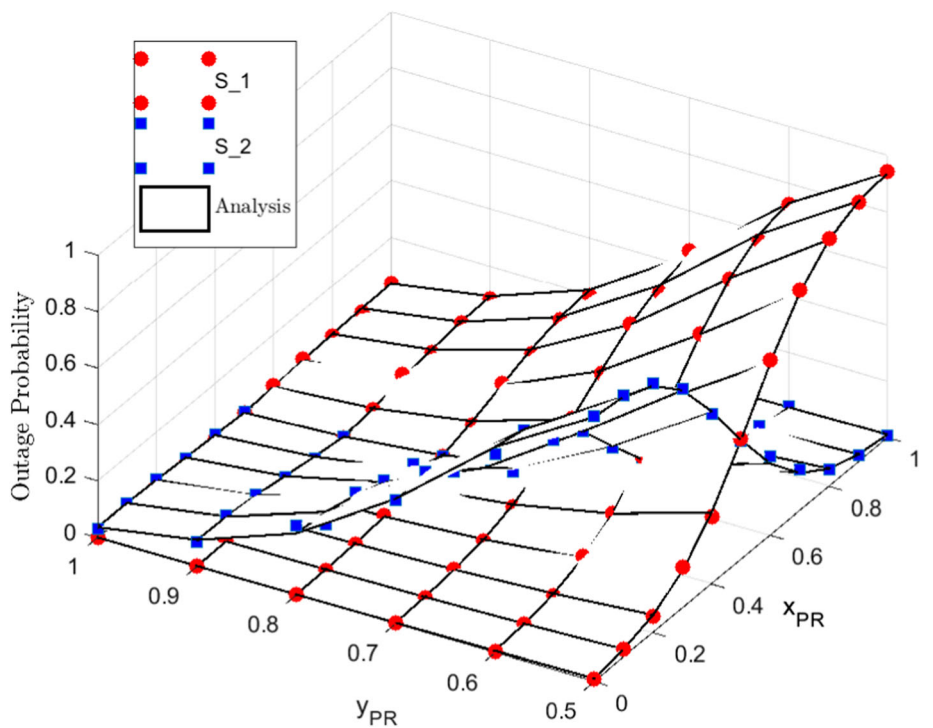
but in the large Q value region, the outage probabilities reach the saturation value region and this value is equal with all the number of primary receivers, it means when Q reaches a sufficiently large value, the number of PRs no longer affects the system's performance. Furthermore, the RIS position equidistant from the two sources gives the best outage probability for both secondary sources when the primary receiver cluster is equidistant from two sources. Next, an important point is evident that RIS-supported two-way systems have system performance outperform the corresponding AF relay-supported ones. Lastly, the
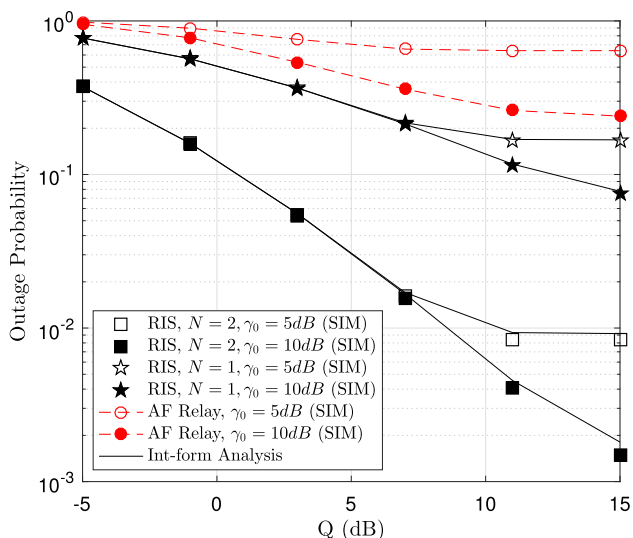
Fig. 9 The outage probabilities of the secondary sources S_1 and S_2 of the protocols MPR-UTW-RIS and two-way full-duplex -AF relay in paper [21] versus Q when $\gamma_0 \in \{5, 10\}$ (dB), $\mu = 0.5$, $T = 2$, $K = 15$, $x_R = 0.5$, $y_R = -0.5$, $x_{PR} = 0.5$, $y_{PR} = 1$

analysis results of the outage probabilities were justified by the Monte Carlo simulations.

Appendix A: Proof of Lemma 1

From (6), Ψ is the sum of T independent and identical double Rayleigh RVs, the PDF and CDF of the Ψ can be tightly approximated as in (10), (11) where the related parameters k_1 and k_2 are solved as [38] (eq.2.74).

$$k_1 = E[\Psi] = E\left[\sum_{t=1}^{T} |h_{1t}| \times |h_{2t}|\right] = \sum_{t=1}^{T} E[|h_{1t}|] \times E[|h_{2t}|],$$
(A.1)

and

$$k_2 = V[\Psi] = V\left[\sum_{t=1}^{T} |h_{1t}| \times |h_{2t}|\right].$$
(A.2)

Likewise $|h_{1t}|$ and $|h_{2t}|$ are independent RVs and follow Rayleigh distribution with variances as $1/\lambda_1$ and $1/\lambda_2$, respectively. Thus [42] (p.162)

$$E[|h_{1t}|] = \sqrt{\frac{\pi}{4\lambda_1}}, E[|h_{2t}|] = \sqrt{\frac{\pi}{4\lambda_2}},$$
(A.3)

$$V[|h_{1t}|] = \left(1 - \frac{\pi}{4}\right)\frac{1}{\lambda_1}, V[|h_{2t}|] = \left(1 - \frac{\pi}{4}\right)\frac{1}{\lambda_2}.$$
(A.4)

Substituting (A.3) into (A.1), we obtain:

$$k_1 = E[\Psi] = \frac{T\pi}{4\sqrt{\lambda_1 \lambda_2}}.$$
(A.5)

Since $|h_{1t}|$ and $|h_{2t}|$ are independent RVs, (A.2) can be rewritten as:

$$k_2 = E\left[\left(\sum_{t=1}^{T} |h_{1t}| \times |h_{2t}|\right)^2\right] - k_1^2 = \sum_{t=1}^{T} E\left[|h_{1t}|^2\right] \times$$
$$E\left[|h_{2t}|^2\right] + +T(T-1)(E[|h_{1v}|]) \times$$
$$(E[|h_{2v}|])(E[|h_{1u}|]) \times (E[|h_{2u}|]) - k_1^2,$$
(A.6)

where $u, v \in \{1, 2, ..., T\}$ and $u \neq v$.

Besides $E[X^2] = V[X] + (E[X])^2$ and substituting (A.3) and (A.4) into (A.6), we obtain:

$$k_2 = \sum_{t=1}^{T} \left(V[|h_{1t}|] + (E[|h_{1t}|])^2\right) \times \left(V[|h_{2t}|] + (E[|h_{2t}|])^2\right) +$$
$$+T(T-1)(E[|h_{1v}|]) \times (E[|h_{2v}|])(E[|h_{1u}|]) \times (E[|h_{2u}|]) - k_1^2$$
$$= T\left(\left(1 - \frac{\pi}{4}\right)\frac{1}{\lambda_1} + \frac{\pi}{4\lambda_1}\right) \times \left(\left(1 - \frac{\pi}{4}\right)\frac{1}{\lambda_2} + \frac{\pi}{4\lambda_2}\right) +$$
$$+T(T-1)\sqrt{\frac{\pi}{4\lambda_1}}\sqrt{\frac{\pi}{4\lambda_2}}\sqrt{\frac{\pi}{4\lambda_1}}\sqrt{\frac{\pi}{4\lambda_2}} - \left(\frac{T\pi}{4\sqrt{\lambda_1\lambda_2}}\right)^2$$
$$= \frac{T}{\lambda_1\lambda_2}\left(1 - \frac{\pi^2}{16}\right).$$
(A.7)

The Lemma 1 is proven completely.

References

1. Basar, E., Di Renzo, M., De Rosny, J., Debbah, M., Alouini, M.-S., & Zhang, R. (2019). Wireless communications through reconfigurable intelligent surfaces. *IEEE Access, 7*, 116753–116773.
2. Liaskos, C., Nie, S., Tsioliaridou, A., Pitsillides, A., Ioannidis, S., & Akyildiz, I. (2018). A new wireless communication paradigm through software-controlled metasurfaces. *IEEE Communications Magazine, 56*, 162–169.
3. Hou, T., Liu, Y., Song, Z., Sun, X., Chen, Y., & Hanzo, L. (2020). Reconfigurable intelligent surface aided NOMA networks. *IEEE Journal on Selected Areas in Communications, 38*, 2575–2588.
4. Wu, Q., & Zhang, R. (2019). Towards smart and reconfigurable environment: Intelligent reflecting surface aided wireless network. *IEEE Communications Magazine, 58*, 106–112.
5. Boulogeorgos, A.-A.A., & Alexiou, A. (2020). Performance analysis of reconfigurable intelligent surface-assisted wireless systems and comparison with relaying. *IEEE Access, 8*, 94463–94483.

6. Diamanti, M., Tsampazi, M., Tsiropoulou, E. E., & Papavassiliou, S. (2021). Energy efficient multi-user communications aided by reconfigurable intelligent surfaces and UAVs. *IEEE International Conference on Smart Computing (SMARTCOMP), 2021,* 371–376.

7. Shi, Z., Wang, H., Fu, Y., Yang, G., Ma, S., & Gao, F. (2021) Outage analysis of reconfigurable intelligent surface aided MIMO communications with statistical CSI. *IEEE Transactions on Wireless Communications.*

8. Perović, N. S., Tran, L.-N., Di Renzo, M., & Flanagan, M. F. (2021) Achievable rate optimization for MIMO systems with reconfigurable intelligent surfaces. *IEEE Transactions on Wireless Communications.*

9. Du, H., Zhang, J., Guan, K., Ai, B., & Kürner, T. (2020) Reconfigurable intelligent surface aided TeraHertz communications under misalignment and hardware impairments,. arXiv preprint arXiv:2012.00267.

10. Chapala, V. K., & Zafaruddin, S. (2021). Exact analysis of RIS-aided THz wireless systems over $\alpha - \mu$ fading with pointing errors. *IEEE Communications Letters, 25,* 3508–3512.

11. Zhang, J., Du, H., Sun, Q., Ai, B., & Ng, D. W. K. (2021). Physical layer security enhancement with reconfigurable intelligent surface-aided networks. *IEEE Transactions on Information Forensics and Security*

12. Son, P. N., & Kong, H. Y. (2017). Improvement of the two-way decode-and-forward scheme by energy harvesting and digital network coding relay. *Transactions on Emerging Telecommunications Technologies, 28,* e2960.

13. Son, P. N., & Duy, T. T. (2020). A new approach for two-way relaying networks: Improving performance by successive interference cancellation, digital network coding and opportunistic relay selection. *Wireless Networks, 26,* 1315–1329.

14. Dao, T.-T. T., & Son, P. N. (2021) Cancel-decode-encode processing on two-way cooperative NOMA schemes in realistic conditions. *Wireless Communications and Mobile Computing 2021*

15. Yue, X., Liu, Y., Kang, S., Nallanathan, A., & Chen, Y. (2018). Modeling and analysis of two-way relay non-orthogonal multiple access systems. *IEEE Wireless Communications and Networking Conference (WCNC), 66,* 3784–3796.

16. Atapattu, S., Fan, R., Dharmawansa, P., Wang, G., & Evans, J. (2020). Two-way communications via reconfigurable intelligent surface. *IEEE Wireless Communications and Networking Conference (WCNC), 2020,* 1–6.

17. Atapattu, S., Fan, R., Dharmawansa, P., Wang, G., Evans, J., & Tsiftsis, T. A. (2020). Reconfigurable intelligent surface assisted two-way communications: Performance analysis and optimization. *IEEE Transactions on Communications, 68,* 6552–6567.

18. Peng, Z., Zhang, Z., Pan, C., Li, L., & Swindlehurst, A. L. (2021). Multiuser full-duplex two-way communications via intelligent reflecting surface. *IEEE Transactions on Signal Processing, 69,* 837–851.

19. Akyildiz, I. F., Lee, W.-Y., Vuran, M. C., & Mohanty, S. (2006). NeXt generation/dynamic spectrum access/cognitive radio wireless networks: A survey. *Computer Networks, 50,* 2127–2159.

20. Goldsmith, A., Jafar, S. A., Maric, I., & Srinivasa, S. (2009). Breaking spectrum gridlock with cognitive radios: An information theoretic perspective. *Proceedings of the IEEE, 97,* 894–914.

21. Al-Zubi, R. T., Abu Issa, M. T., Jebreil, O., Darabkh, K. A., & Khattabi, Y. (2020) Outage performance of cognitive two-way amplify-and-forward relay network under different transmission schemes. *Transactions on Emerging Telecommunications Technologies,* p. e4004.

22. Zhang, X., Zhang, Z., Xing, J., Yu, R., Zhang, P., & Wang, W. (2014). Exact outage analysis in cognitive two-way relay networks with opportunistic relay selection under primary user's interference. *IEEE Transactions on Vehicular Technology, 64,* 2502–2511.

23. Son, P. N., Duy, T. T., & Ho-Van, K. (2020) SIC-coding schemes for underlay two-way relaying cognitive networks. *Wireless Communications and Mobile Computing, 2020.*

24. Zhong, B., & Zhang, Z. (2016). Opportunistic two-way full-duplex relay selection in underlay cognitive networks. *IEEE Systems Journal, 12,* 725–734.

25. Rodriguez, L. J., Tran, N. H., & Le-Ngoc, T. (2014). Performance of full-duplex AF relaying in the presence of residual self-interference. *IEEE Journal on Selected Areas in Communications, 32,* 1752–1764.

26. Cheng, X., Yu, B., Cheng, X., & Yang, L. (2013) Two-way full-duplex amplify-and-forward relaying. *MILCOM 2013–2013 IEEE Military Communications Conference* pp. 1–6.

27. Yuan, J., Liang, Y.-C., Joung, J., Feng, G., & Larsson, E. G. (2020) Intelligent reflecting surface (IRS)-enhanced cognitive radio system. *ICC 2020–2020 IEEE International Conference on Communications (ICC)* pp. 1–6.

28. Xu, D., Yu, X., Sun, Y., Ng, D. W. K., & Schober, R. (2020). Resource allocation for IRS-assisted full-duplex cognitive radio systems. *IEEE Transactions on Communications, 68,* 7376–7394.

29. Ni, Y., Liu, Y., Wang, J., Wang, Q., Zhao, H., & Zhu, H. (2021). Performance analysis for RIS-assisted D2D communication under Nakagami-m fading. *IEEE Transactions on Vehicular Technology.*

30. Dao, T.-T.T., & Son, P. N. (2021). Two-way cognitive network supported by reconfigurable intelligent surface. *International Conference on Advanced Technologies for Communications (ATC), 2021,* 7–12.

31. Ryzhik, I. S. G. a. I. M. (2007). Table of integrals, series, and products, Seventh ed., Elsevier.

32. Yang, L., Yang, Y., Costa, D. B. d., & Trigui, I. (2021). Outage probability and capacity scaling law of multiple RIS-aided networks. *IEEE Wireless Communications Letters, 10*(2), 256–260.

33. Al-Zubi, R. T., Issa, M. T. A., Zghoul, A. A., Darabkh, K. A., & Khattabi, Y. M. (2020). Analysis of system outage probability in underlay cognitive two-way amplify-and-forward relay networks. *Computer Communications, 160,* 253–262.

34. Van Toan, H., Bao, V.-N.Q., & Nguyen-Le, H. (2017). Cognitive two-way relay systems with multiple primary receivers: Exact and asymptotic outage formulation. *IET Communications, 11,* 2490–2497.

35. Tang, W., Chen, M. Z., Chen, X., Dai, J. Y., Han, Y., Di Renzo, M., et al. (2020). Wireless communications with reconfigurable intelligent surface: Path loss modeling and experimental measurement. *IEEE Transactions on Wireless Communications, 20,* 421–439.

36. Le, C.-B., Do, D.-T., Li, X., Huang, Y.-F., Chen, H.-C., & Voznak, M. (2021). Enabling NOMA in backscatter reconfigurable intelligent surfaces-aided systems. *IEEE Access, 9,* 33782–33795.

37. Zhao, W., Wang, G., Atapattu, S., Tsiftsis, T. A., & Tellambura, C. (2020). Is backscatter link stronger than direct link in reconfigurable intelligent surface-assisted system? *IEEE Communications Letters, 24,* 1342–1346.

38. Primak, S., Kontorovich, V., & Lyandres, V. (2004). *Stochastic methods and their applications to communications, Stochastic differential equations approach.* Wiley.

39. Son, P. N., & Kong, H. Y. (2014). Exact outage probability of two-way decode-and-forward scheme with opportunistic relay selection under physical layer security. *Wireless Personal Communications, 77,* 2889–2917.

40. López, O. L. A., Fernández, E. M. G., Souza, R. D., & Alves, H. (2018). Ultra-reliable cooperative short-packet communications

with wireless energy transfer. *IEEE Sensors Journal, 18*, 2161–2177.

41. Du, H., Zhang, J., Cheng, J., & Ai, B. (2021). Millimeter wave communications with reconfigurable intelligent surfaces: Performance analysis and optimization. *IEEE Transactions on Communications, 69*, 2752–2768.

42. Papoulis, A., & Pillai, S. U. (2002). Probability random variables and Stochastic processes, McGraw-Hill.

Publisher's Note Springer Nature remains neutral with regard to jurisdictional claims in published maps and institutional affiliations.

Thu-Thuy Thi Dao received the B.E. and M.E. degrees in electronics and telecommunications engineering from the Ho Chi Minh City University of Technology (HCMUT), Ho Chi Minh City, Vietnam, in 2001 and 2004, respectively. She is currently pursuing the Ph.D. degree with the Ho Chi Minh City University of Technology and Education (HCMUTE). She has been working as a Lecturer with the Faculty of Electronics Technology, Industrial University of Ho Chi Minh City (IUH), since 2001. Her major research interests include cooperative communication, two-way networks, physical layer security, energy harvesting, and non-orthogonal multiple access.

Pham Ngoc Son received the B.E. degree (2005) and M.Eng. degree (2009) in Electronics and Telecommunications Engineering from Post and Telecommunication Institute of Technology, Ho Chi Minh City and Ho Chi Minh City University of Technology, Vietnam, respectively. In 2015, he received the Ph.D. degree in Electrical Engineering from University of Ulsan, South Korea. He is currently a Lecturer in the Faculty of Electrical and Electronics Engineering of Ho Chi Minh City University of Technology and Education (HCMUTE). His major research interests are cooperative communication, cognitive radio, physical layer security, energy harvesting, non-orthogonal multiple access, intelligent reflecting surface and short packet communications.

ICATSD2F.111

PERFORMANCE ANALYSIS OF TWO-WAY NETWORK WITH NONLINEAR ENERGY HARVESTING RELAY AND DIGITAL NETWORK CODING

THU- THUY THI DAO[1,2], PHAM NGOC SON[2]

[1]*Industrial University of Ho Chi Minh City, Ho Chi Minh City, Vietnam*

[2]*Ho Chi Minh City University of Technology and Education, Ho Chi Minh City, Vietnam*

daothithuthuy@iuh.edu.vn, thuydtt.ncs@hcmute.edu.vn, sonpndtvt@hcmute.edu.vn

Abstract. This article studies a two-way cooperative scheme including two sources and the assist of a decode-and-forward relay which equipped a non-linear energy harvester. This scheme operates under a half-duplex mode and has three-time slots to communicate information. In two first slots, the relay uses power splitting method to harvest energy and decode signal from sources, then the digital network coding technique is used to make a new signal by the XOR operation. The relay uses harvested energy in two first time slots to send back the encoded signal to two sources. The exact expressions of the outage probabilities are analyzed to evaluate the effect of a non-linear energy harvesting on the system performance over Rayleigh fading channels. Besides, the outage probabilities of two sources are compared with cases in linear energy harvesting. Finally, the Monte Carlo simulation results verify the exactly of the analysis expressions.

Keywords. two-way network, nonlinear energy harvesting, decode-and-forward relay, digital network coding.

1 INTRODUCTION

In recent years, the fast growth number of users and applications of wireless communication have led to more challenges for wireless networks as improving system performance, spectrum efficiency and energy efficiency. Specially, energy efficiency are critical problems for low-cost and resource-constrained wireless networks like wireless sensor networks and Internet of Things systems. Energy harvesting (EH) via radio-frequency signals in wireless cooperative networks has been appealing many attentions, the relay can harvest energy from the sources signals and then spend the harvested energy to aid its transmission. There are two main methods to energy harvesting at relay base on time switching (TS) and power splitting (PS) techniques. Relay node divides the received signal into two-time phases for EH and signal decoding in TS method, whereas it splits the received signal power for EH and signal decoding in PS method [1]. The cooperative network has been well-known solution for these challenges because it brings an improvement in the performance, coverage, and reliability of wireless networks. There are two methods for relay nodes to process signals as decode-and-forward (DF) and amplify-and-forward (AF) [2]. Besides, the two-way relay network (TWR) combines with the digital network coding (DNC) technique bring to rise bandwidth use efficiency by reducing transmission time among devices [3].

In [4, 5], the performance of EH schemes for a two-way half-duplex relay model with two sources and a relay had been analyzed over block Rayleigh fading channels. The relay harvests the energy from two sources by PS protocol then using that energy to send the information back sources. In [4], the DF relay collects energy from the received signals of two sources in the first two time-slots and then uses the acquired energy and DNC technique for signal transmission in the third one. In [5], the authors use the direct channel between two sources to improve the overall performance and consider three relay styles as AF, DF and hybrid-DF. However, the authors in two papers studied the linear EH model, this may be unrealistic as the electronic devices executed in the energy harvester at the relay are nonlinear elements. The nonlinear energy-harvesting at relays was studied in [6-8]. In [6], the DF relay collects energy from the source and interference signals with TS technique in one-way network over Nakagami-m fading channels. In [7], the authors studied a hybrid TS-PS harvest energy scheme in case of transceiver hardware impairments of two-way AF relay network. In [8], the authors analyzed the outage probability (OP) of a three-step two-

way DF relay network with the nonlinear EH using PS method, where the PS ratios are animatedly changed according to instantaneous channel gains to maximize the capacity of the system.

Motivated by prior works for the two-way network to enhance spectrum utilization efficiency, system performance and energy efficiency, we propose a two-way DF relay system with two sources and a relay which equipped a non-linear energy harvester. In the proposed model, there are three-time slots to communicate information, in two first slots the relay uses PS method to harvest energy and decode signal from to sources, then it uses the DNC technique to create a new signal and uses harvested-energy to send back this signal to two sources, called as NEH-TW-DNC protocol. To evaluate the system performance, the exact expressions of the source OPs are considered. Additionally, we compare the OP of the proposed protocol with the ideal linear EH ones. Our proposed system can be applicated in low-cost and resource-constrained wireless networks like wireless sensor networks, vehicular networks and Internet of Things systems.

The rest of our article includes sections as follows. A two-way cooperative model with nonlinear energy harvesting and DNC technique is described in Section 2. Then Section 3 analyzes the OPs of the two sources. Section 4 displays the results and discussions. Lastly, Section 5 is conclusions.

The notations: $f_\square(\cdot)$ and $F_\square(\cdot)$ are the probability density function (PDF) and the cumulative distribution function (CDF) of a random variable (RV) $\square$, respectively; $Pr[\quad]$ is the probability operation; $\Gamma[.,.]$ is the upper incomplete Gamma function [9] (eq. 8.350.2) ; $X \sim CN(0, \sigma^2)$ is a complex Gaussian random variable (RV) X with zero mean and variance σ^2.

2 SYSTEM MODEL

The system model of the NEH-TW-DNC scheme gives in Figure 1. In this model, there are two sources S_1, S_2 communicate to each other through the DF relay R. The sources and the relay have a single antenna. The direct link among the sources S_1 and S_2 is absent owing to severe fading and path-loss, so communication among S_1 and S_2 just be established via relay. We denote h_{RS_i}, h_{S_iR} and d_i as the fading channel coefficients and the normalized distances between S_i and R respectively, where $i \in \{1,2\}$. The relay has a limited power and so it must harvest the energy from the radio frequency signals of two sources to send the information of these sources by working the three-time slots protocol as Table 1.
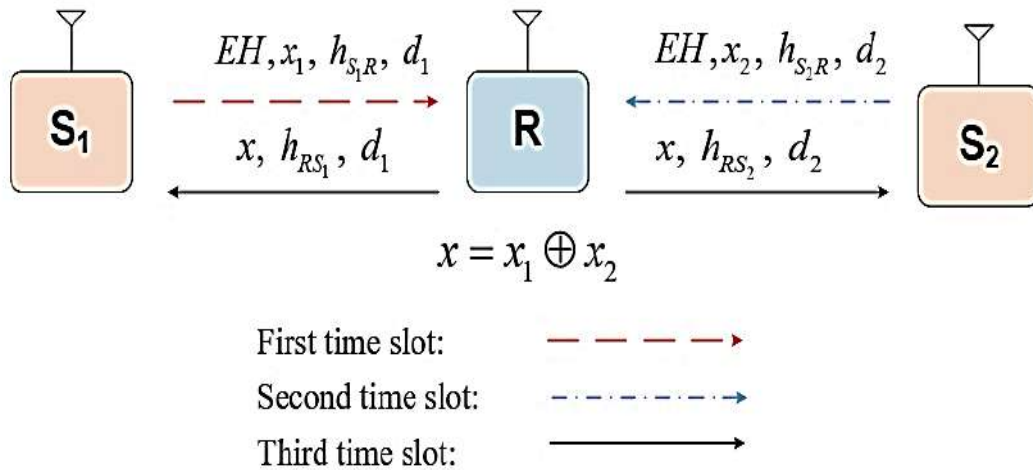
Figure 1. System model of the NEH-TW-DNC scheme.

Table 1: The three-time slots protocol of the NEH-TW-DNC scheme.

$S_1 \rightarrow R$	$S_2 \rightarrow R$	$R \rightarrow S_1, S_2$
NEH at Relay (ρ)	NEH at Relay (ρ)	$x = x_1 \oplus x_2$
Decoding signal x_1 from S_1	Decoding signal x_2 from S_2	Relay forwards signal x to sources
Time slot 1 αT	Time slot 2 αT	Time slot 3 $(1 - 2\alpha T)$
	T	

The first time slot
The receiver signals at R

$$y_{S_1 R} = \sqrt{P_1} h_{S_1 R} x_1 + n_R, \tag{1}$$

where n_R is the additive Gaussian noise $CN(0, N_0)$ at the relay.
The signal-noise ratio (SNR) at R

$$\gamma_{S_1 R} = \frac{(1-\rho)|h_{S_1 R}|^2 P_1}{N_0}. \tag{2}$$

The EH at R in the first time slot:

$$E_{h1} = \eta \rho \alpha P_1 |h_{S_1 R}|^2 T, \tag{3}$$

where $0 < \eta \le 1$ and $0 < \rho < 1$ denote the energy conversion efficiency and the power allocation efficiency, respectively.

The second time slot
The receiver signals at R:

$$y_{S_2 R} = h_{S_2 R} x_2 + n_R. \tag{4}$$

The SNR at R:

$$\gamma_{S_2 R} = \frac{(1-\rho)|h_{S_2 R}|^2 P_2}{N_0}. \tag{5}$$

The EH at R in the second time slot:

$$E_{h2} = \eta \rho \alpha P_2 |h_{S_2 R}|^2 T. \tag{6}$$

From **Error! Reference source not found.** and **Error! Reference source not found.** we have sum of EH at the R following:

$$E_h = E_{h1} + E_{h2} = \eta \rho \alpha \left(P_1 |h_{S_1 R}|^2 + P_2 |h_{S_2 R}|^2 \right) T. \tag{7}$$

Reality, the electronic devices used in the energy harvester at the relay are nonlinear elements. If the values of the input power are under the saturation threshold power P_{th}, the harvested energy is linearly relative to the input power. When the saturation effect happens, the harvested energy does not rise though the input power still rises. Hence, the transmit power of the relay is presented as [6]:

$$P_R = \frac{E_h}{(1-2\alpha)T} = \begin{cases} \frac{\eta \rho \alpha}{1-2\alpha} \left(P_1 |h_{S_1 R}|^2 + P_2 |h_{S_2 R}|^2 \right) & if \quad \left(P_1 |h_{S_1 R}|^2 + P_2 |h_{S_2 R}|^2 \right) \le P_{th} \\ \frac{\eta \rho \alpha}{1-2\alpha} P_{th} & if \quad \left(P_1 |h_{S_1 R}|^2 + P_2 |h_{S_2 R}|^2 \right) > P_{th} \end{cases}. \tag{8}$$

Assuming that the power of two source equal $P = P_1 = P_2$

$$P_R = \begin{cases} \varsigma \, P\left(\left|h_{S_1R}\right|^2 + \left|h_{S_2R}\right|^2\right) & if \quad P\left(\left|h_{S_1R}\right|^2 + \left|h_{S_2R}\right|^2\right) \le P_{th} \\ \varsigma P_{th} & if \quad P\left(\left|h_{S_1R}\right|^2 + \left|h_{S_2R}\right|^2\right) > P_{th} \end{cases}, \tag{9}$$

where $\varsigma = \frac{\eta \rho \alpha}{1-2\alpha}$.

The third time slot, the relay creates an encoded signal $x = x_1 \oplus x_2$ by the DNC techniques [10] and uses P_R to broadcasts this signal to two sources.

$$y_{RS_i} = \sqrt{P_R} h_{RS_i} x + n_{RS_i}, \tag{10}$$

$$\gamma_{RS_i} = \frac{\left|h_{RS_i}\right|^2 P_R}{N_0} = \begin{cases} \dfrac{\left|h_{RS_i}\right|^2}{N_0} \varsigma \, P\left(\left|h_{S_1R}\right|^2 + \left|h_{S_2R}\right|^2\right) & if \quad P\left(\left|h_{S_1R}\right|^2 + \left|h_{S_2R}\right|^2\right) \le P_{th} \\ \dfrac{\left|h_{RS_i}\right|^2}{N_0} \varsigma P_{th} & if \quad P\left(\left|h_{S_1R}\right|^2 + \left|h_{S_2R}\right|^2\right) > P_{th} \end{cases}. \tag{11}$$

The SNR at the source S_1, S_2 can be obtained as:

$$\gamma_{S_1} = min\{\gamma_{S_2R}, \gamma_{RS_1}\}, \gamma_{S_2} = min\{\gamma_{S_1R}, \gamma_{RS_2}\}. \tag{12}$$

The estimated channel gains $g_{S_iR} = \left|\hat{h}_{S_iR}\right|^2$ and $g_{RS_i} = \left|\hat{h}_{RS_i}\right|^2$ are exponentially distributed RVs with probability density function (PDF) and cumulative distribution function (CDF):

$$f_{g_{S_iR}}(z) = \frac{1}{\lambda_i} e^{-z/\lambda_i}, f_{g_{RS_i}}(x) = \frac{1}{\lambda_{i+2}} e^{-z/\lambda_{i+2}}, \tag{13}$$

$$F_{g_{S_iR}}(z) = 1 - e^{-z/\lambda_i}, F_{g_{RS_i}}(z) = 1 - e^{-z/\lambda_{i+2}}, \tag{14}$$

where $\lambda_i = d_i^{-\beta_i}, \lambda_{i+2} = d_{i+2}^{-\beta_{i+2}}$ and β_i, β_{i+2} are path-loss exponents.

3 OUTAGE PROBABILITY ANALYSIS

In this section, we consider the outage probabilities of the sources. The outage at S$_i$ happens when the equivalent SNR exceeds the threshold $\gamma_{S_i} < \gamma_{th}$, where $\gamma_{th} = 2^R - 1$, R(bits/s/Hz) is the threshold data rate [11]. Specifically, the outage probability of the S$_1$ in model present as:

$$OP_{S_1} = Pr[\gamma_1 \le \gamma_{th}] = Pr[\gamma_{S_2R} \le \gamma_{th}] + Pr\left[\gamma_{RS_1} \le \gamma_{th}, \gamma_{S_2R} > \gamma_{th}\right]. \tag{15}$$

Substituting (5) and (11) into (15), we obtain [6]:

$$OP_{S_1} = Pr\left[\frac{(1-\rho)\left|h_{S_2R}\right|^2 P}{N_0} \le \gamma_{th}\right] + Pr\left[\frac{\left|h_{RS_1}\right|^2}{N_0} \varsigma \le \frac{\gamma_{th}}{P_{th}}, \frac{(1-\rho)\left|h_{S_2R}\right|^2 P}{N_0} > \gamma_{th}\right] +$$

$$+ Pr\left[P\left(\left|h_{S_2R}\right|^2 + \left|h_{S_1R}\right|^2\right)\frac{\left|h_{RS_1}\right|^2}{N_0} \varsigma \le \gamma_{th}, \frac{\left|h_{RS_1}\right|^2}{N_0} \varsigma > \frac{\gamma_{th}}{P_{th}}, \frac{(1-\rho)\left|h_{S_2R}\right|^2 P}{N_0} > \gamma_{th}\right] \tag{16}$$

The formula (16), can rewrite as:

$$OP_{S_1} = \Pr\left[g_{S_2R} \leq k_1 \right] + \Pr\left[g_{RS_1} \leq k_3, g_{S_2R} > k_1 \right] +$$

$$+ \Pr\left[\left(g_{S_2R} + g_{S_1R} \right) g_{RS_1} \leq k_2, g_{RS_1} > k_3, g_{S_2R} > k_1 \right] \tag{17}$$

$$= \int_0^{k_1} f_{g_{S_2R}}(y)dy + \int_{k_1}^{\infty} f_{g_{S_2R}}(y)dy \int_0^{k_3} f_{g_{RS_1}}(x)dx + \int_{k_3}^{\frac{k2}{k1}} f_{g_{RS_1}}(x) \int_{k_1}^{\frac{k2}{x}} f_{g_{S_2R}}(y) \int_0^{\frac{k2}{x}-y} f_{g_{S_1R}}(z)dzdydx$$

where $\gamma_0 = \frac{P}{N_0}, k_1 = \frac{\gamma_{th}}{(1-\rho)\gamma_0}, k_2 = \frac{\gamma_{th}}{\varsigma\gamma_0}, k_3 = \frac{\gamma_{th}N_0}{\varsigma P_{th}}$.

After applicating Taylor's series [5]: $exp\left(-\frac{x}{\lambda_{p+2}}\right) = \sum_{k=0}^{\infty} \frac{(-x)^k}{k!\lambda_{p+2}^k}$ and calculating the complex integrations,

we have the OP as the two case follows:

- In case of $\lambda_1 = \lambda_2 = \lambda$:

$$OP_{S_1}\big|_{\lambda_1=\lambda_2=\lambda} = 1 - e^{-(k_1/\lambda + k_3/\lambda_3)} + e^{-k_1/\lambda}\left(e^{-k_3/\lambda_3} - e^{-k2/(k_1\lambda_3)}\right) +$$

$$+ (\frac{k_1}{\lambda} - 1)\sum_{k=0}^{\infty} \frac{(-1)^k}{k!}\left(\frac{k_2}{\lambda\lambda_3}\right)^{k+1}\left[\Gamma\left(-k-1,\frac{k_1}{\lambda}\right) - \Gamma\left(-k-1,\frac{k_2}{k_3\lambda}\right)\right]$$

$$+ \sum_{k=0}^{\infty} \frac{(-1)^{k-1}}{k!}\left(\frac{k_2}{\lambda\lambda_3}\right)^{k+1}\left[\Gamma\left(-k,\frac{k_1}{\lambda}\right) - \Gamma\left(-k,\frac{k_2}{k_3\lambda}\right)\right]. \tag{18}$$

- In case of $\lambda_1 \neq \lambda_2$:

$$OP_{S_1}\big|_{\lambda_1 \neq \lambda_2} = 1 - e^{-(k_1/\lambda_2 + k_3/\lambda_3)} + e^{-k_1/\lambda_2}\left(e^{-k_3/\lambda_3} - e^{-k_2/(k_1\lambda_3)}\right) +$$

$$+ \frac{\lambda_2}{(\lambda_1 - \lambda_2)}\sum_{k=0}^{\infty} \frac{(-1)^k}{k!}\left(\frac{k_2}{\lambda_2\lambda_3}\right)^{k+1}\left[\Gamma\left(-k-1,\frac{k_1}{\lambda_2}\right) - \Gamma\left(-k-1,\frac{k_2}{k_3\lambda_2}\right)\right]$$

$$- \frac{\lambda_1 e^{-(1/\lambda_2 - 1/\lambda_1)k_1}}{(\lambda_1-\lambda_2)}\sum_{k=0}^{\infty} \frac{(-1)^k}{k!}\left(\frac{k_2}{\lambda_1\lambda_3}\right)^{k+1}\left[\Gamma\left(-k-1,\frac{k_1}{\lambda_1}\right) - \Gamma\left(-k-1,\frac{k_2}{k_3\lambda_1}\right)\right]. \tag{19}$$

Likewise, the OP of the S_2 in the model is presented as (20) and (21):

$$OP_{S_2}\big|_{\lambda_1=\lambda_2=\lambda} = 1 - e^{-(k_1/\lambda + k_3/\lambda_4)} + e^{-k_1/\lambda}\left(e^{-k_3/\lambda_4} - e^{-k2/(k_1\lambda_4)}\right) +$$

$$+ (\frac{k_1}{\lambda} - 1)\sum_{k=0}^{\infty} \frac{(-1)^k}{k!}\left(\frac{k_2}{\lambda\lambda_4}\right)^{k+1}\left[\Gamma\left(-k-1,\frac{k_1}{\lambda}\right) - \Gamma\left(-k-1,\frac{k_2}{k_3\lambda}\right)\right]$$

$$+ \sum_{k=0}^{\infty} \frac{(-1)^{k-1}}{k!}\left(\frac{k_2}{\lambda\lambda_4}\right)^{k+1}\left[\Gamma\left(-k,\frac{k_1}{\lambda}\right) - \Gamma\left(-k,\frac{k_2}{k_3\lambda}\right)\right]. \tag{20}$$

$$OP_{S_2}\big|_{\lambda_1 \neq \lambda_2} = 1 - e^{-(k_1/\lambda_1 + k_3/\lambda_4)} + e^{-k_1/\lambda_1}\left(e^{-k_3/\lambda_4} - e^{-k_2/(k_1\lambda_4)}\right) +$$

$$+ \frac{\lambda_1}{(\lambda_2 - \lambda_1)}\sum_{k=0}^{\infty} \frac{(-1)^k}{k!}\left(\frac{k_2}{\lambda_1\lambda_4}\right)^{k+1}\left[\Gamma\left(-k-1,\frac{k_1}{\lambda_1}\right) - \Gamma\left(-k-1,\frac{k_2}{k_3\lambda_1}\right)\right]$$

$$- \frac{\lambda_2 e^{-(1/\lambda_1 - 1/\lambda_2)k_1}}{(\lambda_2-\lambda_1)}\sum_{k=0}^{\infty} \frac{(-1)^k}{k!}\left(\frac{k_2}{\lambda_2\lambda_4}\right)^{k+1}\left[\Gamma\left(-k-1,\frac{k_1}{\lambda_2}\right) - \Gamma\left(-k-1,\frac{k_2}{k_3\lambda_2}\right)\right] \tag{21}$$

When $P_{th} \to \infty$ we have linear energy harvesting at relay nearly like the paper [5]

4 RESULTS AND DISCUSSIONS

In the section, we analyze and evaluate the outage probabilities of NEH-TW-DNC scheme. To validate the accuracy of the exact theory expressions, we use Monte Carlo simulations (markers point to simulated results in all figures). At all our analyzations and assessments, we set the target SNR as $\gamma_t = 1$, the path-loss exponent as $\beta_k = 3$ and the variance of noise at the nodes as $N_0 = 1$. Besides, we use the first 20 terms for all the infinite sum formulas.

Figure 2 illustrations the OPs of the S_1 aid S_2 of NEH-TW-DNC system versus $P_s/N_0(dB)$ when $P_{th} \in \{20, 40, \infty\}dB$, $\rho = 0.5$, $\eta = 0.8$ $\alpha = 1/3$, $d_1 = 0.3$, $d_2 = 1 - d_1$. Due to the symmetry of the model, when the relay is equidistant from the two sources, the OP of the two sources are equal. With these values of d_1, d_2, the relay is nearer S_1 than S_2. Observing Figure 2, when P_s is less than P_{th}, the OP_{S_2} has better

than OP_{S_1}, conversely when P_s is more than P_{th}, the OP_{S_1} has better than OP_{S_2}. It is worth noting that when $P_{th} = P_s$, the OP of the two sources are equal. When $P_s/N_0(dB)$ is in the small value region, the OP of the two sources decrease as P_s/N_0 increases, and the OP of each source is roughly equal for all values of P_{th}. Besides, when P_s/N_0 reaches a large enough value, the OP will reach a threshold value (OP_{th}), that means P_s/N_0 increases but OP no longer increase. This OP_{th} depends on the value of P_{th}, when the P_{th} is larger the OP_{th} is smaller. Moreover, the OP curves of the nonlinear EH model will approach the OP of the linear EH model as P_{th} approaches infinity.
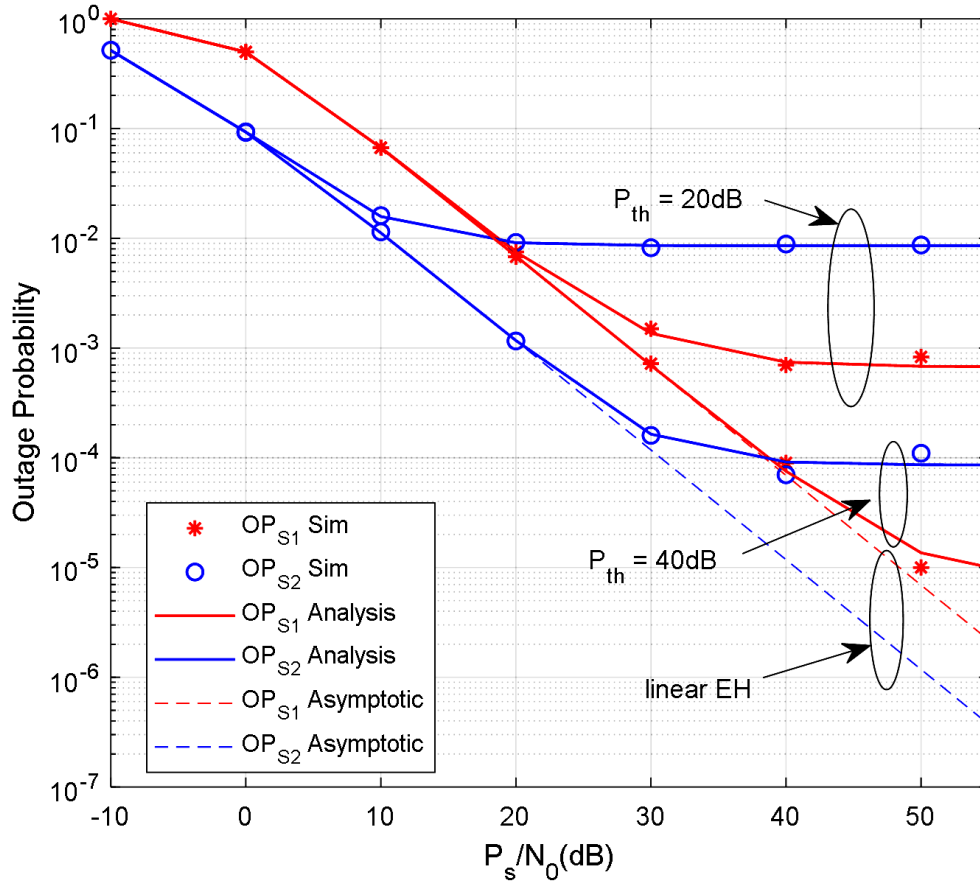
Figure 2. The outage probabilities of the S_1 and S_2 versus $P_s/N_0(dB)$ with three values $P_{th} \in \{20, 40, \infty\}(dB)$

Fig.3 shows the outage probabilities of the source S_1 of NEH-TW-DNC system as a function of the saturation threshold power $P_{th}(dB)$ when $P_s/N_0 \in \{20, 40\}dB$, $\rho = 0.5$, $\eta = 0.8$ $\alpha = 1/3$, $d_1 \in \{0.3, 0.5, 0.7\}$, $d_2 = 1 - d_1$. Due to symmetry of the system model, the OP_{S_1} is equal the OP_{S_2} if the equivalent parameters of the two sources are the same, so in fig.3 we just draw the curves of OP_{S_1}. We can observe that the OP_{S_1} is better when P_{th} and P_s/N_0 increases and the OP_{S_1} achieves the saturation values when P_{th} increases to a high value, and this value is change according to the values of P_s/N_0, and d_1. Besides, when P_{th} is smaller than P_s/N_0 the smaller d_1 is the better OP_{S_1} and when P_{th} is bigger than P_s/N_0 the higher d_1 is the better OP_{S_1}.
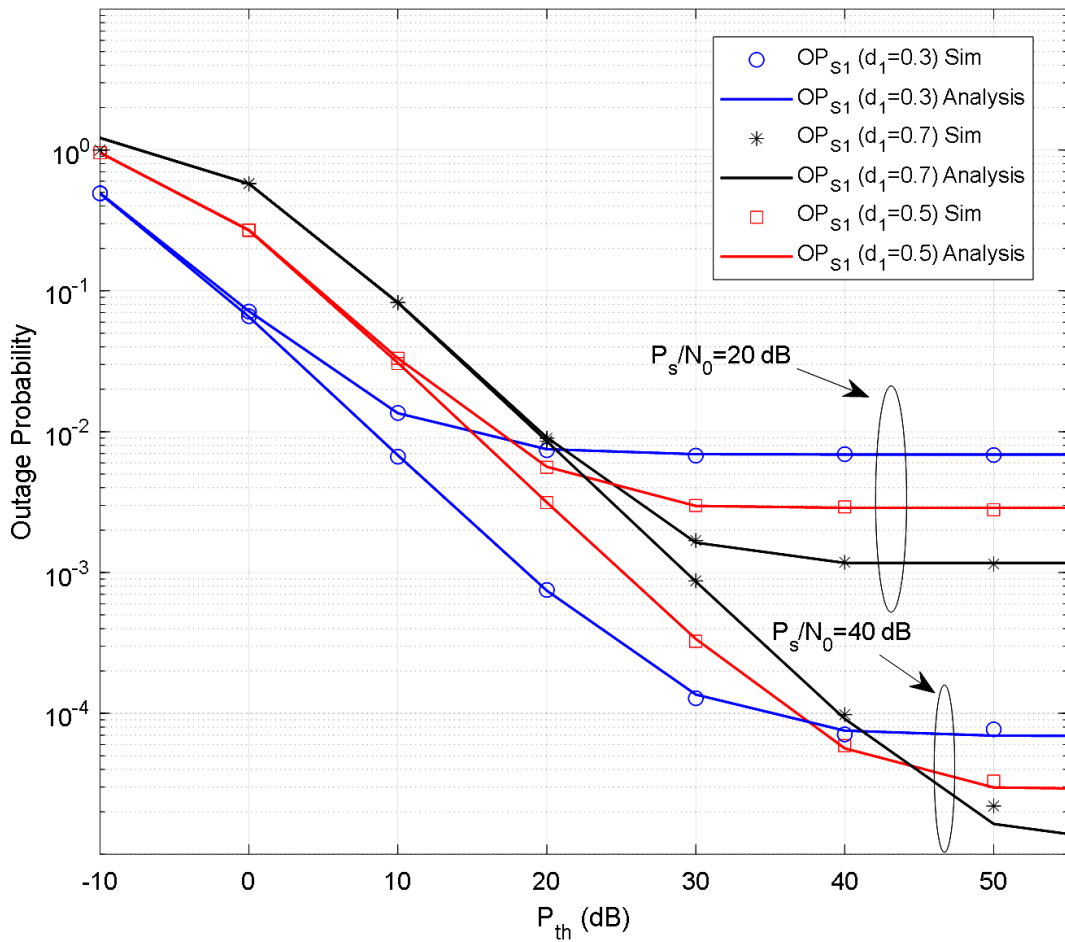
Figure 3. The outage probabilities of the S_1 versus $P_{th}(dB)$ with two values of P_s/N_0 and three values of d_1

Fig. 4 shows the outage probabilities of the source S_1 of NEH-TW-DNC system as a function of the power allocation coefficient ρ when $P_s/N_0 = 30(dB)$, $P_{th} \in \{20,30,40\}dB$, $\eta = 0.8$ $\alpha = 1/3$, $d_1 = 0.5$, $d_2 = 1 - d_1$. It is observed that the OP_{S_1} decreases as the P_{th} increases. Moreover, for each set of parameters, there is always a value of ρ so that the source has the smallest outage probability.

Finally, the theory analyses and the Monte Carlo simulations coincide for all figures.
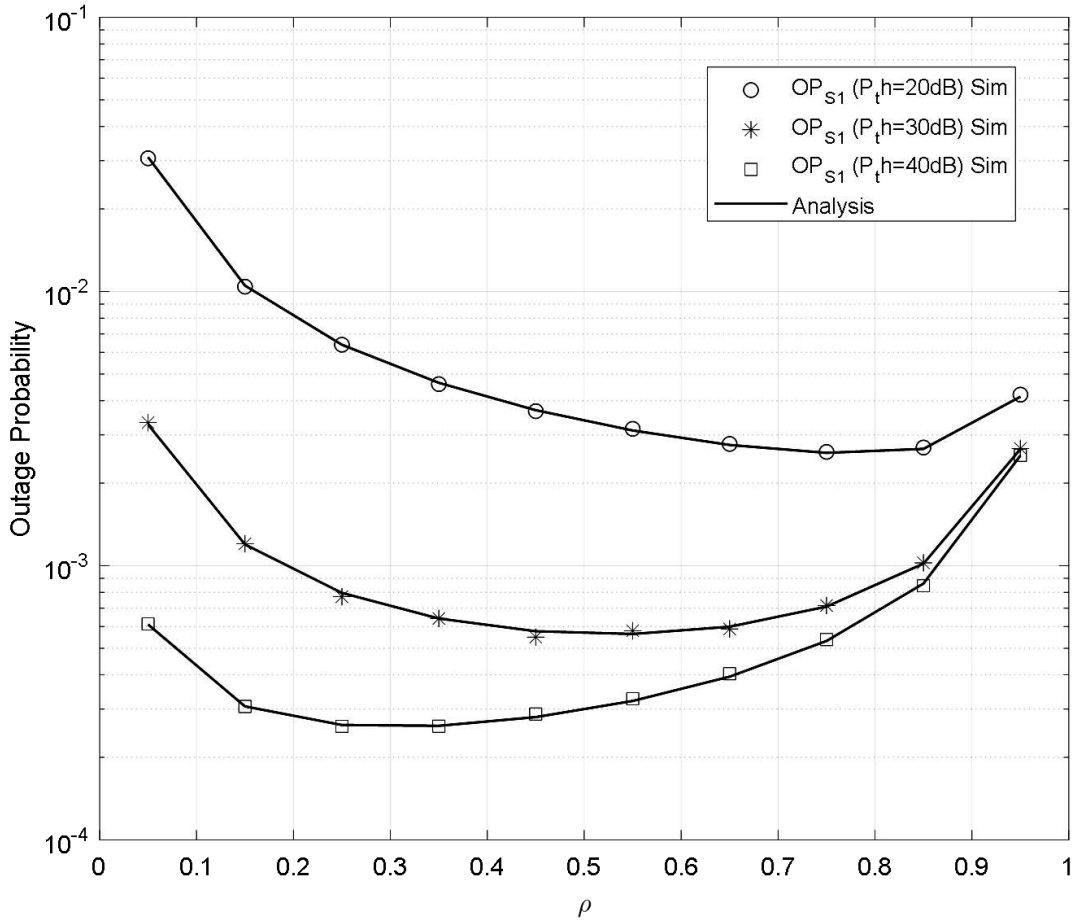
Figure 4. The outage probabilities of the S_1 versus ρ with three values of P_{th} and d_1

5 CONCLUSIONS

In this article, we have derived the exact sources outage probabilities of a two-way cooperation system. And the relay has a non-linear equip to collect the energy from the received radio frequency signals in two first time slots. Then it converts this energy into the broadcast power in the third time slot. The outage probabilities are investigated according to the saturation threshold power, the power allocation coefficient, and the relative position of the relay and two sources. Numerical results show that when the saturation threshold power of a non-linear equip to harvest the energy at relay increases, the outage probabilities decrease. And the outage probabilities achieve the saturation value when P_s/N_0 and P_{th} are enough large. Furthermore, we can define the optimal the power allocation coefficient where the outage probability is minutest. Finally, the theory analyses and the Monte Carlo simulations coincide for all figures. Our future work may consider more techniques and reality conditions in the NEH two-way system to enhance the system performance.

REFERENCES

[1] A. A. Nasir, X. Zhou, S. Durrani, and R. A. Kennedy, "Relaying protocols for wireless energy harvesting and information processing," *IEEE Transactions on Wireless Communications,* vol. 12, no. 7, pp. 3622-3636, 2013.

[2]T.-T. T. Dao and P. N. Son, "Uplink non-orthogonal multiple access protocol in two-way relaying networks: realistic operation and performance analysis," in *2020 7th NAFOSTED Conference on Information and Computer Science (NICS)*, 2020, pp. 399-404: IEEE.

[3] T.-T. T. Dao and P. N. Son, "Cancel-Decode-Encode Processing on Two-Way Cooperative NOMA Schemes in Realistic Conditions," *Wireless Communications and Mobile Computing,* vol. 2021, 2021.

[4] H. V. Toan and T. M. Hoang, "Outage Probability Analysis of Decode-and-Forward Two-Way Relaying System with Energy Harvesting Relay," *Wireless Communications and Mobile Computing,* vol. 2020, 2020.

[5] T. N. Nguyen, P. T. Tran, and M. Voznak, "Wireless energy harvesting meets receiver diversity: A successful approach for two-way half-duplex relay networks over block Rayleigh fading channel," *Computer Networks,* p. 107176, 2020.

[6] A. Cvetkovic, V. Blagojevic, and P. Ivaniš, "Performance analysis of nonlinear energy-Harvesting DF relay system in interference-limited Nakagami-m fading environment," *ETRI journal,* vol. 39, no. 6, pp. 803-812, 2017.

[7] D. Kumar, P. K. Singya, and V. Bhatia, "Performance Analysis of Hybrid Two-Way Relay Network with NLPA and Hardware Impairments," in *2021 IEEE Wireless Communications and Networking Conference (WCNC)*, 2021, pp. 1-6: IEEE.

[8] L. Shi, W. Cheng, Y. Ye, H. Zhang, and R. Q. Hu, "Heterogeneous power-splitting based two-way DF relaying with non-linear energy harvesting," in *2018 IEEE Global Communications Conference (GLOBECOM)*, 2018, pp. 1-7: IEEE.

[9] I. S. G. a. I. M. Ryzhik, *Table of integrals, series, and products*, Seventh ed. Elsevier, 2007.

[10] P. N. Son and T. T. Duy, "A new approach for two-way relaying networks: improving performance by successive interference cancellation, digital network coding and opportunistic relay selection," *Wireless Networks,* pp. 1-15, 2019.

[11] T.-T. T. Dao and P. N. Son, "Multi-constraint two-way underlay cognitive network using reconfigurable intelligent surface," *Wireless Networks,* p. 14, 2022/04/06 2022.